Fabrication & Characterization of an Effective Electron Transport Layer for Perovskite Solar Cells

By

Bushra Batool

171853

Session 2016-18

Supervised by

Dr. Nadia Shahzad

MASTERS of SCIENCE in

ENERGY SYSTEMS ENGINEERING

US-Pakistan Center for Advanced Studies in Energy (USPCAS-E)

National University of Sciences and Technology (NUST)

H-12, Islamabad 44000, Pakistan

November, 2019

Fabrication & Characterization of an Effective Electron Transport Layer for Perovskite Solar Cells

By

Bushra Batool

171853

Session 2016-18

Supervised by

Dr. Nadia Shahzad

A Thesis Submitted to the US-Pakistan Center for Advanced Studies in Energy in partial fulfillment of the requirements for the degree of

MASTERS of SCIENCE in

ENERGY SYSTEMS ENGINEERING

US-Pakistan Center for Advanced Studies in Energy (USPCAS-E)

National University of Sciences and Technology (NUST)

H-12, Islamabad 44000, Pakistan

November, 2019

THESIS ACCEPTANCE CERTIFICATE

Certified that final copy of MS/MPhil thesis written **Ms. Bushra Batool (Registration No. 171853)** of **U.S. – Pakistan Center for Advanced Studies in Energy** has been vetted by undersigned, found complete in all respects as per NUST Statues/Regulations, is within the similarity indices limit and is accepted as partial fulfillment for the award of MS/MPhil degree. It is further certified that necessary amendments as pointed out by GEC members of the scholar have also been incorporated in the said thesis.

Signature: _____

Name of Supervisor _____

Date: _____

Signature (HoD):

Date: _____

Signature (Dean/Principal): _____

Date: _____

This is to certify that work in this thesis has been carried out by **Ms. Rida Mansoor** and completed under my supervision in **Biofuel** laboratory, US-Pakistan Center for Advanced Studies in Energy (USPCAS-E), National University of Sciences and Technology, H-12, Islamabad, Pakistan.

Supervisor: _____

Dr. Nadia Shahzad
USPCAS-E
NUST, Islamabad

GEC member # 1: _____

Dr. Naseem Iqbal
USPCAS-E
NUST, Islamabad

GEC member # 2: _____

Dr. Afzal Kombo
USPCAS-E
NUST, Islamabad

GEC member # 3: _____

Dr. Parvez Akhter
USPCAS-E
NUST, Islamabad

HoD- (dept) _____

Principal/ Dean _____

Dr. Bilal
USPCAS-E
NUST, Islamabad

To the quest of everlasting curiosity;

the essence of scientific minds.

Abstract

With the expanding need for energy production and the collateral damage caused by the emissions released as a consequence of conventional energy producing technologies, there is a constant search for an alternative means of fulfilling global energy requirements**.** Owing to the vigorous research and rapid advancements, many new types of semiconducting photovoltaic materials have been developed in addition to the old-fashioned Silicon based solar cells. PV technologies are divided into three generations. Perovskite Solar Cells (PSCs) so far the highest Power conversion efficiency achievers at research level, are prior most candidates for solar energy. This research is aimed to fabricate and characterize low temperature processed Electron transport layer (ETL) for PSCs. Three different ETLs were deposited on the Fluorine doped Tin oxide glass. The aim was achieved by using sol-gel and solution processing technique and we got good results. This work was considered to discover the potential of a suitable electron transport layer. First of all the nanoparticles of the desired material was synthesized using co-precipitation technique, characterized using X-ray Diffraction (XRD) and Scanning Electron microscopy (SEM) to study the crystal structure and morphological properties. Furthermore the thin film technology used to fabricate the ETLs, was spin-coating and films were characterized using XRD technique, SEM, EDX, UV-Vis spectrophotometer, optical Microscopy and hall Effect. As an additional task, to obtain the efficiency results via IV curve tracer, the device fabrication was also performed for all the ETLs fabricated. The hole transport layer was fabricated via thermal evaporation. The light harvesting absorber layers were fabricated via spin coating and later dip coating inside the glove box for better sustainability of the PSCs.. The contact deposition was done for optimization samples using a physical Vapor deposition system. Hence the whole device fabrication was processed but no good results were achieved. But the task of complete device is being recommended by using better absorber layer and hence efficient PSCs to be tested.

Key words: Electron Transport Layer, Perovskite Solar Cells, Tin Oxide, Titanium dioxide, Solar Energy

.

Table of Contents

List of Figures

List of Tables

List of Journal/Conference Papers

1. **Bushra Batool**, Nadia Shahzad, Imran Shahzad, Anum Ameer, " *Sintering and pH effect on Low Temperature Processed Tin Oxide Nanoparticles for Perovskite Solar Cells Application"*, presented and accepted for the proceedings of MSNANO-2019, conference held at GCU Faisalabad, under review in Journal of Nanoscience and Nanotechnology (JNN)

2- **Bushra Batool**, Nadia Shahzad, Imran Shahzad,"*Optimization of synthesis and deposition of Electron transport layer For Perovskite Solar Cells"* to be sent to Solar Energy Journal **(drafting)**

3- Anum Ameer, **Bushra Batool**, Nadia Shahzad, Imran Shahzad,"*Synthesis and Characterization of Nickel Oxide Nanostructures for Perovskite Solar Cell Application*", presented and accepted for the proceeding of MSNANO-2019, Conference held at GCU, Faisaslabad

4- Farhan Ahmed, Nadia Shahzad, **Bushra Batool**, M. Imran Shahzad, "*Hydrophobic Hole Transport Material For Perovskite Solar Cells*" presented and accepted for the proceedings of MSNANO-2019, conference held at GCU Faisalabad

List of Abbreviations

PSCs	Perovskite Solar Cells
DSSCs	Dye sensitized solar cells
GHG	Greenhouse gas
RE	Renewable energy
KWh	Kilowatt-hours
ITO	Indium tin oxide
FTO	Fluorine doped tin oxide
CB	Conduction Band
VB	Valance band
HOMO	Highest occupied molecular orbital
LUMO	Lowest unoccupied molecular orbital
ETL	Electron Transport Layer
HTL	Hole Transport Layer
FF	Fill Factor
J_{sc}	Short Circuit Current
V_{oc}	Open Circuit Voltage
PEC	Power Conversion Efficiency
DMSO	Dimethyl sulfoxide
DMF	Dimethyl formamide
XRD	X-ray diffraction
SEM	Scanning electron microscopy
UV-Vis	Ultra Violet Visible

Chapter # 1
Introduction

1.1 Energy Mix of Pakistan:

With growing worldwide energy consumption and environmental pollution fossil fuels as energy sources are not sufficient for the sustainable development of human society. Advancement in terms of technology is exclusively reliant upon energy in today's world. With the increase in energy demand and supply gap, researchers have begun focusing on ways to provide steady and constant supply of energy. Non-renewable resources have been the prime source of energy generation over the past few decades. However, recently, due to depletion of non-renewable resources, problem of non-sustainability and emission of greenhouse gases, focus has been shifted to the integration of renewable resources into the energy mix in order to provide a more sustainable, reliable and clean energy supply. The utilization of renewable energy sources is now a requirement for the sustainable development.

1.2 Environmental Impacts:

Burning fossil fuels adds up to the 56.6% of all the greenhouse gasses (GHGs) and increasing concentrations of methane (CH_4), nitrous oxide (NO_x), sulfur oxide (SO_x) and carbon dioxide (CO_2), which contributes significantly to global warming [1]. An increase in the amount of these gases caused increase in temperature and this phenomenon generally known as global warming. Global warming is growing with the rate of 0.13°C per decade and there is a prediction that the rate may increase to 0.5°C in upcoming ten decades [2]. Amongst the few antagonistic health effects of fossil fuels consumption are respirational and skin related diseases. Also phenomenon like acid rain and smog which are caused by harmful emissions in the environment lead to various other problems. According to the report of World Energy Outlook 2017, two of the four large scale shifts in the worldwide energy system include the fast deployment and decrease in prices of green energy technologies and secondly the rapid electrification of energy [1].

1.3 Renewable and Conventional Energy Resources:

With this expanding need for energy production and the collateral damage caused by the emissions released as a consequence of conventional energy producing technologies, there is a constant search for an alternative means of fulfilling global energy requirements**.** Also the costs of obtaining fuels both from local and foreign sources is increasing rapidly because of the nonstop depletion of fossil fuel resources. If the current situation prevails for a while, there might be an alarming increase in the cost of these fuels. Due to. this rapid increase in energy consumption which cause emission of greenhouse gases (GHG) and depletion of fossil fuels with passage of time, there is a need of finding new innovative ways for producing energy at lower costs with less environmental impact. According to the World Energy Outlook 2017 report, renewable sources are expected to capture 2/3rd of the global investment on power plants by 2040, as they will soon become the most affordable sources of electricity generation in many countries throughout the world [1].

Renewable energy technologies like solar, wind, bio-fuel and geothermal are acquired from sources that are never-ending and can be replenished time after time. There is an enormous amount of energy that can be produced by renewable energy resources. Renewable energy not only helps contribute to the world energy crisis but it is also sustainable and eco-friendly (zero gas emissions). Among the possible alternatives to conventional energy technology solar is being most reliable and affordable choice. Received in abundance by the earth (23,000 TW per year), solar energy can help reduce our dependence on carbon-based fuels and progressively eliminate the threat of global warming [3].

1.4 Pakistan's Energy Mix:

According to recent estimates by NEPRA and IEEFA, wind and solar are now the most economical sources of energy in Pakistan [6]. Solar irradiance levels in the southwest of Pakistan, are at par with the best in the world, with Global Horizontal Irradiance of up to 1500 kWh/m^2 in almost 90 percent of the land area [3]. Pakistan is capable of producing 92% of its electricity necessities through solar PV technologies at a very good rate and considering that, over 58.1% of that electricity production is through solar plants and 15 percent via Concentrated Solar Plants (CSP) [7].

1.5 Solar Energy:

Harvesting Sun's energy is major form of solar energy. There are two major classifications of this renewable energy: the first one is the solar thermal power generation, the second type is solar power generation [8].

1.5.1 Solar thermal power generation

Solar thermal power generation converts energy from the sun into heat, and transforms this heat into electricity. Hence there are two types of conversions. Firstly converting the sunlight directly into electric energy, for example like semiconductors and other metallic thermo-electrical power generation and magnetic liquefied power generation etc. [8]. The second is that the conversion of heat energy through the turbines to operate the generator to supply electric power. This Power generation and traditional thermal is analogous, however the heat is from marketable solar power rather from the fuel.

1.5.2 Solar power generation

Solar power generation is an elegant method of harnessing Sun's energy. A solar device transforms the incident solar radiations straight into electrical energy via photo-voltaic effects otherwise photochemical reactions. Solar power generation uses solar cell technology i.e. Photovoltaic cell technology. In comparison to other renewable technologies, photovoltaic solar cell is required to do a two-step function. First the material (semiconductor) which is used in fabrication of the cell must absorb light (photon) and excite electron from lower energy state to a higher energy state. Second function of the photovoltaic demands the movement of electron shifted to advanced energy state, from solar device to the externally connected circuit, so generation of the current is ensured.

1.6 Working of a Solar Cell

A solar cell is a device that converts the incident solar radiations directly into electrical energy via photovoltaic effect. It works on the principle that whenever light falls on the surface of the solar cell, an electron hole pair is generated which produces a current and voltage. Almost all devices that act a solar cell are in form of PN junction. The energy of the incident photon (light) must be greater than the band-gap of the semiconductor material used. The generated electron-hole pair is in a meta-stable state. The four basic steps on which a solar cell functions are [11]:

I. the production of photons
II. the collection of the produced photons to generate an electric flow
III. A huge voltage generation across the device
IV. The power dissipation through the load and resistances

A typical silicon based solar cell consists of p-n junction where electron hole pair is generated, an anti-reflective coating for maximum absorption of sunlight, and front metal contacts for the collection of generated electrons as displayed in figure 1 [9].

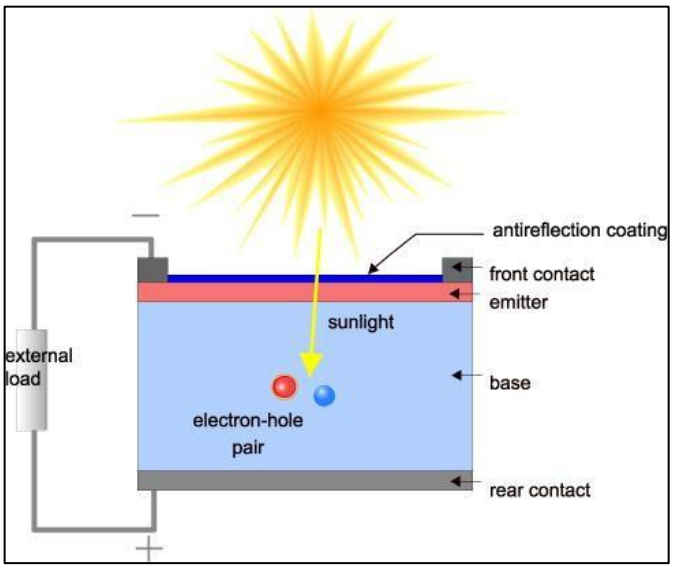

Figure 1.1 Cross section of a Solar Cell [9]

Solar energy placement requires an area of 5.5 acres/megawatt (MW) and 1MW generates enough power to provide for around 120 homes. Ballasted systems can be installed without troubling or using up ground space [13].

1.7 Generations of Photovoltaic Technologies

Owing to the vigorous research and rapid advancements, many new types of semiconducting photovoltaic materials have been developed in addition to the traditional Silicon based solar cells. PV technologies are divided into three generations and are discussed briefly in this section. Figure 1.2 illustrates the categorization of materials employed for solar device fabrication, the solar generation containing perovskite, which are studied in this thesis, are part of the organic structure group of solar cells [14].

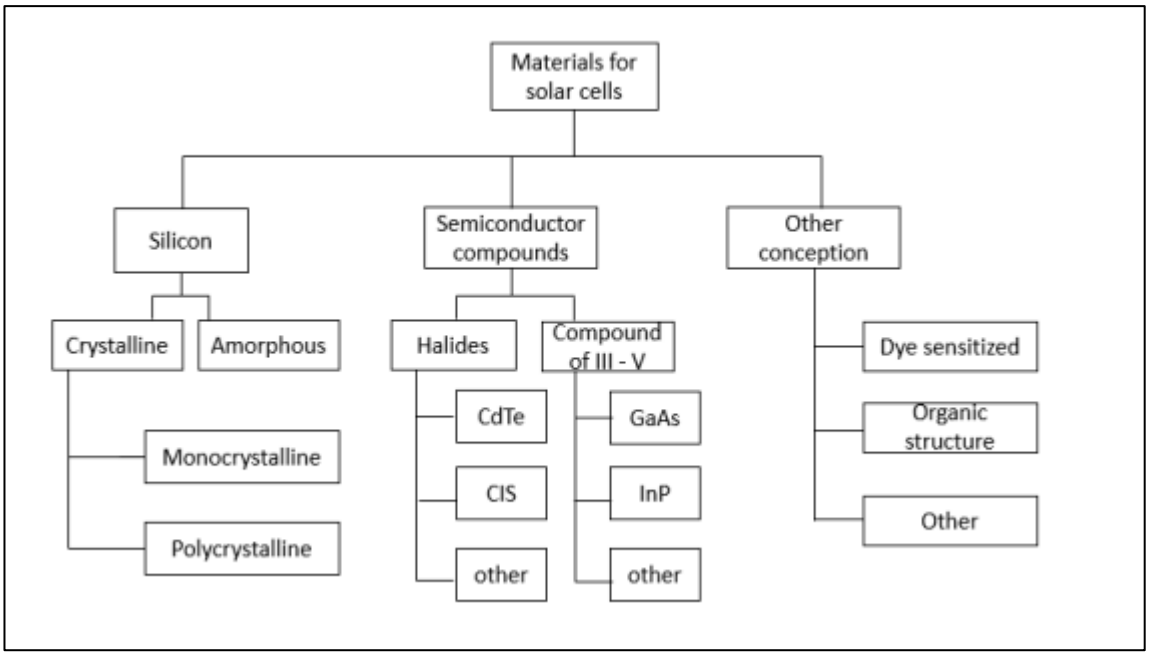

Figure 1.2 Categorization of solar cell materials [14]

1.7.1 First Generation Solar Cells

The first generation solar photovoltaics are well-matured in terms of their technology, and fabrication process. They represent the oldest commercially available photovoltaics technologies [15] . Silicon solar cells based on silicon wafer and hetro-junction silicon based solar cells have achieved an excellent efficiency (15% to 20%) and are widely used for residential purpose. Silicon solar cell technology is mainly based on two kinds of cells, Monocrystalline (single junction) and Multicrystalline (Polycrystalline) solar cells which are further categorized on the basis of number of grain boundaries.

Monocrystalline solar cells are thin wafers of silicon sliced from a bulk of single crystal of silicon. A number of such thin wafers are combined together in order to form a panel. Presently mono-crystalline solar cells have achieved a lab efficiency of 26.2%.

Polycrystalline silicon solar cells are cheaper than mono-crystalline solar cells. These silicon wafers are produced from multiple silicon crystals, hense multi-crystalline unlike the monocrystalline or single-crystal silicon cells. Due to crystal defects and grain-boundaries, these solar cells lack efficiency.

1.7.2 Second Generation Solar Cells

Second-generation solar cells are usually called thin-film solar cells. These types of cells are made from thin layers of semi-conductor materials. Because of less cost and less material usage in these type of solar cells, these are preffered generation

over the first one. But mass production of this type of solar cells are difficult to achieve, moreover the techniques like vacuum processing and high temperature treatments of thin films still require a large amount of energy consumption. The types of cells in this generation are of three types, Cadmium Telluride (CdTe), Amorphous Silicon hetero-junction and Copper Indium Gallium diSelenide (CIGS). These type of solar cells have achieved a power conversion efficiency of around 9%-18% and the highest efficiency is measured for CIGS so far is 22.9% [16].

1.7.3 Third Generation Solar Cells

To achieve higher efficiency at low cost, researchers have developed another generation of solar cells. This generation of solar cells mainly includes quantum dots solar cells, organic solar cells, dye-sensitized solar cells and perovskite solar cells. These solar cells are low in cost of materials and manufacturing but have not achieved efficiency equal or greater than silicon based solar cells.

The highest record efficiency obtained with perovskite solar cells thus far is 23.3% and 12.9% for organic solar cells, whereas that for DSSCs is still only 11.9% as demonstrated in the graph [16]. Now a days perovskite material solar cells, which are the part of organic structure are under research phase and highest lab efficiency of value 21% is achieved but it holds little share of market.

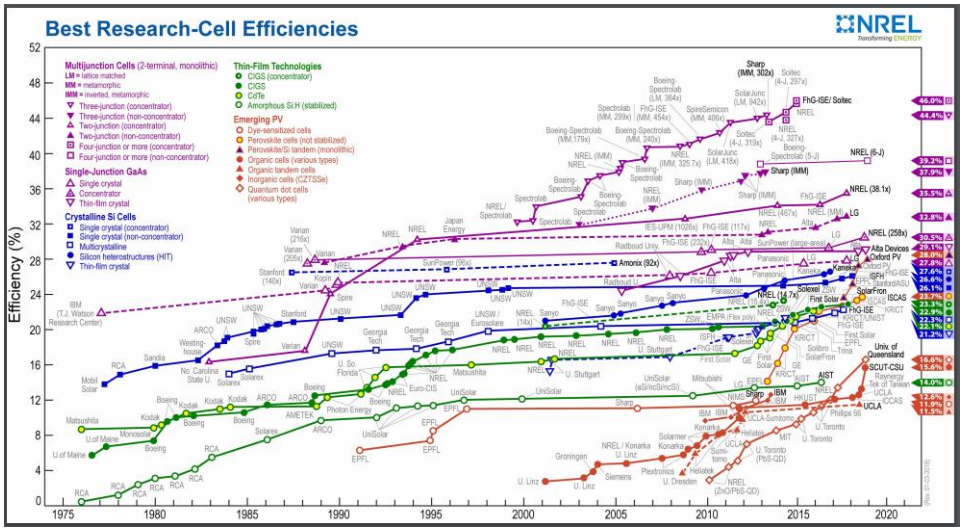

Figure 1.3 Recorded efficiencies of solar cells, national renewable energy laboratory (NREL) [16]

1.8 Perovskite Solar Cells

Recently Methylammonium lead halide, centered hybrid perovskite solar cells (PSCs) are being studied intensively not only because of their low processing costs but

also their high efficiency. This class of solar cells belongs to the third-generation solar cell technology and resemble closely with the DSSCs with few alterations in the device architecture. The efficiency of the PSCs has improved since 2009 (3.8%) to 27.3% (Perovskite silicon tandem cell) in 2018. Perovskite solar cells (PSCs) have high efficiencies that are increased speedily in the short time. According to national research engineering laboratory efficiencies of solar cells based on perovskite material increased from 3.8% to 21% within year 2009 to 2016.

1.8.1 Structure of Perovskite Solar Cell

The third generation of solar cells technology holds PSCs and resemble closely with the DSSCs with a few alterations in the device architecture. They have a hybrid organic-inorganic light absorbing layer instead of a liquid dye. The basic types of perovskite devices include the planner hetero-junction and Meso-super structured PSCs based on whether they possess a mesoporous TiO_2 electron transport layer. The main light absorbing layer that is made up of perovskite material is sandwiched in between two charge transporting layers, one is hole blocking/electron transporting layer and the second is electron blocking/hole transporting layer. The basic structure of a Perovskite solar cell is shown below

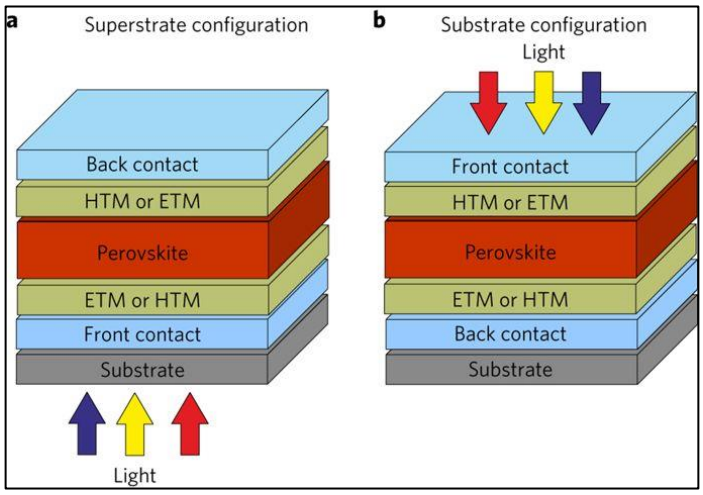

Figure 1.4 Schematic of a perovskite solar cell in (a) the conventional superstrate configuration and (b) the substrate configuration

1.9 Brief Description and Aim of Research

This research is aimed to fabricate and characterize Electron transporting layer (ETL) processed on low temperature for Perovskite solar cell. Three different ETLs were deposited on the FTO, Fluorine doped Tin oxide glass slides. The aim was

achieved by employing sol-gel and solution processing technique for good results. This work was considered to discover the potential of a suitable electron transport layer. First of all the nanoparticles of the desired material were synthesized Co-precipitation technique, characterized using X-ray Diffraction and Scanning Electron microscopy to study the crystal structure and morphological properties. Furthermore the thin film technology used to fabricate the ETLs, was spin-coating and films were characterized using x-ray diffraction technique, SEM, EDX, UV-Vis spectrophotometer, optical Microscopy and hall Effect. To obtain the efficiency results via IV curve tracer, the device fabrication was also performed for all the ETLs fabricated. The hole transport layer was fabricated via thermal evaporation. Two comparative light harvesting absorber layers were fabricated via dip coating inside the glove box for better sustainability of the perovskite solar cell. The contact deposition was done using a physical Vapor deposition system. Hence the whole device fabrication was processed.

Summary:

This chapter gives an overview of world energy consumption. Focusing the significance of renewable energy, the solar potential of Pakistan is discussed under Pakistan's Energy Mix. Considering solar energy, solar thermal power generation and solar power generation is briefly discussed. Working of the solar Cell is explained. Discussing solar photovoltaic technology, the various generations of solar cells and have been overviewed. First generation deals with silicon based solar cells, 2nd class deals with thin film technology based solar cells, while third generation deals with different nano-materials based solar cells. Perovskite solar cells are among this last category of photovoltaic cells. These cells have achieved an efficiency of 26%-27.3%.

References:

[1] K. S. Ottmar Edenhofer (Germany), Ramon Pichs- Madruga (Cuba), Youba Sokona (Ethiopia/Mali) and (Germany/USA), "IPCC Special Report on Renewable Energy Sources and Climate Change Mitigation Summary for Policymakers," no. May 2011, pp. 5–8.

[2] A.H. khan, "A Primer on Pakistan's Energy Mix - Daily Pakistan Global," *daily pakistan global*, (2018) 3.

[3] E. Y. Book, "Primary energy mix," pp. 203–221, California ISO, 2012.

[4] M. Sarim, “Pakistan’s energy mix | The Express Tribune,” *Tribune*, Pakistan p. 3, 2019.

[5] H. B. Khalil and S. J. H. Zaidi, “Energy crisis and potential of solar energy in Pakistan,” *Renew. Sustain. Energy Rev.*, 31, (2014) 194–201.

[6] heliscsp, “Pakistan can achieve highest solar power potential by 2050 – HELIOSCSP,” 2016. Available: http://helioscsp.com/pakistan-can-achieve-highest-solar-power-potential-by-2050/

[7] solar energy Austrailia, “A brief introduction of solar energy - Solar Energy Australia Medium,”2014 Available: https://medium.com/@solarenergy/a-brief-introduction-of-solar-energy-ea561c0cf6b8/

[8] Christina Honsberg and Stuart Bowden, “Solar Energy | PVEducation,” 2019. Available: https://www.pveducation.org/pvcdrom/introduction/solar-energy.

[9] J. Salasovich and G. Mosey, “Feasibility Study of Economics and Performance of Solar Photovoltaics, Golden, CO (Unites States), 2011.

[10] Honsberg Christina and Bowden Stuart, “Solar Cell Structure | PVEducation,” 2019. https://www.pveducation.org/pvcdrom/solar-cell-operation/solar-cell-structure/

[11] J. Simon and G. Mosey, “Feasibility Study of Economics and Performance of Solar Photovoltaics,” Golden, CO (United States), 2013.

[12] F. Dinçer, “The analysis on photovoltaic electricity generation status, potential and policies of the leading countries in solar energy,” *Renew. Sustain. Energy Rev.*,15, . 1,(2011) 713–720.

[13] JONAS STASIULIONIS, “Life cycle assessment of perovskite solar cells and comparison to silicon solar cells Master’s Thesis within the Sustainable Energy Systems programme.”, 52. (2018), 413-419.

[14] Editor by, “4.1 Generations of solar cells - Jlanka Technologies,” 2018. [Online]. Available: https://jlankatech.com/generations-of-solar-cells/

[15] Alchemie Limited, “3 Generations of Solar Cells: Solar Facts and Advice,” 2013. [Online]. Available: http://www.solar-facts-and-advice.com/solar-

cells.html/

[16] F. Fu *et al.*, “High-efficiency inverted semi-transparent planar perovskite solar cells in substrate configuration,” *Nat. Energy*. 2, no. 1,(2017) p. 16190.

Chapter # 2

Literature Review

In the past few years methylammonium lead halide, centered hybrid PSCs have been studied intensively not only because of their low processing costs but also their high efficiency. The efficiency of the PSCs has improved since 2009 (3.8%) to 27.3% (Perovskite silicon tandem cell) in 2018. Perovskite solar cells (PSCs) have high efficiencies that are increased speedily in the short time. According to national research engineering laboratory efficiencies of solar cells based on perovskite material increased from 3.8% to 21% within year 2009 to 2016.

2.1 Perovskite Solar Cells:

This class of solar cells belongs to the third-generation solar cell technology and resemble closely with the DSSCs with a little alterations in the device architecture [1]. They have a hybrid organic-inorganic light absorbing layer instead of a liquid dye. The basic types of perovskite devices include the planner hetero-junction and meso-super structured PSCs based on whether they possess a mesoporous TiO_2 electron transport layer. General structure of the perovskite (non-inverted) is given in the figure 2.1.

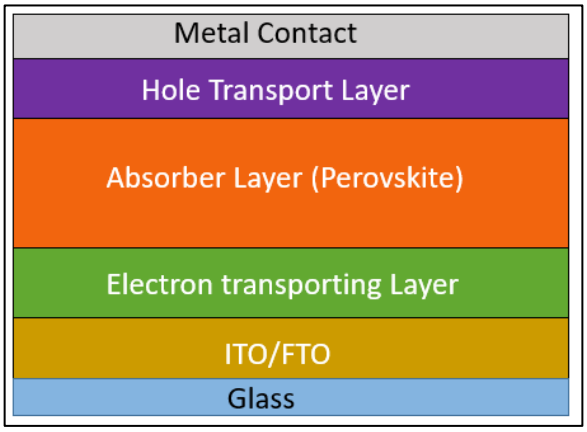

Figure 2.1 Generic structure of Perovskite Solar cell

2.1.1 Top/bottom glass substrate

A bare glass slide acts as the substrate upon which the remaining layers are deposited,

2.1.2 Indium or Fluorine doped tin oxide (ITO/FTO)

Glass is covered with material which is an electrically conductive as well as transparent layer. Other than solar cell technology ITO/FTO have an extensive range of uses.

2.1.3 Electron transport layer

ETL is a semiconducting layer used as a charge carrier, materials like TiO_2 and SnO_2 are commonly employed in PSCs. Usually a compact n-type layer of TiO_2 is fabricated on FTO or the ITO functioning as a blocking layer for holes and on thiscompact layer, meso-porous layer of TiO_2 is employed for charge tranport [2].

2.1.4 Light harvester/sensitizer

This layer is composed of the perovskite material (ABX_3) and functions as the absorber material. Electron and hole pairs are produced when light hits this layer, from where they are transported to the particular charge transport layers.

2.1.5 Hole transporting layer

HTL in perovskite based solar devices is used for hole (charge carrier) transportation. Vareity of materials are used for this Layer, for example Spiro MeOTAD, NiO, PbPc, CUSCN, PEDOT [3].

2.1.6 Metal contacts

With high values of conductivity these contacts are employed for the charge extraction and transportation. Choice of metallic contacts hinge on the HOMO and LUMO levels of the materials employed for both charge transporting layers, ETL and HTL.

2.2 Working of Perovskite Solar Cells (PSCs):

Physics of hybrid organic-inorganic lead halide solar cells can be explained with the help of following processes. These progressions from conversion of light into electric energy show a significant part in performance of PSCs.

2.2.1 Light absorption

Perovskite material is termed as light absorber in PSCs. When light falls on the active layer of solar cell, sensitizer absorbs the incident sunlight and electron is excited from the ground state i.e. HOMO of valance band to excited state LUMO of conduction band. Working principal of perovskite solar cells is represented in figure 2.2 given below

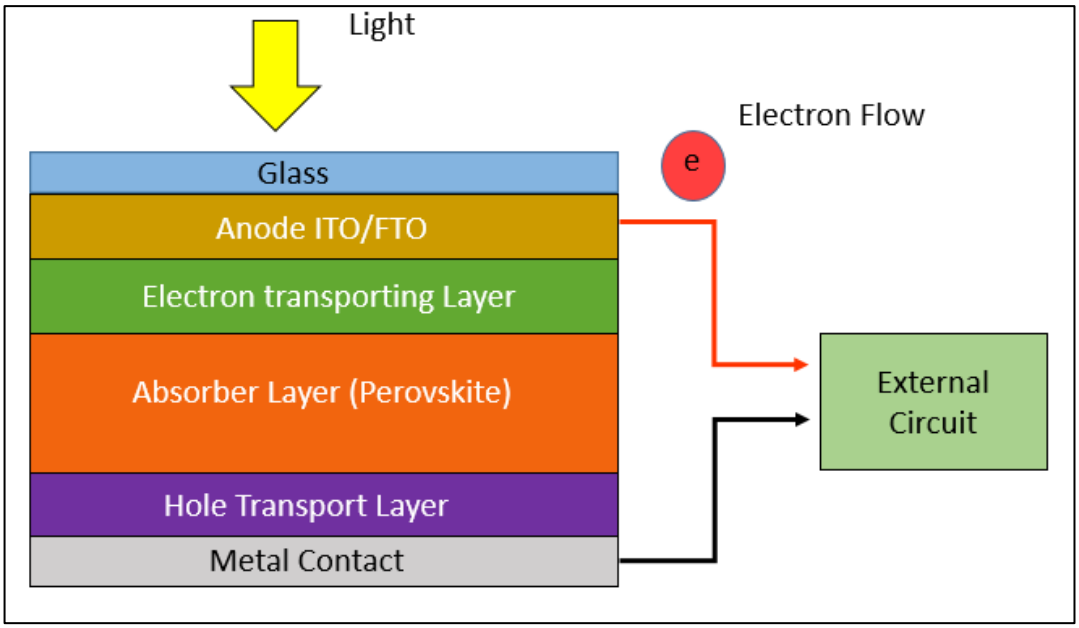

Figure 2.2 Working Principal of Perovskite Solar Cell

2.2.2 Exciton Generation and Diffusion

The light incident on the cells when passes on to light absorber layer generating electron-hole pairs, namely exciton. When a light absorber semiconductor material is illumined an exciton can be formed depend upon the material absorption coefficient and bandgap. These generated excitons are diffuses in the material and only a small numbers of excitons are able to reach donor/ acceptor junction these excitons have high probability to be dissociated in to charge carriers if the material has short diffusion lengths [5]. In planar bilayer organic photovoltaic cells (OPVs) excitons diffusion is the main efficiency blockage. The bulk hetero junction has mixed donor and acceptor solution therefore donor/ acceptor junction active layers give an efficient exciton dissociation to get rid of diffusion length blockage [6]. Therefore the short diffusion length restricts the morphologies that can be used to construct efficient solar cell. The phenomena is shown in figure 2.3.

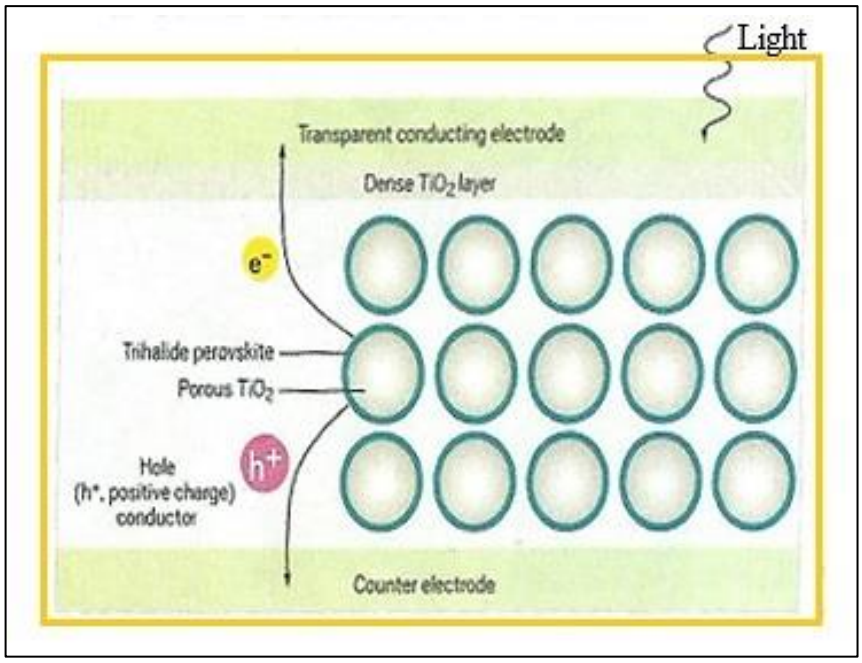

Figure 2.3 Electron Hole pair generation [4]

2.2.3 Charge Separation

When solar cell absorbs photons it generates excitons then these excitons required separation in to charge carriers for the generation of electrical current. Same time without an external field this is not an efficient process to separate exciton in bulk organic material [8]. Charge transfer state is the state at which both electron and hole are in front of each other and there is a chance of recombination which leads the excitons to ground state. If the same process is happen the loss in efficiency occur. Recombination is the key reasons for decrease in efficiency of Photovoltaic devices.

2.2.4 Charge Extraction

After charge separation in the sensitizer the next step is electron injection to the electron transport layer from the conduction band of absorber layer material. The photo-generated charge is quickly injected into two different transporting layers: one for ETL, normally a wide band gap semiconductor like TiO_2, and the second one for HTL [9]. Hole injection is occurred when hole crated by electron injection is transfer to HOMO level of HTL. The process is demonstrated in the energy level diagram of PSCs shown in figure 2.4 [10]. In which electron moves from conduction band of $MAPbI_3$ to ETL i.e. TiO_2 [10] [11].

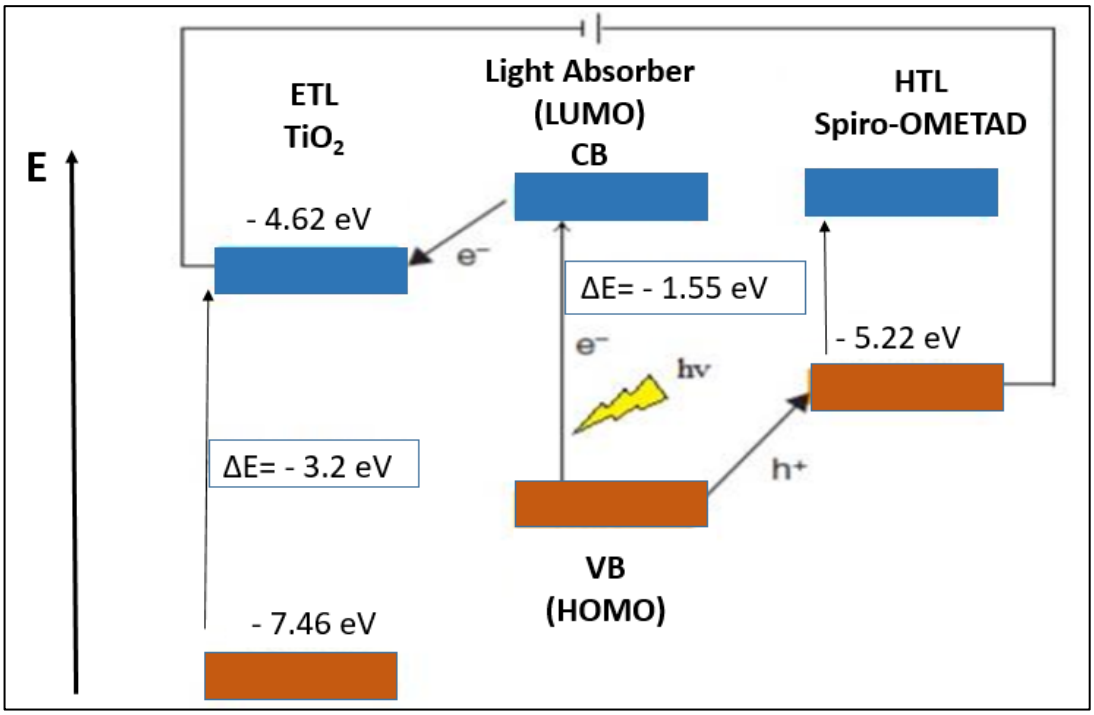

Figure 2.4 Energy level diagram of perovskite solar cells, image modified from [10]

2.3 Electron Transport Layer:

ETL is responsible for extracting the electrons from absorber layer. The n-type semiconductors having high carrier mobility are recommended. The transparency of the film matters, it must be transmitting in visible region which means the materials must have a relatively wide band gap. The band structure should match the perovskite materials.

An efficient electron transport material should have suitable energy level alignment with the perovskite active layer, high electron mobility for electron extraction and stable structures for long-term stability [12] [13] [14] 15].

2.3.1 Different ETL materials used in Perovskite solar cells

Variety of metal oxides such as TiO_2, SnO_2, ZnO, SiO_2, ZrO_2, can either be used as ETL or scaffold material [16]. The traditional electron transport materials in perovskite solar cells, such as TiO_2, are not very efficient for electron extraction at the interface causing current-voltage hysteresis, and they also suffer from the degradation under UV illumination [12]. ZnO and other n-type semiconductor materials are also often used as composites, as ETLs and are employed in flexible perovskite solar cells. The electron transport materials in perovskite solar cells that have been studied so far

are mainly divided into metal oxide, organic ETLs, multilayer electron transport layer involving Doped ETLs and ETLs using composite materials and nanostructured ETLs.

2.3.2 Metal oxide ETLs

Metal oxides such as TiO_2, ZnO, SnO_2, SiO_2, ZrO_2, can be used as ETLs. TiO_2 has been used extensively as an Electron transport material because of a wide band gap. For the reasons that rutile phase of TiO_2 increases the charge extraction and prevents recombination another metal oxide layer of materials Such as SnO_2 are fabricated in addition to the compact TiO_2 layer [18].

Incorporation of Acteylacetonate-based additives into TiO_2 to improve the ETL in perovskite solar cells, with enhanced device performances, particularly pertaining to short circuit current (Jsc) and Fill factor (FF)[19]. Some research have also been undertaken to investigate the route of fabricating ETLs, like sputtering and anodization processed TiO_2 in comparison with solution processed spin-coated TiO_2 [20]. To increase air stability, research demonstrating effective substation of organic transport layers with p-type NiO_x and n-type ZnO with superior cell PCE have been done [21].

Sputtered Si_3N_4 and SiO_2 electron barrier layer between a redox electrolyte and the WO_3 film in electro-chromic devices [22]. To demonstrate novel inverted light emitting devices based on n-typed tungsten trioxide nanostructures, it was reported that prepared WO_3 nanostructures show high transmittance in the wavelength of 400-700 nm and band-gaps of 3.5-3.75 eV [23]. To demonstrate the differences between two electron transporting materials used as n-type selective, it was reported that WO_3 offers advantage of being printable and does not require high annealing temperature, allowing cheap, expendable and efficient solar cells [24]. To demonstrate the impact of using Zinc oxide as ETL on performance and shelf life of OBHD (Organic Bulk Hetero-junction Devices), it was reported that incorporation of zinc oxide as ETL improves device shelf life dramatically for un-encapsulated devices under ambient conditions [25]. To highlight the impact of introducing low temperature (<150°C) processed sol-gel ZnO thin film on PSCs [26]. To demonstrate the impact of incorporating Ionic layer (IL) between ZnO ETL and perovskite layer upon stability of the PSCs using two step-sequential spin-coating deposition method [27]. It is found that ZnO bears good electron transfer ability and a low recombination rate at interface, works well for high performance PSC [28]. Zirconium dioxide can also be

incorporated in PSCs as an electron transmission layer. To propose organic/inorganic quantum dots hybrid LEDs with Cd-free InP QDs as light emitting layer and inorganic ZrO_2 nanoparticles as ETL [29]. To narrate physical, chemical and electrical characteristics of intercalated nano-layers of Y_2O_3 and ZrO_2, research has been done [30]. The typical TiO_2 in some research case was replaced by In_2O_3, which is not only transparent and conductive, but also has little photo-catalytic effect and it has higher electron mobility than TiO_2 [31]. Another work reported tin oxide nanoparticles based ETL manufactured via wet chemical techniques delivered a power conversion efficiency (PCE) of 19.17% [32]. Atomic layer deposition of Tin oxide annealed up to 180 °C, the structural results proved SnO_2 to be more effective an ETL with comparison to TiO_2 [33] [35]. Multiple research works have concluded that SnO_2 based PSCs have conversion efficiencies higher than TiO_2, and also have an improved device stability [36]. Considering SnO_2 ETL with a deep conduction band and high electron mobility, it was used by Q. Jiang et al. to enhanced electron extraction caused by the reduction of the energy barrier at the perovskite/ETL interface [37].

2.3.3 Organic ETLs

Many groups have reported organic ETL such as PEHT, PCBM, PEHT:PCBM composites to achieve high efficiency in inverted PSC. To highlight the significance of double ETL layer PCBM/ZnO (NPs) in perovskite solar cells work was reported [38]. To conclude and highlight role of interfacial layers (IFLs) between organic semiconductors and electrical contacts to enhance charge injection, extraction research was also done [39]. Study have been conducted to highlight the impact of additional mp-TiO_2 along with main TiO_2 as ETL layer for organic- inorganic perovskite solar Cells [40]. To investigate the impact of PDI copolymers as ETL materials and study its effect on energy alignment, electron mobility and film morphology [41]. An innovative method to fabricate low- temperature- processed, hysteresis- free, and stable PSCs with a large area up to 1 cm^2 is demonstrated using a versatile organic nano-composite that combines an electron acceptor and a surface modifier, this nano-composite forms an ideal, self- organized electron transport layer (ETL) via a spontaneous vertical phase separation, which leads to hysteresis- free, planar hetero-junction PSCs with stabilized PCEs of over 18% [42] [43]. A recent research demonstrated an inverted PSCs, metal-oxide free, using sulfur small compounds as an ETL with a PCE approximately 18.2% [44]. Fluorinated PDI films were used as novel

organic electron transport material in perovskite solar cells, the morphology control is critical to achieve high efficiency perovskite solar cells and the morphology of ETL layer could be controlled by convenient solvent treatments [45]. In few studies to overcome the stability issues of the PSCs, it was demonstrated that by adding carbon 60 and PFN to the PCBM ETL improved the conversion efficiency as well as the buffering of the interfacial contacts was improved [46].

2.3.4 Multilayer ETLs

To investigate impact of introducing TiO_2/ZnO electron transport bilayer on electron extraction and interface recombination planar PSCs, it was reported that TiO_2/ZnO bilayer combines advantages of high electron extraction and low interfacial recombination and this bilayer together with the perovskite absorber forms a type-II band structure, benefiting for electron transport and avoiding charge accumulation [48]. To prepare ultrathin and high quality WO_3 compact layers and compare performance of WO_3 and TiO_2 based devices, It is reported that optimum thickness of WO_3 and TiO_2 compact layers is 15nm and 60 nm, respectively ii)The Planar PSCs with WO_3 compact layer exhibited average 9.69% and 10.14% maximum PCE, TiO_2 compact layer with 60nm exhibited 11.79% and 12.64% maximum PCE [49]. Research titling ZrO_2/TiO_2 Electron Collection Layer for Efficient Meso-Superstructured Hybrid Perovskite Solar Cells for finding that mesoporous alumina-based cell applying c-TiO_2 as ETL is reported with high stabilized PCE value around 17% and the champion device exhibited with maximum current efficiency around 18%, V_{oc}=1V and FF=80% [50] It is found that hybrid IL improves electron injection and transport and suppresses triple exciton quenching at the EML/ZnO interface, resulting in lower driving voltage and doubled luminous efficiency compared with those of the control device without IL [51].Ternary oxides in the TiO_2–ZnO system to find new materials for the ETL were explored [52]. Further to increase the efficiency of the cell, optimization of TiO_2/ZnO bilayer Transport layer has also been done [53]. For better charge extraction a study reported a novel titanium oxide (TiO_2) bilayer with different Fermi energy levels by combing atomic layer deposition and spin-coating technique and the Energy band alignments of TiO_2 bilayer can be modulated by controlling the deposition order of layers [54]. A group of researchers demonstrated that a few tens of nanometers thick bilayer, made of two types of inorganic oxide nanoparticles (SnO_2/TiO_2), can perform as a robust and low-temperature-processed

electron-selective contact for planar perovskite solar cells [55]. The bilayer TiO_2-SnO_2 film exhibits efficient electron extraction and hole blocking ability even at a low processing temperature of 150 °C [56]. The SnO_2-TiO_2 composite films based solar cells acquire a high power conversion efficiency (PCE) of 14.8%, which is higher than PCEs of devices based on individual SnO_2 layer and sintered TiO2 layer [57].

2.3.5 Doped ETLs

Doping is essentially done for improving the properties of the Electron Transport Materials. Doping can improve the effectiveness of the hybrid organic–inorganic perovskite (HOIP) layer and the ETL [58]. Ru-doped TiO_2 ETL offers a power conversion efficiency (PCE) of over 15.7% [59]. Zn-doped TiO_2 ETL can be grown on FTO substrate below 100 °C also Zn dopant raises the Fermi level of TiO_2 by 0.1 eV [60]. La doped SnO_2 was ETL for planar PSCs with PCE of 17.08% and La doping is a feasible strategy for improving the PCE [61]. The Al-dopant in SnO_2 enhances the charge transport and electron extraction behavior of the PSCs and then the JSC of the devices is improved also the champion cell based on Al-SnO_2 exhibited a higher efficiency of 12.10% than that using SnO2 (9.02%) as ETLs [62]. To develop an electron transfer layer composed of PCBM doped with graphdiyne with superior electron transferring performance, research was conducted [63]. Various studies has been done to investigate the impact of Nb doping mesoporous TiO_2 on electronic structure and photovoltaic properties of PSCs [64]. Impedance spectroscopy study showed that prohibited hole-electron recombination at the interface between the perovskite layer and Ag cathode, resulting in enhanced electron collection efficiency under efficiency enhancement of Inverted assembled PSCs with a PCBM as an ETL [39]. To investigate the impact of PDI copolymers as ETL materials and study its effect on energy alignment, electron mobility and film morphology [65]. Shin *et al.* report a low-temperature colloidal method for depositing La-doped $BaSnO_3$ films as a replacement for TiO_2 to reduce such ultraviolet-induced damage [66]. Mamblona et al. presented a PSCs, with an absorber layer in the middle of an intrinsic and doped organic transporting layers [67]. Yang bi. et al. demonstrated tin oxide nano-crystals with antimony doping (Sb) through temperature less than 100°C solution processing techniques [68].

2.3.6 Nanostructured ETLs

Reduced graphene oxide (rGO) is incorporated into SnO_2 nanoparticles to form composite ETL. For planar PSC on AZO substrates, SnO_2-rGO with a low incorporation ratio of 3 wt% rGO significantly enhances the device short circuit current density (J_{sc}) and the fill factor when compared to the device with pristine SnO_2 ETL, leading to an overall power conversion efficiency of 16.8% with negligible hysteresis [69]. To highlight the role of incorporating low temperature solution processed WO_X Nano particular layer in combination with a mixed fullerene functionalized self-assembled monolayers, research was conducted [70]. To demonstrate comparative analysis, PCE versus Stability of PSCs with two renowned architecture planar and scaffold (rutile nanorods, NRs) vs. Planar [71]. To mitigate effects of morphological defects by fabricating TiO_2 through sputtering and anodization rather than conventional spin-coating [72] [73]. Tin oxide has emerged as a potential candidate for ETL, different techniques are adapted for the processing of SnO_2 as an ETL, some researcher has reported that the SnO_2 produced through e-beam technology have more uniform structure and low production cost [74]. Where some of them had hydrothermally grown SnO_2 Electron Transport Layers for enhancing the stability [75]. A highly crystalline SnO_2 has been fabricated through a low-temperature (below 100 ^{O}C) electro-deposition technique, the SnO_2 film thus fabricated served as electron-transporting layer facilitating the fabrication of *n-i-p* planar perovskite solar cell [76]. A solvothermal route was adapted to stabilize gelled dispersions of tin oxide nanoparticles with diameters in the range of 2–4 nm by Bob et al. [77] [78]. A high power conversion efficiencies have been reported by using SnO_2 as an ETL, it is fabricated through different methodologies and recently a very interesting technique low temperature solution based was adopted, named Ultrasonic- synthesis of very fine tin oxide nano-crystal using tin tetrachloride pentahydrate as a precursor salt [79]. J. Zhu et al. has presented an investigation into mesoporous perovskite solar cells incorporating mesoporous SnO_2 nanoparticle films as electron-transporting materials and scaffold layers, to replace traditional mesoporous TiO_2 films [80].

2.4 Absorber Layer:

Many studies have been published on the substances with the formula AMX3, such as BaTiO3, NaNbO3 and CsPbCl3, CsMAPbI3. 10% Cs doped perovskite based inverted type planner heterojunction solar cell device i.e. CSxMA1-xPbI3 showed remarkable improvement of cell efficiency from 5.51% to 7.68% by increasing short-

circuit current density (Isc) and open circuit voltage (Voc) via increasing light absorption, improvement in film morphology and bandgap tuning [81][82][83][84]. Though methylammonium ($CH_3NH_3PbI_3$ or $MAPbI_3$) perovskite (Organic-Inorganic) as the light absorber material in perovskite solar cells (PSCs) by Kojima et al. in 2009 appeared to be promising with high power conversion efficiency (PCE) [85]. These efficiencies have been improving as much as 23% over the past few years. Unfortunately, organic-inorganic PSCs regardless of their high efficiencies and performances still suffer from certain degradations because of the weak level of the hydrogen-bonding between monovalent organic cation and octahedral PbI_2 [86] . Such a PSC break downs to PbI_2 under common external stresses, like: electric charge, moisture, photo-oxidation and UV irradiation. $CsPbI_3$ was used earlier as perovskite absorber layer but the phase responsible to absorb light was quite hard to control. $CsPbI_2Br$ is recently been under work due to rather ease in phase control with promising light absorption capabilities and high stabilities [87] [88].

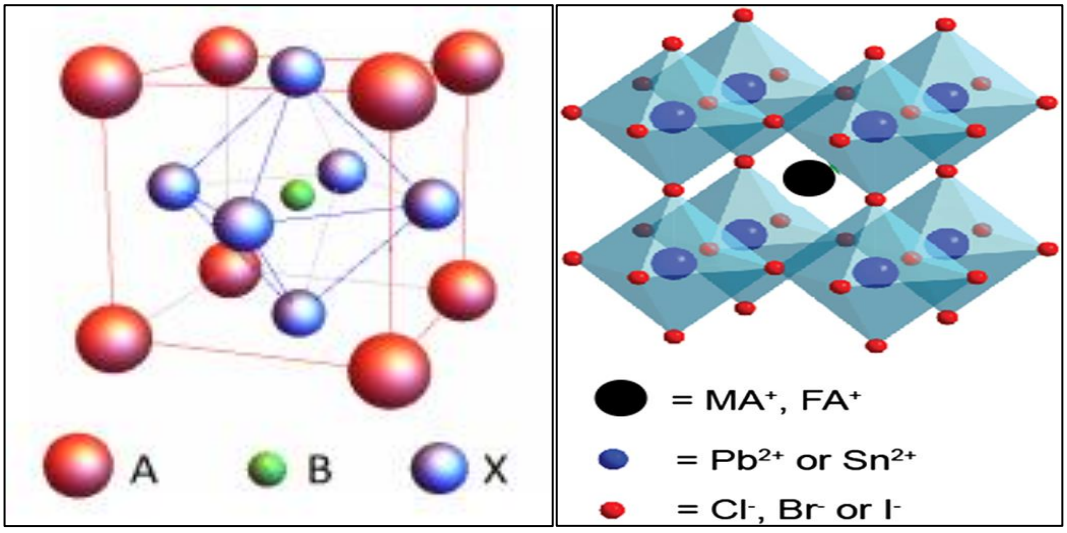

Figure 2.5 Generic perovskite ABX3 crystal unit cell structure. In most typical PSCs A is the organic cation CH_3NH_3 , B is the metallic cation Pb and X is the halide anion (I, Cl, Br or mixed) [89]

Another promising way to keep the organic-inorganic PSCs intact is with a mixture containing DMSO (Dimethyl sulfoxide) & DMF (Dimethylformamide) in solution processing of MAI with PbI_2 [90]. DMF is a polar solvent and have extensively been used in solution processing of various organic-inorganic PSCs. But using DMSO in appropriate proportion alongside DMF can not only enhance the solubility of PbI_2 in DMF which typically is no more than 0.4 Molar, but also enhance the thickness and stability of absorber layer. Excess usage of DMSO though is not advisable as it may

result in recombination. In some cases Hydroiodic acid is added to the methyl ammonium Apart from DMSO, Caffeine is also reported to be used in the mix, which has shown good results in past few years [91].

2.5 Hole Transport Layer

HTL is essential to complete the flow of electric current. HTL must possess:

- Efficient electron blocking
- Efficient hole extraction

Uniform coverage and high mobilities of HTM should be ensured for efficient PSCs because the high mobility accounts for the Ohmic losses which then effects the fill factor of the cell.

2.5.1 Hole Transporting materials in PSCs:

HTMs employed in PSCs can be categorized as inorganic (NiO, CuSCN, CuI, CuxO, and Graphene oxide (GO)) or organic materials. Different types of materials have been studied and used as HTLs thus far, including inorganic, polymeric, and small organic molecules. Spiro-OMeTAD [2,20,7,70-tetrakis(N,N-di-p-methoxyphenyl-amine)9,90-spirobifluorene] has extensively been used as a HTM over the last six years and has shown great efficiencies [92]. Further classified into three groups (i) small molecules such as Spiro-OMeTAD (ii) polymers such as P3HT, PEDOT: PSS and PTAA or (iii) Oligomers. Other molecules like ZnO, CuI, Cu_2O, CuSCN, GO, MoO_3, VO_x, WO_x, PTAA and thiphene cores have been used as HTLs [93].

The perovskite material, $CH_3NH_3PbI_3$ undergo decomposition under thermal stress at a temperature between 100°C and 140°C [94]. The perovskite material under moisture or heat stress, decomposes which results into breakage of $MAPbI_3$ into its components. Its occurrence is as following:

$$\mathbf{CH_3NH_3PbI_3 \longrightarrow PbI_2 + CH_3NH_2 + HI} \qquad \mathbf{2.1}$$

To overcome the degradation of perovskite material due to moisture, the HTL should be composed of hydrophobic material. Various hydrophobic materials can be utilized as HTL bearing the basic hole transport properties along with their hydrophobic capabilities. CuO, NiO [95] and various Metal Phthalocyanines have shown fair results when incorporated in PSCs.

2.5.2 Lead Phthalocyanines PbPc

Metal phthalocyanines are aromatic molecules comprised of a macrocyclic ring with a large π-conjugated system which stack through π–π supramolecular interactions [96], [97], [98] . In general, they possess highly symmetrical square planar D_{4h} structures with high thermal and chemical stabilities [99]. Their lower costs, exceptional stability, flexibility, decent electrical reaction and comfortable manufacture have presented them as diverse ingredients. These prevailing materials deem potent in the fields of molecular electronics and optoelectronics [100], [101].

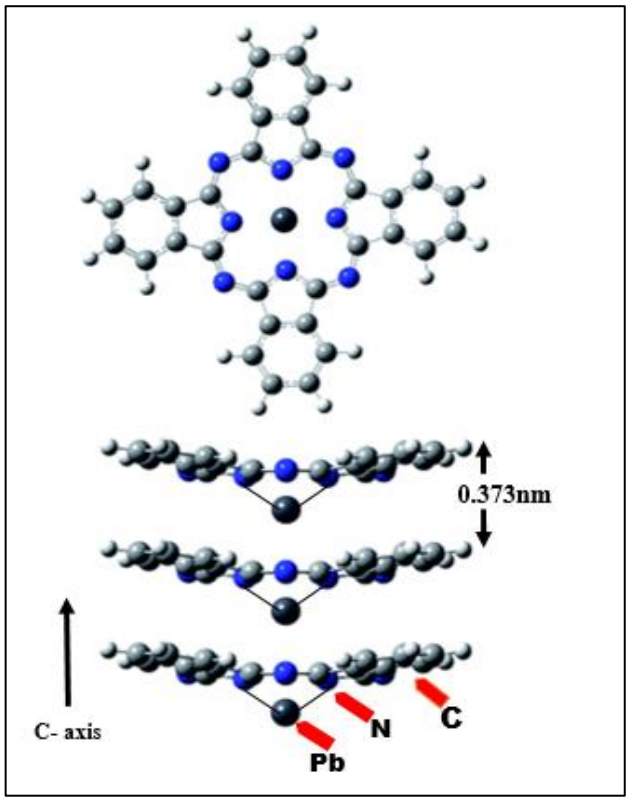

Figure 2.6 Structure of PbPc, modified from [99]

Among many Metal phthalocyanines' compounds, lead (II) phthalocyanine (PbPc) has an unusual structure with C_{4v} symmetry like a shuttlecock [102]. Studies certify that there are two polymorphs of PbPc crystals, the monoclinic (α-phase) and the triclinic (β-phase) [97] [103]. Both these crystalline polymorphs have shown varied responses to air, nitrogen oxide and water vapors [97]. PbPc has been also used as non-linear optical materials, organic solar cells and a lot more.

Summary:

In the past few years methyl ammonium lead halide – based hybrid perovskite solar cells (PSCs) have been studied intensively not only because of their low processing costs but also their high efficiency. The PSCs belongs to the third generation of solar cell technology. In this chapter firstly the structure of the PSCs was discussed followed by the working mechanism of PSCs. After that the three major layers ETL, Absorber (perovskite) layer and HTL are discussed with their major characteristics and materials. ETL materials were classified under the groups metal oxide, organic, multilayers, doped and nanostructured ETLs. The perovskite materials can be used not only as a light-absorbing layer, but also as an electron/hole transport layer due to the advantages of its high extinction coefficient, high charge mobility, long carrier lifetime, and long carrier diffusion distance. Followed by the HTL materials and explaining the required hydrophobicity of the layer leading to the selection of the PbPc HTL.

References

[1] S. F. Shaikh, H. Kwon, W. Yang, R. S. Mane, and J. Moon, "Performance enhancement of mesoporous TiO 2 -based perovskite solar cells by ZnS ultrathin-interfacial modi fi cation layer," *J. Alloys Compd,* 738,(2018) 405–414

[2] D. Wang, M. Wright, N. K. Elumalai, and A. Uddin, "Solar Energy Materials & Solar Cells Stability of perovskite solar cells," *Sol. Energy Mater. Sol. Cells*, 147,(2016)255–275

[3] RF Wireless, "Advantages of Perovskite solar cell | disadvantages of Perovskite solar cell." https://www.rfwireless-world.com/Terminology/Advantages-and-Disadvantages-of-Perovskite-solar-cell.html/

[4] P. Peumans and S. R. Forrest, "Separation of geminate charge-pairs at donor–acceptor interfaces in disordered solids," *Chem. Phys. Lett.*, 398, 1–3,(2004) 27–31

[5] J.-S. Yeo *et al.*, "Highly efficient and stable planar perovskite solar cells with reduced graphene oxide nanosheets as electrode interlayer," *Nano Energy*,12 (2015) 96–104

[7] P. Qin *et al.*, “Inorganic hole conductor-based lead halide perovskite solar cells with 12.4% conversion efficiency,” *Nat. Commun.*, 5, 1, (2014) 3834

[8] P. Peumans, A. Yakimov, and S. R. Forrest, “Small molecular weight organic thin-film photodetectors and solar cells,” *J. Appl. Phys.*, 93, 7, (2003)3693–3723,

[9] V. Gonzalez-Pedro *et al.*, “General Working Principles of $CH_3NH_3PbX_3$ Perovskite Solar Cells,” *Nano Lett.*, 14, 2, (2014) 888–893

[10] I. Chung, B. Lee, J. He, R. P. H. Chang, and M. G. Kanatzidis, “All-solid-state dye-sensitized solar cells with high efficiency,” *Nature*, 7399, (2012) 486–489,

[11] N. Marinova, S. Valero, and J. L. Delgado, “Organic and perovskite solar cells: Working principles, materials and interfaces,” *J. Colloid Interface Sci.*, 488,(2017) 373–389

[12] S. Zheng, G. Wang, T. Liu, L. Lou, S. Xiao, and S. Yang, “Materials and structures for the electron transport layer of efficient and stable perovskite solar cells,” . *Sci. China Chem.*, 62, 7,(2019) 800–809

[13] M. F. Mohamad Noh *et al.*, “The architecture of the electron transport layer for a perovskite solar cell,” *J. Mater. Chem. C*, 6, 4, (2018) 682–712

[14] F. Huang *et al.*, “Perovskite Solar Cells: Effect of the Microstructure of the Functional Layers on the Efficiency of Perovskite Solar Cells (Adv. Mater. 20/2017),” *Adv. Mater.*, , 29, (2017) 20

[15] G. Yang, H. Tao, P. Qin, W. Ke, and G. Fang, “Recent progress in electron transport layers for efficient perovskite solar cells,” *J. Mater. Chem. A*, 4, 11, (2016) 3970–3990

[16] K. Mahmood, S. Sarwar, and M. T. Mehran, “Current status of electron transport layers in perovskite solar cells: materials and properties,” *RSC Adv.*, 7, 28, (2017) 17044–17062

[17] Y. Wang, J. Wan, J. Ding, J.-S. Hu, and D. Wang, “A Rutile TiO_2 Electron Transport Layer for the Enhancement of Charge Collection for Efficient Perovskite Solar Cells,” , *Angew. Chemie Int. Ed.*, 58, 28, (2017) 9414–9418

[18] M. M. Tavakoli, P. Yadav, R. Tavakoli, and J. Kong, “Surface Engineering of TiO 2 ETL for Highly Efficient and Hysteresis-Less Planar Perovskite Solar Cell (21.4%) with Enhanced Open-Circuit Voltage and Stability,” *Adv. Energy Mater.*, 8, 23, (2018) 1800794

[20] J. Choi, S. Song, M. T. Hörantner, H. J. Snaith, and T. Park, “Well-Defined Nanostructured, Single-Crystalline TiO 2 Electron Transport Layer for Efficient Planar Perovskite Solar Cells,” *ACS Nano*, 10, 6,(2016) 6029–6036,

[21] J. You *et al.*, “solution-processed metal oxide transport layers,” , 56, (2015) 1–8

[22] S. Bogati and W. Graf, “Solar Energy Materials & Solar Cells Sputtered Si 3 N 4 and SiO 2 electron barrier layer between a redox electrolyte and the WO 3 fi lm in electrochromic devices,” *Sol. Energy Mater. Sol. Cells*, 159, (2017) 395–404

[23] C. Chang, S. Wang, S. Yang, and A. Puaud, “Superlattices and Microstructures Hybrid light-emitting devices by incorporating WO 3 nanorod arrays as the electron transport layer and PEIE as the buffer layer,”*Superlattices Microstruct.*, 113, (2018) 667–677.

[24] A. Gheno *et al.*, “Solar Energy Materials & Solar Cells Printable WO 3 electron transporting layer for perovskite solar cells : In fl uence on device performance and stability,” *Sol. Energy Mater. Sol. Cells*, 116, (2016) 347–354

[25] S. R. Ferreira, P. Lu, Y. Lee, R. J. Davis, and J. W. P. Hsu, “Effect of Zinc Oxide Electron Transport Layers on Performance and Shelf Life of Organic Bulk Heterojunction Devices,”132 (2011) 13471–13475

[26] A. Mahmud *et al.*, “Solar Energy Materials & Solar Cells Low temperature processed ZnO thin fi lm as electron transport layer for ef fi cient perovskite solar cells,” 159, (2017) 251–264

[27] W. Zhang, Z. Ren, Y. Guo, X. He, and X. Li, “AC SC,” *Electrochim. Acta*, 182. 64278 (2018) 153-164

[28] L. Chen, Z. Tseng, L. Chen, and Z. Tseng, “ZnO-Based Electron Electron Transporting Transporting Layer Layer for for Perovskite Perovskite Solar

Cells Solar Cells.” 76., 254 (2018) 387-399

[29] H. Y. Kim *et al.*, “Transparent InP Quantum Dot Light-Emitting Diodes with ZrO 2 Electron Transport Layer and Indium Zinc Oxide Top Electrode,” 354 (2018) 3454–3461,

[30] J. Molina *et al.*, “Physical and electrical characterization of yttrium-stabilized zirconia (YSZ) thin films deposited by sputtering and atomic-layer deposition,” *J. Mater. 2018 Sci. Mater. Electron.*, 29,18, (2018)15349–15357

[31] Q. Dong *et al.*, “In_2O_3 based perovskite solar cells,”9749, 97491, (2018) 5687-5693

[32] K.-H. Jung, J.-Y. Seo, S. Lee, H. Shin, and N.-G. Park, “Solution-processed SnO_2 thin film for a hysteresis-free planar perovskite solar cell with a power conversion efficiency of 19.2%,” *J. Mater. Chem. A*,. 5. 47, (2016) 24790–24803

[33] S. Jeong, S. Seo, H. Park, and H. Shin, “Atomic layer deposition of a SnO_2 electron-transporting layer for planar perovskite solar cells with a power conversion efficiency of 18.3%,” *Chem. Commun.*, 55, 17, (2019) 2433–2436,

[34] Q. Jiang, X. Zhang, and J. You, “SnO 2 : A Wonderful Electron Transport Layer for Perovskite Solar Cells,”, 1801154, 32 (2018)1–14

[35] N. Hamdadou, “IMPROVED PROPERTIES OF SnO 2 THIN FILMS OBTAINED VIA SPIN COATING METHOD BY VARYING THE SOLUTION CONCENTRATION,” J. Mater. Chem. 25, 7, (2018) 1–9

[36] L. Xiong, Y. Guo, J. Wen, H. Liu, G. Yang, and P. Qin, “Review on the Application of SnO 2 in Perovskite Solar Cells,” J. Mater. Nano 1802757, (2018)1–18

[37] Q. Jiang *et al.*, “Enhanced electron extraction using SnO2 for high-efficiency planar-structure HC(NH2)2PbI3-based perovskite solar cells,” J. Sustain Energy Rev. 253, 76. (2016) 542-560

[38] W. Qiu *et al.*, “High efficiency perovskite solar cells using a PCBM / ZnO double electron transport layer and a short air-aging step,” *Org. Electron.*, 26, 14 (2016)30–35

[39] F. Xia, Q. Wu, P. Zhou, Y. Li, and X. Chen, “Efficiency Enhancement of Inverted Structure Perovskite Solar Cells via Oleamide Doping of PCBM Electron Transport Layer,” 47, 23. (2018) 176-182

[41] Q. Guo *et al.*, “E ff ect of Energy Alignment , Electron Mobility , and Film Morphology of Perylene Diimide Based Polymers as Electron Transport Layer on the Performance of Perovskite Solar Cells,” *Adv. Energy Mater.*, 7, 15 (2017) 1700226,

[42] J. Lee *et al.*, “A Printable Organic Electron Transport Layer for Low-Temperature-Processed, Hysteresis-Free, and Stable Planar Perovskite Solar Cells,”.*Adv. Energy Mater.*, 7, 15, (2017) 1700276

[43] Z. Zhu *et al.*, “A Low-Temperature, Solution-Processable Organic Electron-Transporting Layer Based on Planar Coronene for High-performance Conventional Perovskite Solar Cells,” ,. *Adv. Mater.*, 28, 48, (2016) 10786–10793

[44] P.-Y. Gu *et al.*, “Pushing up the efficiency of planar perovskite solar cells to 18.2% with organic small molecules as the electron transport layer,” ,.*J. Mater. Chem. A*, 5, 16, (2017) 7339–7344

[45] J. Huang, Z. Gu, L. Zuo, T. Ye, and H. Chen, “Morphology control of planar heterojunction perovskite solar cells with fluorinated PDI films as organic electron transport layer,” ,.*Sol. Energy*, 133, (2017) 331–338

[46] J. Xie *et al.*, “A ternary organic electron transport layer for efficient and photostable perovskite solar cells under full spectrum illumination,” ,.*J. Mater. Chem. A*, 6, 14, (2018)5566–5573

[47] H. Dong *et al.*, “Improving electron extraction ability and device stability of perovskite solar cells using a compatible PCBM/AZO electron transporting bilayer,” , J. *Nanomaterials,* 8, 9, (2018) 654-663

[48] X. Xu *et al.*, “Highly efficient planar perovskite solar cells with a TiO_2/ZnO electron transport bilayer,” ,. *J. Mater. Chem. A,* 3, 38, (2017)19288–19293

[49] J. Zhang, C. Shi, J. Chen, Y. Wang, and M. Li, “Journal of Solid State Chemistry Preparation of ultra-thin and high-quality WO 3 compact layers and

comparision of WO 3 and TiO 2 compact layer thickness in planar perovskite solar cells," , *J. Solid State Chem.*, 238, (2016) 223–228

[50] M. Alejandro, S. Pathak, J. Liu, H. J. Snaith, and F. Jaramillo, "ZrO 2 / TiO 2 Electron Collection Layer for E ffi cient Meso- Superstructured Hybrid Perovskite Solar Cells," *J. Mater. Chem. A*, 338, (2016) 19288–19293

[52] X. Yin, Z. Xu, Y. Guo, P. Xu, and M. He, "Ternary Oxides in the TiO_2 –ZnO System as Efficient Electron-Transport Layers for Perovskite Solar Cells with Efficiency over 15%," *ACS Appl. Mater. Interfaces*, 8, 43, (2016) 29580–29587

[53] N. Kumari, J. V. Gohel, and S. R. Patel, "Optimization of TiO2/ZnO bilayer electron transport layer to enhance efficiency of perovskite solar cell,", *Mater. Sci. Semicond. Process.*, 75, (2018) 149–156

[54] H. Lu, W. Tian, B. Gu, Y. Zhu, and L. Li, "TiO_2 Electron Transport Bilayer for Highly Efficient Planar Perovskite Solar Cell," *Small,*. 13, 38, (2018) 1701535,

[55] G. Martínez-Denegri, S. Colodrero, M. Kramarenko, and J. Martorell, "All-Nanoparticle SnO_2 /TiO_2 Electron-Transporting Layers Processed at Low Temperature for Efficient Thin-Film Perovskite Solar Cells," *ACS Appl. Energy Mater.*, 1788, 234. (2018) p. 2014

[56] H. Xie *et al.*, "Low temperature solution-derived TiO2-SnO2 bilayered electron transport layer for high performance perovskite solar cells," , *.Appl. Surf. Sci.,*. 464, (2019) 700–707

[57] X. Huang *et al.*, "Low-temperature processed SnO2 compact layer by incorporating TiO2 layer toward efficient planar heterojunction perovskite solar cells," , *Sol. Energy Mater. Sol. Cells*, 164, (2017) 87–92

[58] Y. Zhou, Z. Zhou, M. Chen, Y. Zong, and J. Huang, "Doping and alloying for improved perovskite solar cells," , *J. Mater. Chem. A Mater. energy Sustain.*, 4, (2016) 17623–17635

[59] Z. Xu, X. Yin, Y. Guo, Y. Pu, and M. He, "Ru-Doping in TiO_2 electron transport layers of planar heterojunction perovskite solar cells for enhanced performance," , *J. Mater. Chem. C*, 6, 17, (2018) 4746–4752

[60] X. Liu, Z. Wu, Y. Zhang, and C. Tsamis, "Low temperature Zn-doped TiO2 as

electron transport layer for 19% efficient planar perovskite solar cells," , *Appl. Surf. Sci.*, 471, (2019) 28–35

[61] Z. Xu *et al.*, "La-doped SnO2 as ETL for efficient planar-structure hybrid perovskite solar cells," *Org. Electron.*, 73, (2019) 62–68

[62] H. Chen *et al.*, "Enhanced Performance of Planar Perovskite Solar Cells Using Low-Temperature Solution-Processed Al-Doped SnO 2 as Electron Transport Layers," , *Nanoscale Res. Lett.*, 12, 1, (2017) 2–7

[63] C. Kuang *et al.*, "Highly E ffi cient Electron Transport Obtained by Doping PCBM with Graphdiyne in Planar-Heterojunction Perovskite Solar Cells," 2015, vol. 6, no. 17, pp. 4746–4752

[65] F. Giordano *et al.*, "Enhanced electronic properties in mesoporous TiO2 via lithium doping for high-efficiency perovskite solar cells," 2016 *Nat. Commun.*, vol. 7, pp. 1–6,

[66] S. S. Shin *et al.*, "Colloidally prepared La-doped BaSnO3 electrodes for efficient, photostable perovskite solar cells.," *Science*, 356, 6334, (2017) 167–171,

[67] C. Momblona *et al.*, "Efficient vacuum deposited p-i-n and n-i-p perovskite solar cells employing doped charge transport layers," *Energy Environ. Sci.*, 9, 11, (2017) 3456–3463

[68] Y. Bai *et al.*, "Low Temperature Solution-Processed Sb:SnO_2 Nanocrystals for Efficient Planar Perovskite Solar Cells," *ChemSusChem*, 9, 18, (2017) 2686–2691,

[69] R. Liu *et al.*, "SnO_2 -rGO nanocomposite as an efficient electron transport layer for stable perovskite solar cells on AZO substrate,". *Nanotechnology*, 30, 7, (2019) 075202,

[70] Y. Hou *et al.*, "Low-Temperature and Hysteresis-Free Electron- Transporting Layers for Effi cient , Regular , and Planar Structure Perovskite Solar Cells," *J. Mater. Chem. C*, 6, 17, (2015) 4754–4767

[71] A. Fakharuddin, F. Di, I. Ahmed, Q. Wali, T. M. Brown, and R. Jose, "Role of morphology and crystallinity of nanorod and planar electron transport layers on

the performance and long term durability of perovskite solar cells," *J. Power Sources*, 283, (2015) 61–67

[72] W. Nanostructured, J. Choi, S. Song, M. T. Ho, H. J. Snaith, and T. Park, "Well-De fi ned Nanostructured, Single- Crystalline TiO 2 Electron Transport Layer for E ffi cient Planar Perovskite Solar Cells," *J. Mater. Chem. C*, 6, 17, (2016)7446–7452

[73] D. Ouyang, Z. Huang, and W. C. H. Choy, "Solution-Processed Metal Oxide Nanocrystals as Carrier Transport Layers in Organic and Perovskite Solar Cells," *Adv. Funct. Mater.*, 29, 1, (2019) 1804660,

[74] J. Ma *et al.*, "Highly Efficient and Stable Planar Perovskite Solar Cells With Large-Scale Manufacture of E-Beam Evaporated SnO_2 Toward Commercialization," , *Sol. RRL*, 1, 10, (2017) 1700118,

[75] Q. Liu *et al.*, "Enhanced Stability of Perovskite Solar Cells with Low-Temperature Hydrothermally Grown SnO_2 Electron Transport Layers," *Adv. Funct. Mater.*, 26, 33 (2017) 6069–6075,

[76] J.-Y. Chen, C.-C. Chueh, Z. Zhu, W.-C. Chen, and A. K.-Y. Jen, "Low-temperature electrodeposited crystalline SnO2 as an efficient electron-transporting layer for conventional perovskite solar cells," , M *Sol. Energy Mater. Sol. Cells*, v64, (2017) 47–55

[77] B. Bob, T.-B. Song, C.-C. Chen, Z. Xu, and Y. Yang, "Nanoscale Dispersions of Gelled SnO_2 : Material Properties and Device Applications,", *Chem. Mater.*, 25, 23, (2013)4725–4730,

[78] L. Xiong *et al.*, "Fully High-Temperature-Processed SnO_2 as Blocking Layer and Scaffold for Efficient, Stable, and Hysteresis-Free Mesoporous Perovskite Solar Cells," , *Adv. Funct. Mater.*, 28,(2018) 1706276

[79] H. Shan, E. Rezaee, X. Leng, X. Wang, Q. Chen, and Z.-X. Xu, "Ultrasonic-Assisted Wet Chemistry Synthesis of Ultrafine SnO_2 Nanoparticles for the Electron-Transport Layer in Perovskite Solar Cells," *ChemSusChem*, vol. 11, (2018) 3000–3006,

[81] F. Prokert, "Neutron Scattering Studies on Phase Transitions and Phonon

Dispersion in CsSrCl3," *Phys. status solidi*, 104 (1981) 261–265,

[82] J. Rubin, E. Palacios, J. Bartolome, and J. Rodriguez-Carvajal, "A single-crystal neutron diffraction study of NH_4MnF_3," ,*J. Phys. Condens. Matter*, 7,3, (1998) 563–575

[83] H. Choi *et al.*, "Cesium-doped methylammonium lead iodide perovskite light absorber for hybrid solar cells," , *Nano Energy*, 7, (2014) 80–85

[84] R. Prasanna *et al.*, "Band Gap Tuning via Lattice Contraction and Octahedral Tilting in Perovskite Materials for Photovoltaics," *J. Am. Chem. Soc.*, 139, 32, (2017)11117–11124,

[85] A. Kojima, K. Teshima, Y. Shirai, and T. Miyasaka, "Organometal Halide Perovskites as Visible-Light Sensitizers for Photovoltaic Cells," , *J. Am. Chem. Soc.*, 131, (2017) 6050–6051

[86] J. Chen and N.-G. Park, "Causes and Solutions of Recombination in Perovskite Solar Cells," , *Adv. Mater.*, (2018) 1803019

[87] K. Wang *et al.*, "All-inorganic cesium lead iodide perovskite solar cells with stabilized efficiency beyond 15%," *Nat. Commun.*, 9 (2018) 4544,

[88] S. Hong *et al.*, "A facile and low-cost fabrication of TiO2 compact layer for efficient perovskite solar cells," , *Curr. Appl. Phys.*, 15, (2015) 574–579

[89] U. Krishnan, M. Kaur, M. Kumar, and A. Kumar, "Factors affecting the stability of perovskite solar cells: a comprehensive review,".*J. Photonics Energy*, 9, 02, (2019) 1-5

[90] N. Ahn, D.-Y. Son, I.-H. Jang, S. M. Kang, M. Choi, and N.-G. Park, "Highly Reproducible Perovskite Solar Cells with Average Efficiency of 18.3% and Best Efficiency of 19.7% Fabricated via Lewis Base Adduct of Lead(II) Iodide,", *J. Am. Chem. Soc.*, 137, 27, (2015) 8696–8699

[91] R. Wang *et al.*, "Caffeine Improves the Performance and Thermal Stability of Perovskite Solar Cells," , *Joule*, 3, 6, (2019)1464–1477

[92] R. L. Vekariya, A. Dhar, P. K. Paul, and S. Roy, "An overview of engineered porous material for energy applications: a mini-review," , *Ionics (Kiel).*, 24, 1,

(2018)1–17

[93] S. Pitchaiya *et al.*, "A review on the classification of organic/inorganic/carbonaceous hole transporting materials for perovskite solar cell application," *Arab. J. Chem.*, 11, 17, (2018)3000–3006,

[94] A. Dualeh, N. Tétreault, T. Moehl, P. Gao, M. K. Nazeeruddin, and M. Grätzel, "Effect of Annealing Temperature on Film Morphology of Organic-Inorganic Hybrid Pervoskite Solid-State Solar Cells," , *Adv. Funct. Mater.*, 24, 21, (2014) 3250–3258

[95] L. J. Tang *et al.*, "A Solution-Processed Transparent NiO Hole-Extraction Layer for High-Performance Inverted Perovskite Solar Cells," , *Chem. - A Eur. J.*, 24, 12, (2018)2845–2849

[96] E. A. Lukyanets and V. N. Nemykin, "The key role of peripheral substituents in the chemistry of phthalocyanines and their analogs," *J. Porphyr. Phthalocyanines*, 14, 01, (2010). 1–40

[97] R. A. Collins and A. Belghachi, "Structural properties of lead phthalocyanine thin films," , *Mater. Lett.*, 8, 9 (1989) 349–352

[98] K. P. Madhuri, P. Kaur, M. E. Ali, and N. S. John, "Nanoscale Conductance in Lead Phthalocyanine Thin Films: Influence of Molecular Packing and Humidity," , *J. Phys. Chem. C*, 121, 17 (2017)9249–9259

[99] N. Hamamoto, H. Sonoda, M. Sumimoto, K. Hori, and H. Fujimoto, "Theoretical study on crystal polymorphism and electronic structure of lead(ii) phthalocyanine using model dimers," , *RSC Adv.*, 7, 14, (2018) 8646–8653

[100] G. Guillaud, J. Simon, and J. P. Germain, "Metallophthalocyanines: Gas sensors, resistors and field effect transistors," *Coord. Chem. Rev.*, 178–180, (1998) 1433–1484,

[101] C. G. Claessens, U. Hahn, and T. Torres, "Phthalocyanines: From outstanding electronic properties to emerging applications," , *Chem. Rec.*, 8, 2, (2008) 75–97

[102] K. Ukei, "Lead phthalocyanine," *Acta Crystallogr. Sect. B Struct. Crystallogr. Cryst. Chem.*, 29, 10, (21973) 2290–2292,

[103] Y. Iyechika, K. Yakushi, I. Ikemoto, H. Kuroda, and IUCr, “Structure of lead phthalocyanine (triclinic form),” , *Acta Crystallogr. Sect. B Struct. Crystallogr. Cryst. Chem.*, 38, 3, (1982) 766–770

Chapter # 3

Review on Experimentation, Characterization and Testing Methods

This chapter includes an overview of all of the experimentation, characterization and testing methods and techniques used or followed in this research work.

3.1 Nano Particles Synthesis & Fabrication Methods

Tin oxide nanoparticles were synthesized using co-precipitation technique. The films were further deposited through spin coating, dip coating and ultrasonic spray deposition. The absorber layer was fabricated inside the glove box. The contacts were deposited via sputtering and the HTM was deposited through thermal evaporation. The layers were later characterized to obtain the results.

3.1.1 Co-Precipitation

Co-precipitation reactions involve the simultaneous occurrence of nucleation, growth, coarsening, and/or agglomeration processes. Nucleation is a key step in the process. Aggregation disturbs the size, morphology, and properties of the products.

The phases involved in the synthesis procedure are presented schematically in figure 3.1 Co precipitation is a simple, low temperature, energy efficient process with easy control of particle size and composition but it cannot be used for uncharged species and trace impurities may also get precipitated with the product.

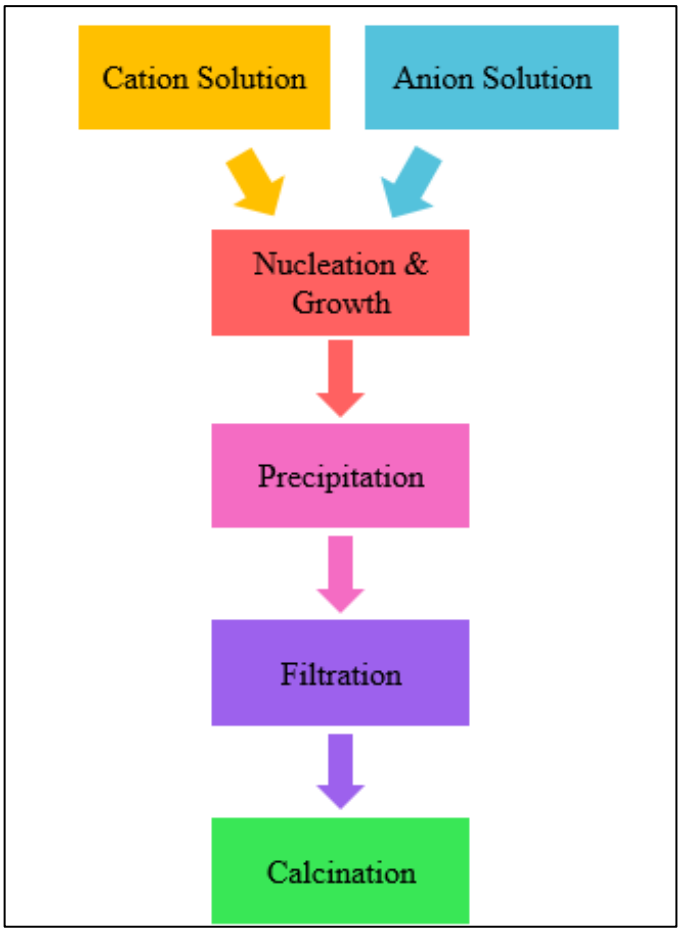

Figure 3.1 Steps involved in Co-precipitation

3.1.2 Spin Coating

This is a relatively simple yet effective technique for thin film deposition, in which a solution (organic, inorganic or hybrid) is dropped onto the substrate at a steady rotation rate [2]. Once the process is optimized, it can be used to produce high quality films of the desired material dissolved in a suitable solvent. The deposited film ranges in thickness from a few nm to many um. The substrate is placed on the spin coater which is held in place by the vacuum generated by rotary pump [3]. The speed of rotation can be adjusted from anywhere between 100-10000 rpm and time duration (in seconds) is adjusted by built-in controlling speed and time functions. The solution is injected on to the substrate through a syringe or pipette. The thickness of the film is related to the speed of rotation in an inverse manner and is dependent upon factors such as solvent evaporation rate, solution concentration, viscosity and temperature of the substrate. Only one substrate can be coated at a time. A large fraction of material goes to waste as it flies off during spinning of the substrate [4].

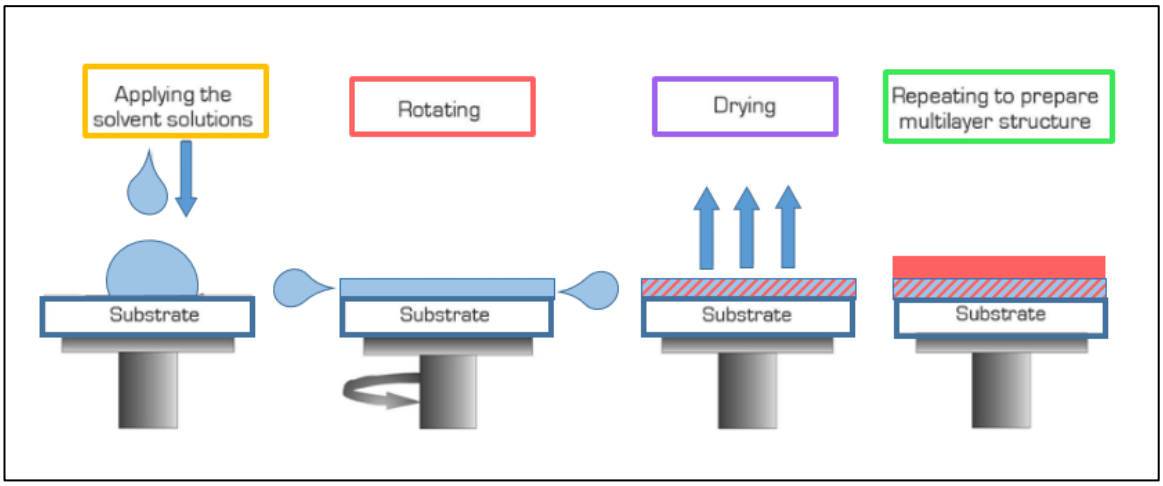

Figure 3.2 Steps of spin coating, modified from [5]

Spin Methods

Static and dynamic dispense spin coating are the main two methods for fabricating thin films by using spin coating technique. a dynamic dispense spin coating technique is better as compared to static due to less use of solution. The drawback of a dynamic distribution is that it cannot be used for low spin speed below 1000 rpm as at low spin it is difficult to get complete coverage of substrate for more viscous solutions. So generally Static dispense technique is used for 500 rpm or below[4].

Advantages

- Fabrication of thin films by spin coating technique involves Simple and easy process.
- At high speed air flow can dry the films fastly.
- Uniform and good quality films can be fabricated at both macro and Nano scale.

Disadvantages

- Process involve only single substrate at a time so has low rate of production as compared to roll to roll process.
- Drying of films fastly can also lead to low performance for Nano scale production.
- Material wastage is there as around 10% material is threw off during the spinning.

3.1.3 Dip coating

Dip coating is a simple and old fashioned technique that can be used for deposition of thin films on substrates, cylinders and blocks. The film thickness depend on the viscosity of solution, surface tension and gravity [6]. It also depend upon the immersion time of substrate into coating solution, the more rapid substrate withdrawal cause the thicker film [7].

The dip-coating process involves following stages:

i. **Immersion**: The first stage of the process is the dipping of substrate in the solution of desired coating material at a constant speed.
ii. **Time duration**: The substrate should be dipped in to the solution for a known time duration. Time duration of immersion of substrate effect the thickness and then drawn up with constant speed.
iii. **Deposition:** When the substrate is drawn up thin layer deposits itself on the substrate. The withdrawal of substrates should be carried out at a constant speed for getting uniform film. The speed of pulling up a substrate defines the thickness of the film.
iv. **Drainage:** After pulling up the substrate the excess liquid will drain from the substrate surface.
v. **Evaporation:** Finally substrate is annealed on the suitable temperature for evaporating the solvents forming thin film.

Advantages

- Technique can be used for deposition of different materials layers on substrates
- Uniform film can be obtained using this technique by using a simple beaker.
- Less material wastage as compared to spin coating technique.

Disadvantages

- Basic flow should be steady i.e. the immersion and pulling of substrate should be at constant speed for obtaining good film.
- More complicated process as control of process is demanding
- Application in limited area like only in R&D sector

3.2 Vacuum Based Deposition Techniques:

3.2.1 Physical Vapour deposition:

Physical vapour deposition is a thin film deposition technique by using ultra-high pressure and vacuum environment. It includes techniques like ion plating, electron beam evaporation and sputtering. The deposited film thickness varies from several angstrom to few millimeters depending upon the requirement. PVD is a flexible technique because it can deposit nearly all type of in-organic materials like alloys, mixtures, metals and others [8] [9].

Physical vapour deposition technique mainly includes,

1. Evaporation
2. Sputtering

3.2.2 Evaporation:

In evaporation, thermal energy is required to deposit films on substrates. Material being deposited is placed inside a crucible and thermal energy is supplied to the crucible for the evaporation of the atoms. These evaporated atoms moves through the evacuated space between the crucible and substrate and stick to the surface of the substrate [10]

a. Resistance - W, Mo, Ta filament.
b. Electron- beam.

The reaction on the surface of the substrate is very fast which lead to the improper arrangement of the atoms on the surface. This affects the topology, film thickness and step coverage of the film deposited. Moreover, in case of deposition of alloy, evaporation is difficult to carry out because of the different vapour pressures.

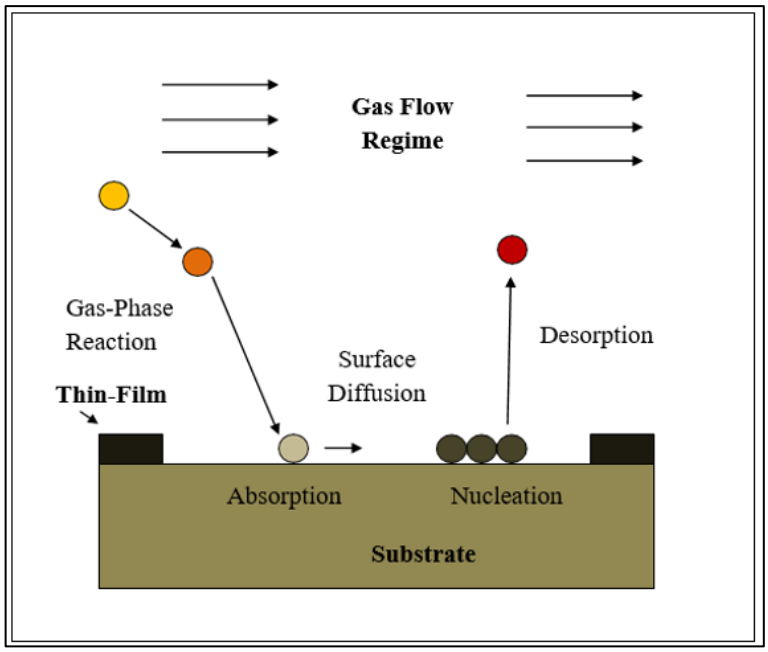

Figure 3.3 Working mechanism of Evaporation

3.2.3 Sputtering:

Sputtering is another type of PVD which involves the ejection of material from the source and deposition of that material onto the substrate. A strong vacuum and plasma is created for the ejection and deposition of the source material.

A typical sputtering process consist of following steps,

a. The source material and the target are placed inside a vacuum chamber.
b. A suitable voltage is applied across the target & source, such that, target is attached to the negative potential cathode and substrate at positive potential anode.
c. Plasma is created inside the chamber by inserting a sputtering gas (usually Argon).
d. Current flow in between the two electrodes (anode and cathode) which leads to the formation of Ar+ ions. These Ar+ ions collide with other Argon molecules to create more Ar+ ions and electrons. This is known as avalanche multiplication effect.
e. The ionized atoms of the sputtering gas bombard the target and sputter the source material.

f. These sputtered atoms are transported to the substrate for deposition/coating.

Sputtering begins when an electron moves from cathode to anode and collides with a sputtering gas atom and forms a positively charged ion. Pressure is maintained inside the chamber for maximum collision between the electron and sputtering gas atom. With increase in collision, current increases which leads the plasma to become self-sustaining. To further maintain the plasma every electron has to maintain and produce sufficient secondary emission. In some cases, collision can also result in glow discharge instead of ions production [11].

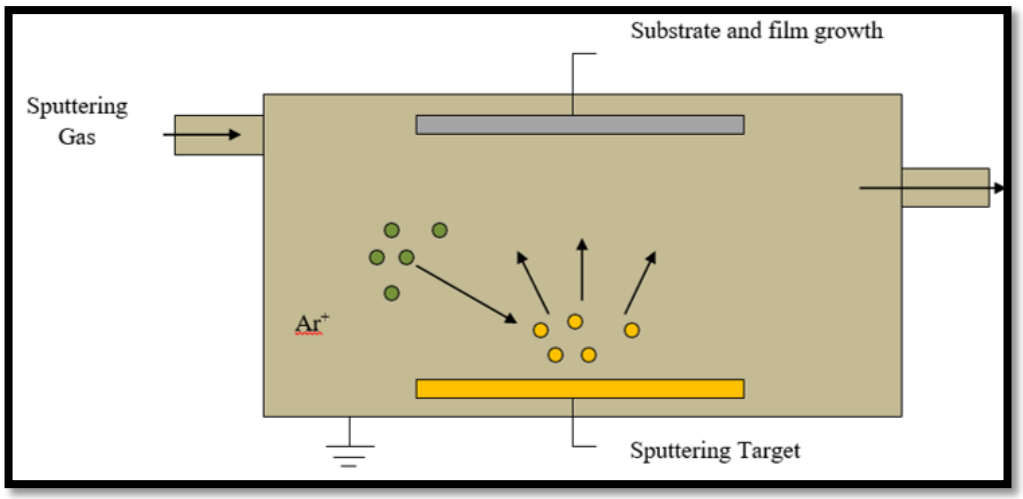

Figure 3.4 Working mechanism of Sputtering

Sputtering is divided into two types depending upon the voltage source,

a. DC Sputtering - utilize a DC gaseous discharge (DC voltage source).
b. RF Sputtering – utilizes a RF source of high voltage, 13.56 MHz.

RF sputtering can be used to deposit metal, semi-conductors as well as insulators. In case of this type of sputtering, in the first cycle the source is given negative charge which lead to polarization on the surface of the source [11]. This polarization results in the attraction of sputter gas atoms on the source and knocking off of the source atoms. In the other cycle when target is given a positive charge, the source atoms are ejected from the surface due to reverse polarization and are accelerated towards the substrate for deposition [11].

Types of Sputtering:

Sputtering is divided into following types,

1. **Magnetron Sputtering**: The sputtering gas is ionized by a magnetic field.

2. **Reactive Sputtering**: A chemical reaction takes place before deposition. Other gas like O2, H2 and N2 are used to assist chemical reaction. The target material is different from the material deposited.

3. **Ion Assisted Sputtering:** A secondary ion beam is exposed on the substrate. Usually used to deposit carbon based materials like diamond.

3.3 Characterization & Testing Techniques

Following are some of the characterization and testing methods employed to study the samples prepared in this research work.

3.3.1 X-ray Diffraction (XRD)

X-ray diffraction (XRD) is a systematic, non-destructive technique employed for phase identification of a crystalline material and calculating dimensions of unit cell. Apart from that it also reveals information on crystal structure type, average crystallite size, crystal defects, and preferred orientation of crystals along with other strain parameters. XRD employs monochromatic x-ray beams which undergo constructive interference to reveal the XRD pattern. The source of x-rays is the cathode tube which filters, directs and concentrates the rays to the sample. The mathematical representation for Bragg's law is given below:

$$n\lambda = 2dsin\theta$$

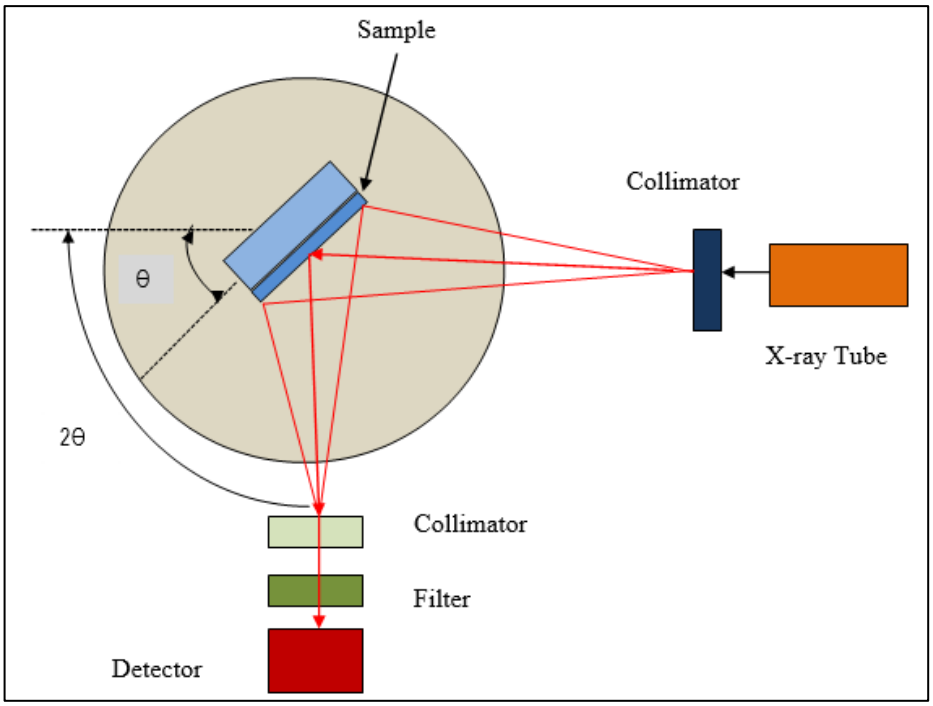

Figure 3.5 Schematic diagram of XRD

Where "n" is any integer, "λ" is the ray's wavelength, "d" the crystal plane separation and "θ" being the angle between incident and reflected beam.

The peaks are obtained from the diffraction of x-rays. Crystallite size "D" of any material in nanometers (nm) can be found from the equation given below using XRD significant peaks:

$$D = \frac{0.9\lambda}{\beta cos\theta}$$

Here "λ" is the wavelength in nm, "θ" is the diffraction angle and "β" is the full width half maximum.

3.3.2 Optical Microscopy (OM)

Optical microscopy (OM) utilizes a type of optical microscope that employs light in the visible region and a specific lens scheme to magnify and observe small samples.

It was invented in the 18th century but it is still applied in researches carried out in today's era. A simple optical microscope employs a single lens for magnification while a compound microscope use a variety of different lenses to achieve high magnification.

Most of the laboratory optical microscopes available today are the compound microscopes.

The schematic of working of a compound microscope is given in **Error! Reference ource not found.**.

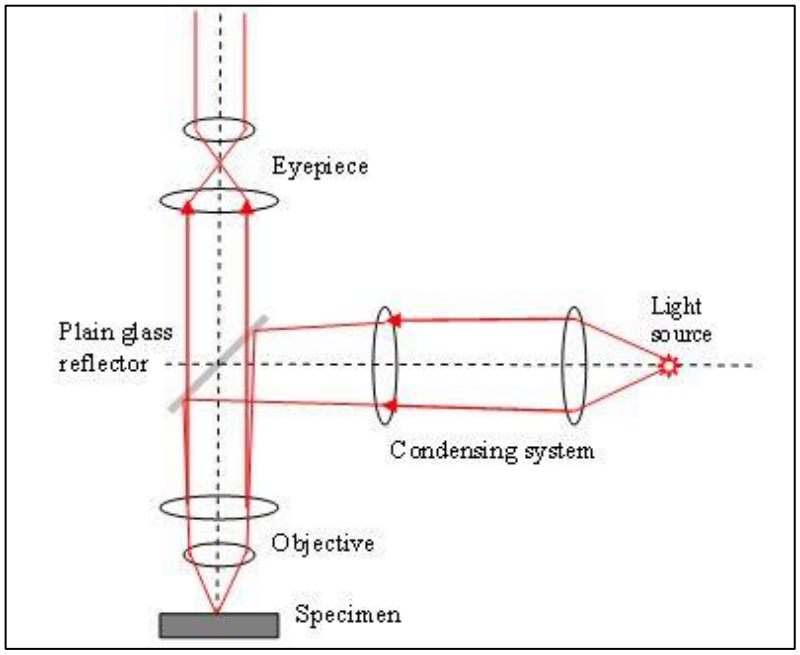

Figure 3.6 Working of Compound Optical Microscope

The main components of a compound microscope is the eyepiece, objective lens, an objective turret, coarse and fine adjustment knobs, a mirror, stage and condenser.

Light sensitive cameras can capture the image from optical microscope producing a micrograph which is the final result from which research related data can be extracted. Compound optical microscopes are used to examine thinly sliced materials especially structure of polished materials and ceramics. A standard compound microscope has three types of objective lens including a scanning lens of 5x power, a low power lens of 10x power and medium and high power lens of 30x and 40x powers. Structures up to few micrometers can be seen and studied using optical microscopy. Porosity can also be studied using this type of lens and areal porosity can be calculated from micrograph produced by OM [14], [15].

3.3.3 Scanning Electron Microscopy (SEM)

Scanning electron microscope (SEM) employs a focused high energy electron beam to produce different signals at the surface of sample under consideration. The working of a SEM can be demonstrated by

Figure 3.7 Schematic of Scanning Electron Microscope (SEM)

given below:

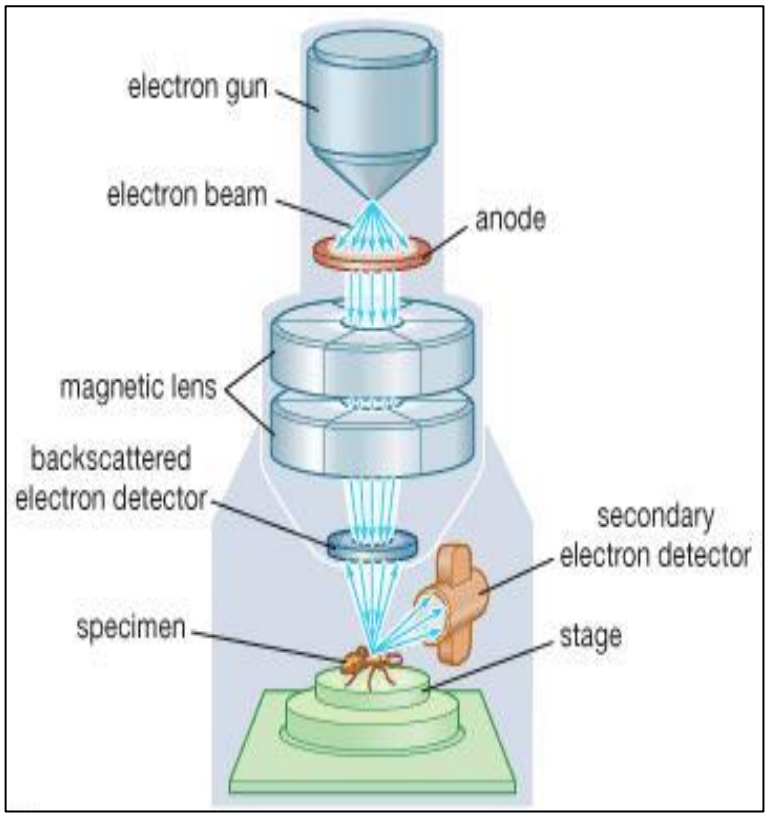

Figure 3.7 Schematic of Scanning Electron Microscope (SEM)

The schematic diagram of SEM is shown in Figure 3.10 which shows the complete flow of process from the start i.e. generation of electron beam to end i.e. the beam strikes the sample. Finally, the generated signals i.e. secondary electrons are analyzed with the help of detector and the output is displayed. When the electron beam hits the sample surface different types of signals generates carrying information about film or surface morphology. These signals include X-rays, secondary electrons and back scattered electrons. Finally, these signals can be detected by specific detectors and the chemical composition of material is analyzed by back scattered electrons while secondary electrons give surface morphology. High vacuum and nonconductive surface of sample are the conditions of using this technique [16]–[19]**.**

3.3.4 Energy Dispersive Spectroscopy (EDS/EDX)

Energy dispersive x-ray spectroscopy (EDX/EDS) is basically an analytical technique that provides information on the elemental composition and chemical analysis of the sample under consideration. It generally uses an electron beam as in

SEM to interact with sample's atoms. However, the EDS spectra that it produces actually results from the x-rays emitted from the sample.

When the sample is bombarded with source of high energy electrons or protons, the atoms on surface of sample eject electrons resulting in generation of vacancies in the structure. These vacancies are subsequently filled with electrons from higher energy state releasing x-ray. These x-rays are distinctive for each element. EDS/EDX is usually combined with SEM unit. The detector in EDS records the abundance of x-rays emitted from sample versus their energy, thus, resulting in an EDS spectra [20]–[22]

3.3.5 Hall Effect Measurement:

Hall Effect measurement system is use to determine the electrical properties of semi- conductor thin films like charge carrier type and density, mobility, conductivity, resistivity and sheet resistance. Hall Effect measurement system work on the principle of Lorentz force. The direction of the magnetic force is determined by right hand rule, i.e. in the opposite direction in which thumb is pointed. In this case the Lorentz force is the combination of both electric and magnetic force and is calculated as, **- q(E + v x B)** where E is electric field and B is magnetic field [23]. Suppose a constant current I flows along the x-axis in presence of z-directed magnetic field. The charges experience a Lorentz force and a hall voltage is produce. In case of negative (n) charge, the current direction is towards the negative y-axis and in case of holes (p type), in the opposite direction. This calculated hall voltage can be used to calculate the bulk density/ charge density by **ns=IB/qlVHl.**

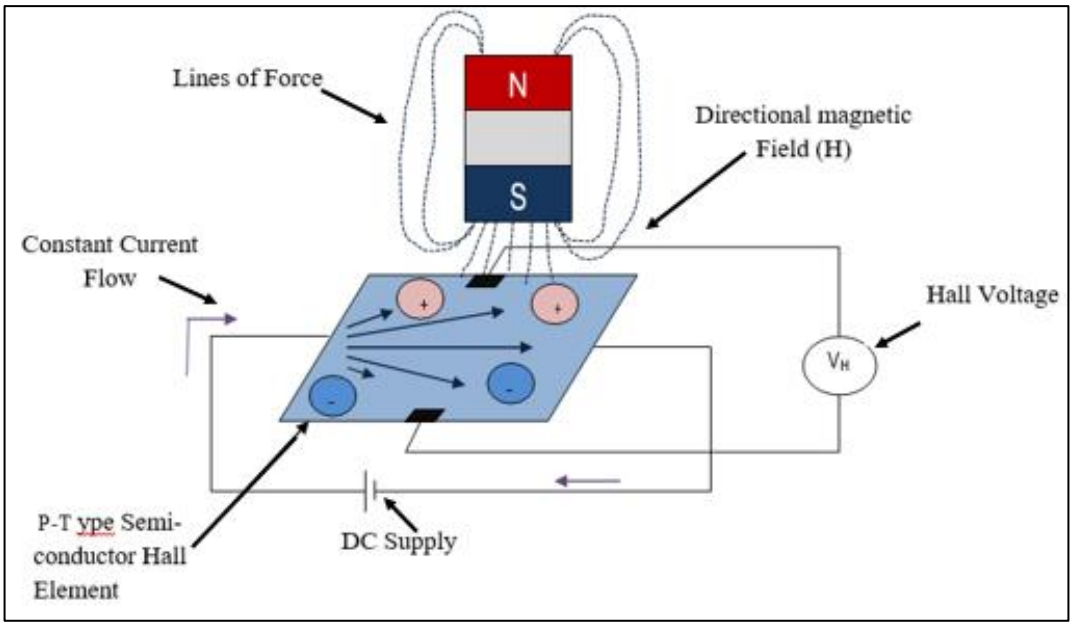

Figure 3.8 Geometry of fields and sample in Hall effect experiment

Hall voltage is negative for n-type materials and positive for p-type materials. This technique requires four ohmic contacts and it require a square sample of the conductive sample. In this measurement , van der Pauw resistivity measurement suggest that there are two types of resistance RA and RB , which are related to sheet resistance as,

$$\mathbf{exp(-\pi RA/RS) + exp(-\pi RB/RS) = 1}$$

Mobility is calculated by ɳ=1/(qnsRs) and similarly bulk resistivity is calculated as ϱ=Rsd is the conductive layer thickness i.e d is known. Hall Effect measurement system can also be use to calculated IV or IR curves for a conductive film in the required range of current. For better measurements, the sample must have:

1. Flat sample of uniform thickness.
2. Better ohmic contacts. Sample must be symmetric.
3. Sample uniformity and its thickness must be known.

3.3.6 Ultraviolet-Visible Spectroscopy

The amount of light transmitted by contacts is a measure of its transparency. Conventionally, the thickness of ITO deposited on thin film solar cells is from 50-200 nm and measurement of transmittance shows that it allows greater than 90% of the incident light to pass through. UV-Vis spectroscopy is a technique which measures absorption, transmittance and reflection in the ultraviolet (190 nm-400 nm) and visible

(400 nm- 700nm) regions. It also gives information about the organic molecules and helps to determine the presence of impurities, heteroatoms, saturation or unsaturation in the material.When a sample is placed under the UV-Vis spectrum the electrons get excited to higher antibonding orbitals. . Lesser the energy gap between HOMO and LUMO of a material, easier is the excitation of electrons by longer wavelength radiations. When a molecule with an energy equal to gap between HOMO-LUMO is exposed to radiation. This is referred to as electronic transition bonding to anti-bonding and denoted by σ - σ*. The graph between absorption or transmittance of light on X-axis and different wavelengths on Y-axis is obtained and analyzed [24].

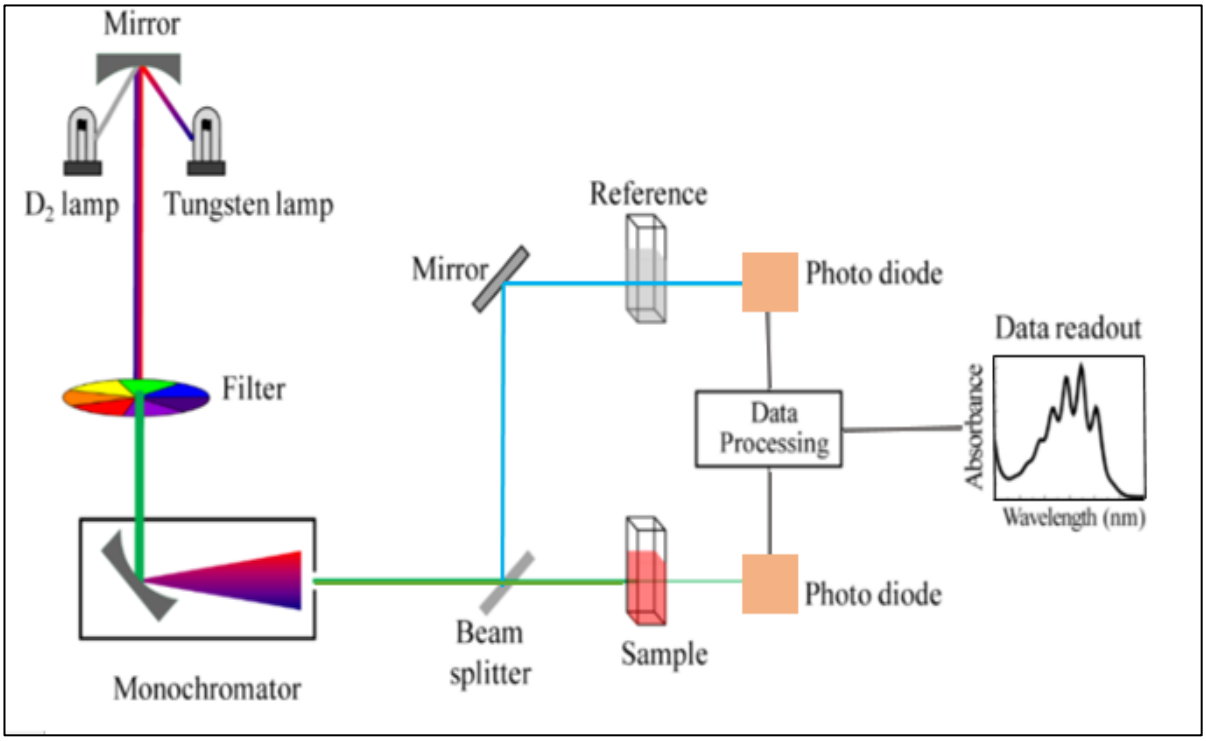

Figure 3.9 Mechanism of UV-vis spectroscopy

3.3.7 IV-curve Measurement:

The I-V curve is a graph of all possible available combinations of voltage and current operated under constant conditions and give the characteristic electrical properties of a solar cell depending upon the active electrode region that enhances charge transport, exciton dissociation and carrier injection. These properties a usually measured using a Keithley source meter under illuminated and dark conditions. Generally, the I-V curve has a characteristic shape point, the behavior is similar however, when it is to the right of the MPP, there is an immediate decline in power output because of sealed charges within the solar cell that do not flow out. These

charges are a result of increased voltage output [25]. IV-curve gives the Isc, Voc and Fill Factor FF for the device under consideration and this information can be used to find efficiency of the cell [26].

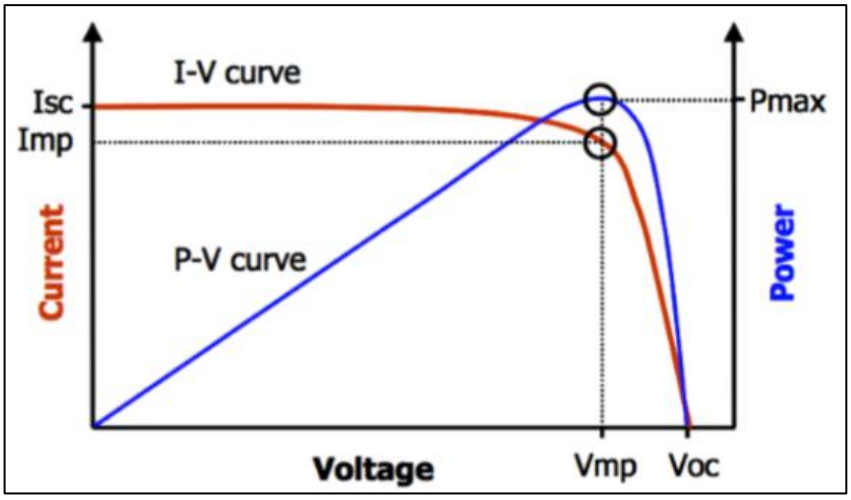

Figure 3.10: IV-curve measurement using one sun solar simulator

Summary

The chapter highlights the review of synthesis, characterization and testing techniques employed for research work on ETL for perovskite solar cells.

The methods used for synthesis and fabrication of ETL, absorber layer are co-precipitation, spin coating, dip coating and ultrasonic spray deposition method and Thermal evaporation for HTL. Contacts for the cell were deposited using sputtering.

The characterization and testing techniques employed are XRD, OM, SEM, EDS/EDX, UV-Vis spectroscopy, Hall Effect measurement and IV curve measurement. XRD analysis can provide information on phase identification and crystal structure of sample, OM and SEM can provide information about shape, morphology and topography and surface defects of samples at microstructural level. EDS/EDX is used for determining the elemental analysis and composition of the material. UV-Vis spectroscopy to measure the Transmittance and absorbance spectra of the materials deposited. Hall Effect is used to measure conductivity, resistivity, the p/n nature and charge mobility of the material. IV- curve measurement for the cell efficiency can be performed using 1 sun solar simulator.

References:

[1] F. C. Krebs, “Fabrication and processing of polymer solar cells: A review of printing and coating techniques,” *Sol. Energy Mater. Sol. Cells*, 93, 4, (2009) 394–412,

[2] “Spin Coating - an overview | ScienceDirect Topics.” [Accessed: 04-Sep-2019].Available: https://www.sciencedirect.com/topics/materials-science/spin-coating/

[3] “Spin Coating, A Complete Guide to Theory and Techniques | Ossila.” [Accessed: 04-Sep-2019].Available: https://www.ossila.com/pages/spin-coating/

[4] “The stages of the deposition thin films by spin coating method | Download Scientific Diagram.”. Available: https://www.researchgate.net/figure/The-stages-of-the-deposition-thin-films-by-spin-coating-method_fig3_277891167/

[6] C. J. Brinker, “Dip coating,” in *Chemical Solution Deposition of Functional Oxide Thin Films*, 9783211993118, (2013) 233–261.

[7] D. L. (Donald L. Smith, Book *Thin-film deposition : principles and practice*. McGraw-Hill, 1995.

[8] “Physical vapor deposition of thin films - John E. Mahan - Free E-Book Download.”2019,http://terment.ru/en/?q=Physical+vapor+deposition+of+thin+films+-+John+E.+Mahan/

[10] L. Wengeler, M. Schmitt, K. Peters, P. Scharfer, and W. Schabel, *Chemical engineering and processing : process intensification.*, vol. 68. Elsevier B.V, 2000

[11] S. Valligatla *et al.*, “High quality factor 1-D Er^3+-activated dielectric microcavity fabricated by RF-sputtering,” , *Opt. Express*, 20, 19, (2012) 21214

[12] J. Goldstein, *Scanning electron microscopy and x-ray microanalysis*. Kluwer Academic/Plenum Publishers, 2003.

[13] R. Green, “Hall Effect Measurements in Materials Characterization Who Needs to Measure Hall Effect ? Growing Interest in the Use of Hall Effect

Measurements," *Keithley White Pap.*, 3111, 440, (1990) 1–12

[14] A. Fakharuddin, F. Di, I. Ahmed, Q. Wali, T. M. Brown, and R. Jose, "Role of morphology and crystallinity of nanorod and planar electron transport layers on the performance and long term durability of perovskite solar cells," , *J. Power Sources*, 283, (2015) 61–67

[15] W. Nanostructured, J. Choi, S. Song, M. T. Ho, H. J. Snaith, and T. Park, "Well-De fi ned Nanostructured, Single- Crystalline TiO 2 Electron Transport Layer for E ffi cient Planar Perovskite Solar Cells," J. power *Joule*, 3, 6, (2016) 1464–1477

[16] D. Ouyang, Z. Huang, and W. C. H. Choy, "Solution-Processed Metal Oxide Nanocrystals as Carrier Transport Layers in Organic and Perovskite Solar Cells," , *Adv. Funct. Mater.*, 29, 1, (2019) 1804660

[17] J. Ma *et al.*, "Highly Efficient and Stable Planar Perovskite Solar Cells With Large-Scale Manufacture of E-Beam Evaporated SnO_2 Toward Commercialization," , *Sol. RRL*, 1, 10, (2017) 1700118

[18] Q. Liu *et al.*, "Enhanced Stability of Perovskite Solar Cells with Low-Temperature Hydrothermally Grown SnO_2 Electron Transport Layers," *Adv. Funct. Mater.*, 26, 33, (2016) 6069–6075

[19] J.-Y. Chen, C.-C. Chueh, Z. Zhu, W.-C. Chen, and A. K.-Y. Jen, "Low-temperature electrodeposited crystalline SnO2 as an efficient electron-transporting layer for conventional perovskite solar cells," *Sol. Energy Mater. Sol. Cells*, 164, (2017) 47–55

Chapter # 4

Materials & Methodology

Numerous experiments were carried out in accordance to the focus of the research work. To meet the research objectives, the sequence defined for the experiments to be carried out is:

1. Tin Oxide Nanoparticle Synthesis
2. ETL Fabrication
3. Absorber Layer Fabrication
4. HTL Fabrication
5. Device Fabrication

4.1 Tin Oxide Nanoparticle Synthesis

Materials:

For Tin Oxide (SnO_2) nanoparticles preparation, the Stannous Chloride dihydrate ($SnCl_2.2H_2O$), Ethyl Alcohol (C_2H_5OH) and sodium hydroxide (NaOH) were purchased from Merck-Sigma Aldrich with purity up to 99.9% trace metal basis. Glucose in a very small amount have been used as template.

Preparation of Tin Oxide Nanoparticles:

SnO_2 nanoparticles were synthesized using co-precipitation technique. The nanoparticle's size was optimized by varying the pH and the sintering temperature. For preparation of the required material firstly 0.1M solution of $SnCl_2.2H_2O$ was prepared in ethanol and 0.1M solution of NaOH in distilled water was added to maintain a pH=5. The solution was refluxed at 90°C for 4 hours in lab tech oven. After cooling, centrifugation was done at 3000 rpm for 15mins and repeated washing was done with deionized water and later collecting the ensuing gel. Then it was kept overnight in vacuum oven at 90°C.

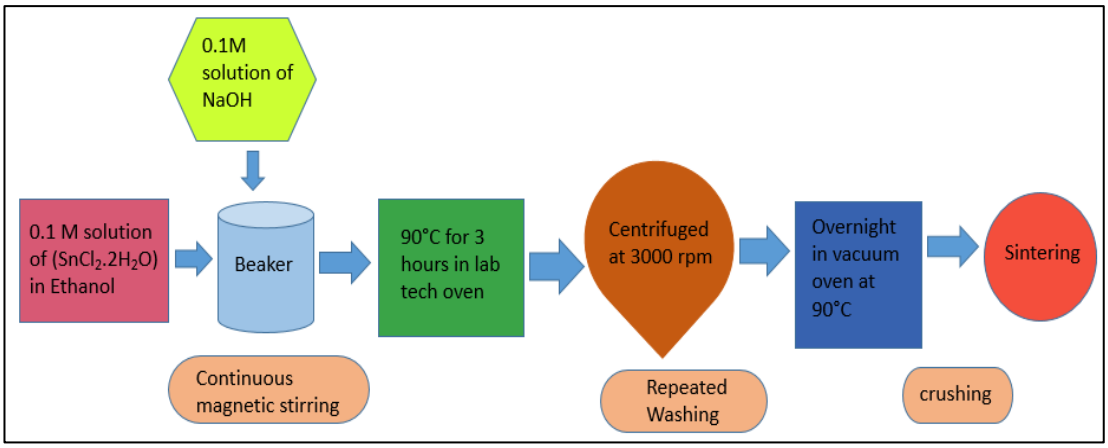

Figure 4.1 Preparation of SnO2 Nanoparticles using Co-precipitation

Sintering at Different Temperatures:

The sintering of the obtained residue was done at different temperature i.e. 400°C, 500, 700°C and 800°C for 1 hour at a rate of 10°C/min in a furnace to obtain SnO_2 nano-powder.

Varying the pH:

The same recipe of preparation was followed up but the pH was varied and nanoparticles at pH=8 and pH=11 were obtained and were characterization was done of the as synthesized SnO_2.

4.2 ETL Fabrication

Three different Electron Transport Layers (ETL) were fabricated and characterized for a comparative analysis.

1. TiO_2 ETL
2. SnO_2 ETL
3. TiO_2/SnO_2 ETL

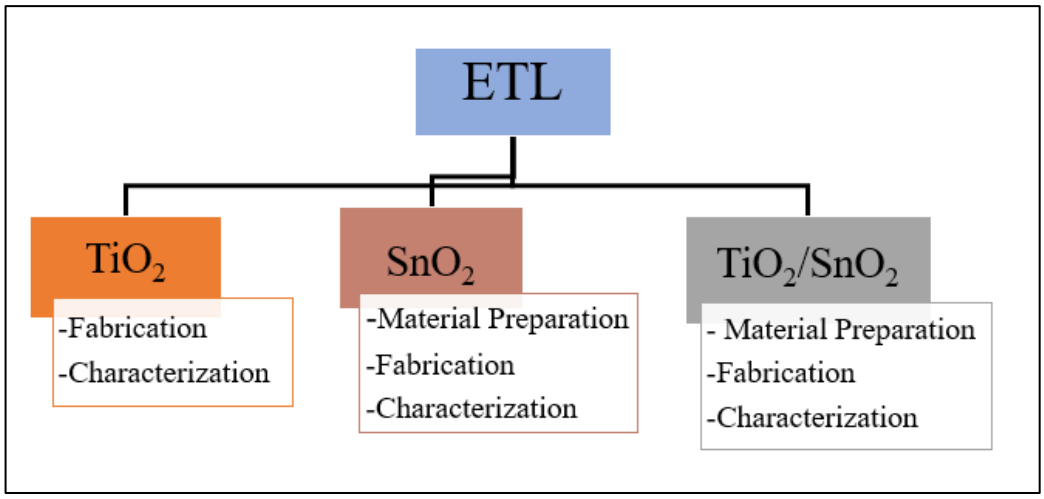

Figure 4.2 Classification of ETLs being fabricated under our study

4.2.1 TiO_2 ETL

ETL used in our case study was Titania (TiO_2). A compact Titania layer was fabricated on FTO glass via spin coating technique. The resultant compact layers, also mentioned as "blocking layer", is a pre-requisite.

Materials:

Titania Paste: Ti-Nanoxide BL/SC was acquired from Solaronix which deems to be an organotitanate formulation.

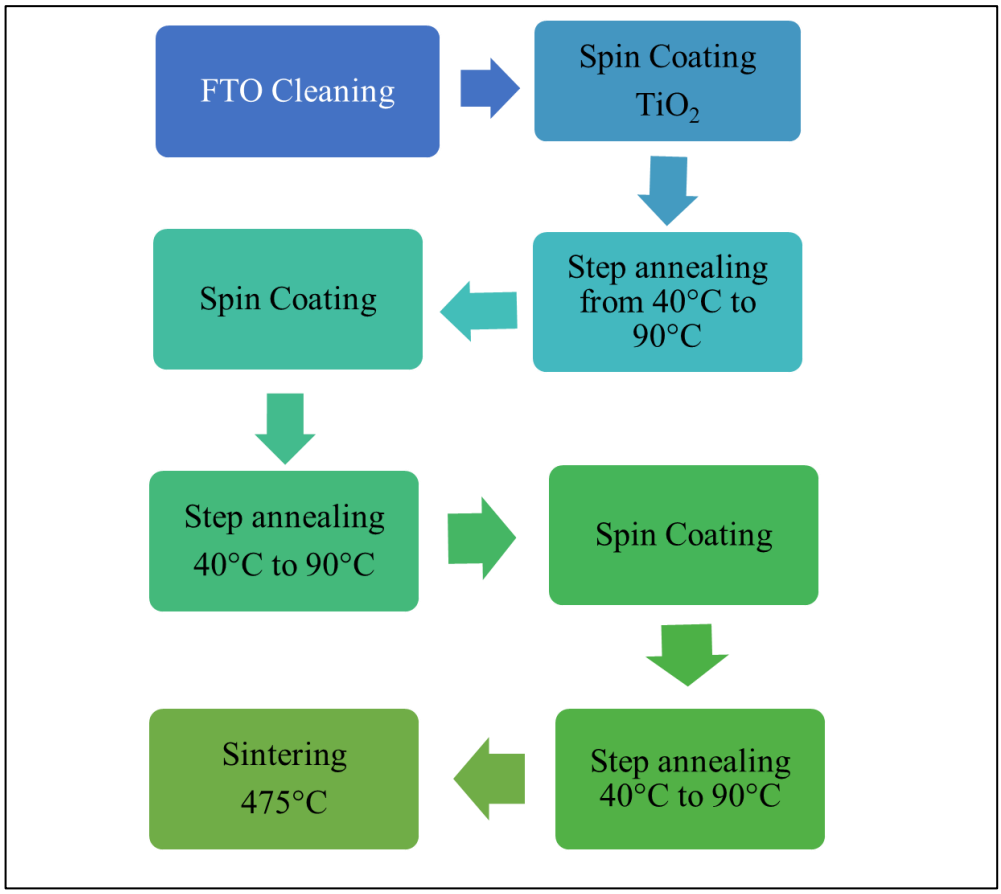

Figure 4.3 Flowchart for the fabrication of TiO_2

Deposition:

Titania was deposited on FTO via spin coating with using single step of 5000rpm for 50 sec. After single coat films were step-annealed from 40°C to 90°C with keeping them stay for two minutes every 5°C rise. Three coats and consequent step-annealing were taken out to achieve the desired thickness of around 50nm. Finally, Titania deposited FTO films were annealed at 475°C in a furnace for 1 hour to acquire the ideal compact Titania layer for electron transport purposes.

4.2.2 SnO_2 ETL

In this case study SnO_2 nanoparticles ETL was fabricated via spin coated. Two set of experiment were lead once the optimization was done. After acquiring the desired thickness of the film, the dried films at 90°C were kept aside for further testing while the other set after being dried at 90°C were further sintered at 450°C in furnace. Hence we obtained sintered films at 90°C named group A and sintered film at 450°C named group B.

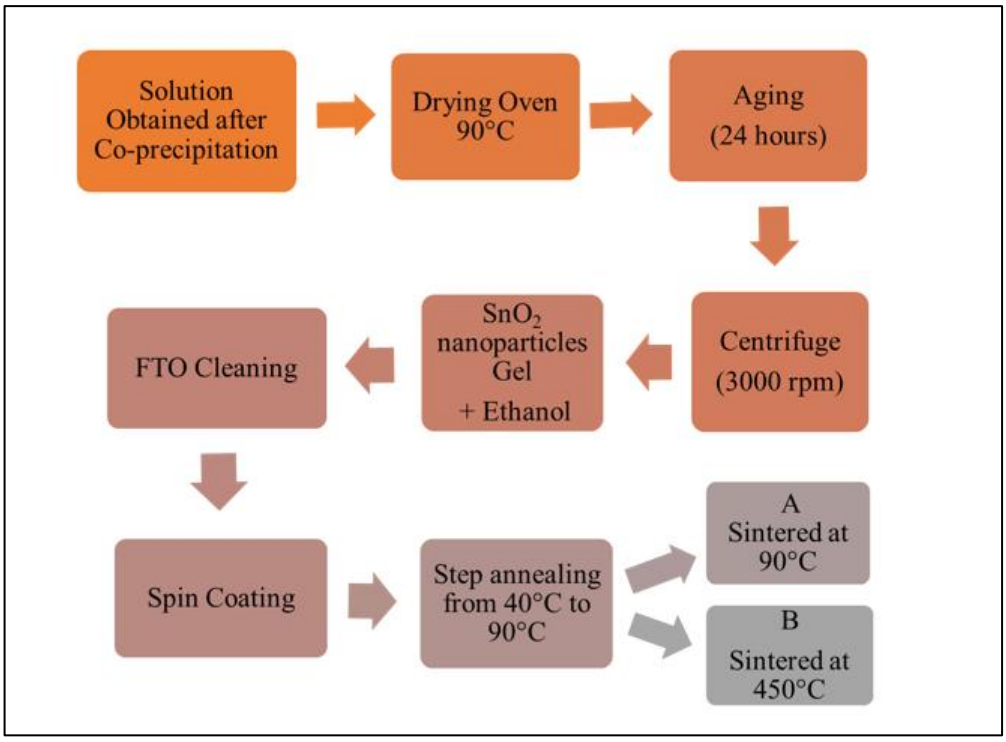

Figure 4.4 Flow chart for fabrication of SnO_2 ETL

Materials:

Stannous chloride dihydrate ($SnCl_2.2H_2O$), Ethyl Alcohol (C_2H_5OH) and sodium hydroxide (NaOH) were purchased from Merck-Sigma Aldrich with purity up to 99.9% trace metal basis. Glucose in a very small amount have been used as template.

Deposition:

SnO_2 films are being deposited using Spin coating. The solution obtained through the process of co-precipitation for synthesis of SnO_2 nanoparticles was used for this purpose. The solution was kept in oven for 5 hours at 90°C. It was left to age for 24 hours. Later centrifuged at 3000 rpm for 15mins and washed repeatedly with deionized water. Ethanol was added to the concentrated nanoparticles gel in a very little quantity of about 1:6 to make it a little dilute for spin coating. It was then spin coated at 10000rpm for 35seconds in a single step dynamic spin coating and then step annealed from 40°C to 90°C with staying for 2 minutes at every 5°C rise in temperature in a drying oven. After the first layer was dried, the second and third film of SnO_2 nanoparticles were deposited and dried at same temperature and time as for the first one. After the desired thickness of the SnO_2 ETL was achieved, one

set was further sintered at 450°C for 45 minutes in a furnace and other was just kept for characterization after being dried at 90°C.

4.2.3 TiO_2/SnO_2 ETL

For a better comparative analysis a third ETL being composite of both, first two ETL described in the chapter. Multilayer ETLs have shown good efficiency for PSCs. Firstly TiO_2 films were deposited and sintered and then the SnO_2 films were deposited and sintered.

Materials:

TiO_2 Blocking paste, stannous chloride dihydrate ($SnCl_2.2H_2O$), Ethyl Alcohol (C_2H_5OH) and sodium hydroxide (NaOH) were purchased from Merck-Sigma Aldrich with purity up to 99.9% trace metal basis. Glucose in a very small amount have been used as template.

Deposition:

Firstly, TiO_2 was deposited on FTO via spin coating with using single step of 5000rpm for 50 sec. After single coat films were step-annealed from 40°C to 90°C with keeping them stay for two minutes every 5°C rise. After depositing TiO_2 films, it was sintered at 475°C for 1 hour. The SnO_2 films were deposited over TiO_2 films using spin coating. The material was prepared exactly like the procedure described for tin oxide nanoparticles films and were dried in oven from 40°C to 90°C.

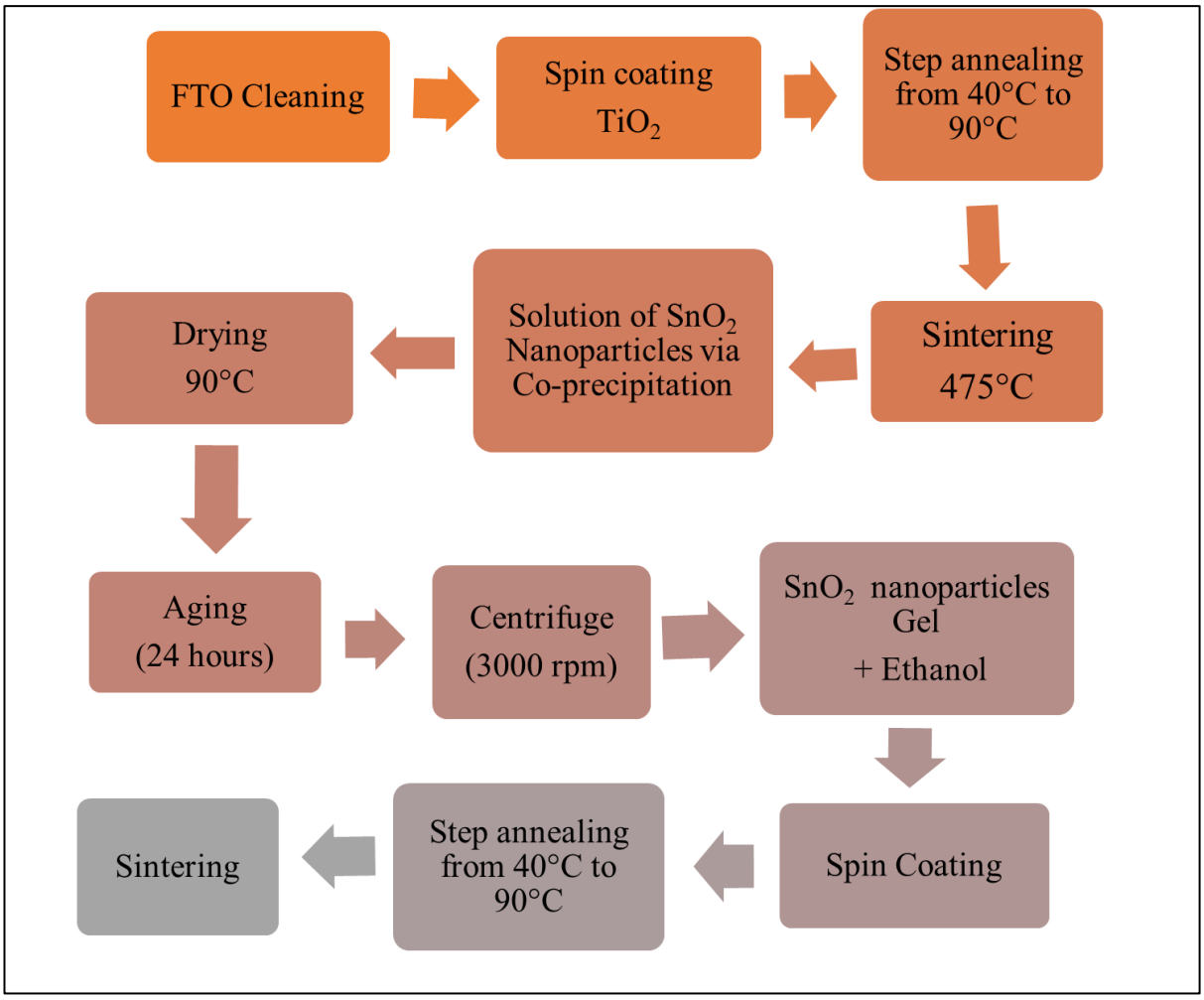

Figure 4.5 Flow chart for the fabrication of TiO_2/SnO_2

4.3 Absorber Layer/ perovskite Layer Fabrication

Absorber layer or Perovskite Layer is typically prepared using solution processing with DMF as solvent to the PbI_2, the solution is then spin coated on to the ETL and obtained films are dipped in $MAPbI_3$ solution to form the perovskite layer. The layer thence formed seem to have degradation issues with moisture on a consistent basis. Therefore, alternate approaches are also been put forth to hinder the issue. One of them was to use an inert environment with low moisture content, which improves the stability. Apart from that Caffeine also showed better stabilities as its molecules tend to generate a molecular lock with Pb^{++}. We are going to consider both the possibilities to device our absorber layer. Experimental procedure for absorber layer was taken out in Argon environment in a glove box to keep the moisture levels at bay.

Materials:

Lead iodide (PbI_2), cesium Bromide (CsBr), Dimethyl Form-amide (DMF) and Dimethyl Sulf-oxide (DMSO), 2- propanol, Caffeine and Methylammonium Iodide ($CH_3NH_3I_3$) were all purchased from Sigma Aldrich.

Deposition:

The first step was to spin coat PbI_2 and then to deposit $CH_3NH_3I_3$ on the lead iodide via dip coating in the glove box. 1M solution of PbI_2 was made in 3ml DMF and 2ml DMSO and was kept on continuous stirring at 1000rpm for 30 minutes while being heated at &70°C. The lead iodide films were spin coated at 6500rpm for 30 sec followed by drying at 70°C. For deposition of Methylammonium Iodide, a solution was prepared inside the glove with 10mg/ml MAI in 2-propanol, kept on stirring for 10 minutes, the PbI_2 films already deposited on samples were then dip coated in MAI solution for 10minutes. The samples were dried at 80°C on a hot plate for 5 minutes.

Case 1:

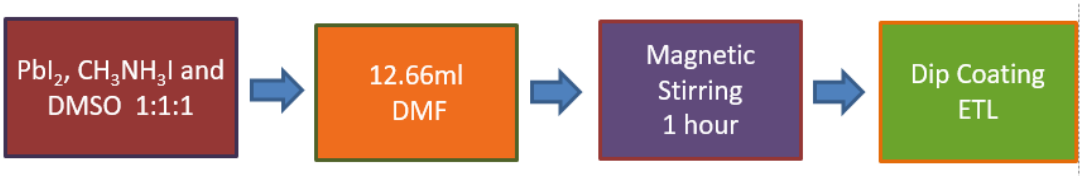

Case 2:

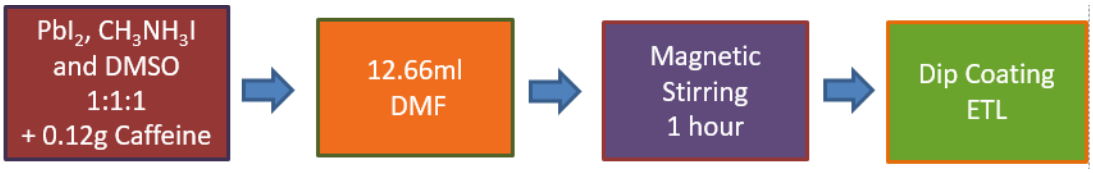

4.4 HTL Fabrication

PbPc is thermally evaporated onto the perovskite surface under high vacuum conditions to achieve sound and smooth HTL. To understand its behavior PbPc was deposited on FTO glass under high vacuum via thermal evaporation.

Materials

PbPc (Lead Phthalocyanine) was purchased from Sigma Aldrich.

Deposition:

Various hydrophobic HTLs (PbPc) were fabricated by depositing upon FTO glass. Thermal evaporation under vacuum ($1.2*10^{-3}$) is to be used to deposit a layer of metal phthalocyanine of about 40-60 nm. Once the film was characterized for the HTL properties, it was then deposited over the Perovskite surface.

4.4.1 Characterization:

XRD

For structural and phase analysis of perovskite material based thin films, X-ray diffraction (XRD) technique was carried out by using Bruker, D8 Advanced at the scan rate of 1.2/min in 2θ range of 5o-70o. The XRD was operated with a CuKα radiation source (λ =1.54056 Å), generated at 40 kV and 40 mA. Xpert HighScore and checkcell software's were used for the analysis of XRD data. **SEM/EDS**

For the surface morphology of the samples scanning electron microscope (SEM) was performed using MIRA3 TESCAN. The SEM scans were recorded for 1.0 Kx and 5.0 Kx magnification, the voltage was set at 10.0 KV for the recording of scans.

UV-Vis Spectroscopy

The optical properties of the film were studied using a UV-3600 plus UV-VIS NIR Spectrophotometer. The Transmittance and Absorbance spectra were measured for the fabricated ETL.

Hall Effect

The Electrical conductivity of the prepared film was measured using Hall Effect measurement system (Ecopia HMS-3000). The results obtained confirmed the p/n type of the material, charge mobility, conductivity and resistivity. The I-V curve for the fabricated film was also acquired through Hall Effect.

Contact Angle Measurement

To understand the hydrophobicity, contact angle was measured using Goniometer. This test was very important for the stability of HTL.

4.5 Device Fabrication

The complete device was fabricated to calculate the cell efficiency. For that purpose firstly ETL was deposited, and the absorber layer followed by the HTL. Contacts were deposited to make the cell complete for the calculation of device efficiency. All the three types of ETL were incorporated with same Absorber layers and then same HTL. Another set of the cells were differentiated with the Absorber layer being caffeinated and not caffeinated.

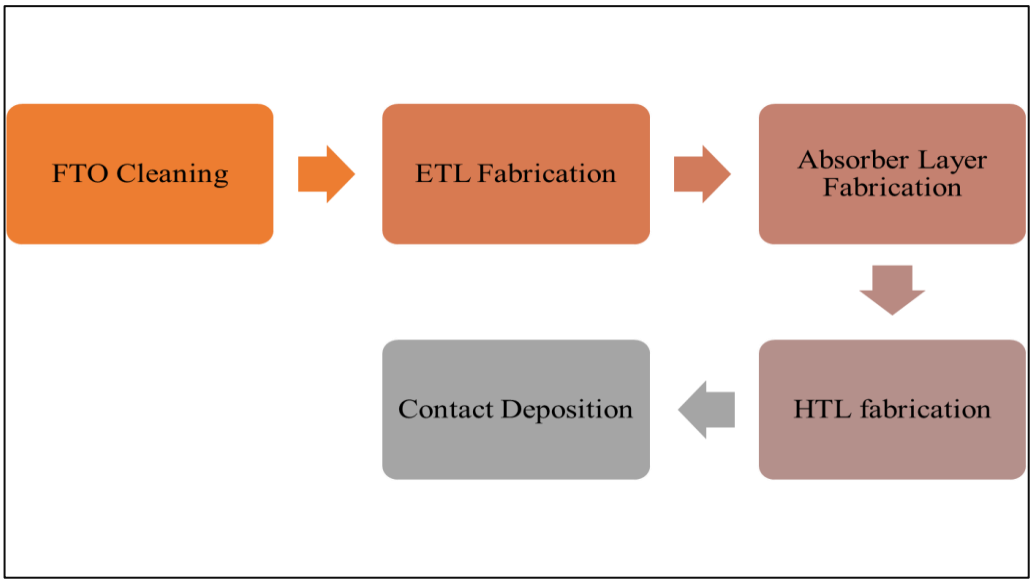

Figure 4.6 Flow chart for the Device fabrication

4.5.1 Types of Cell

As describe earlier three types of ETL and two types of Absorber layer were incorporated for the device fabrication, hence leading to 6 different types of PSCs. Firstly all the three types of ETL, TiO_2, SnO_2 and TiO_2/SnO_2 were fabricated and two sets were made. The first set was further deposited with the Absorber layer (PbI_2+$CH_3NH_3I_3$ + Caffeine) and the second set was subjected to the deposition of Absorber layer (PbI_2+$CH_3NH_3I_3$) without Caffeine. HTL (PbPc) was thermally evaporated and deposited over the Absorber layer for all the cells.

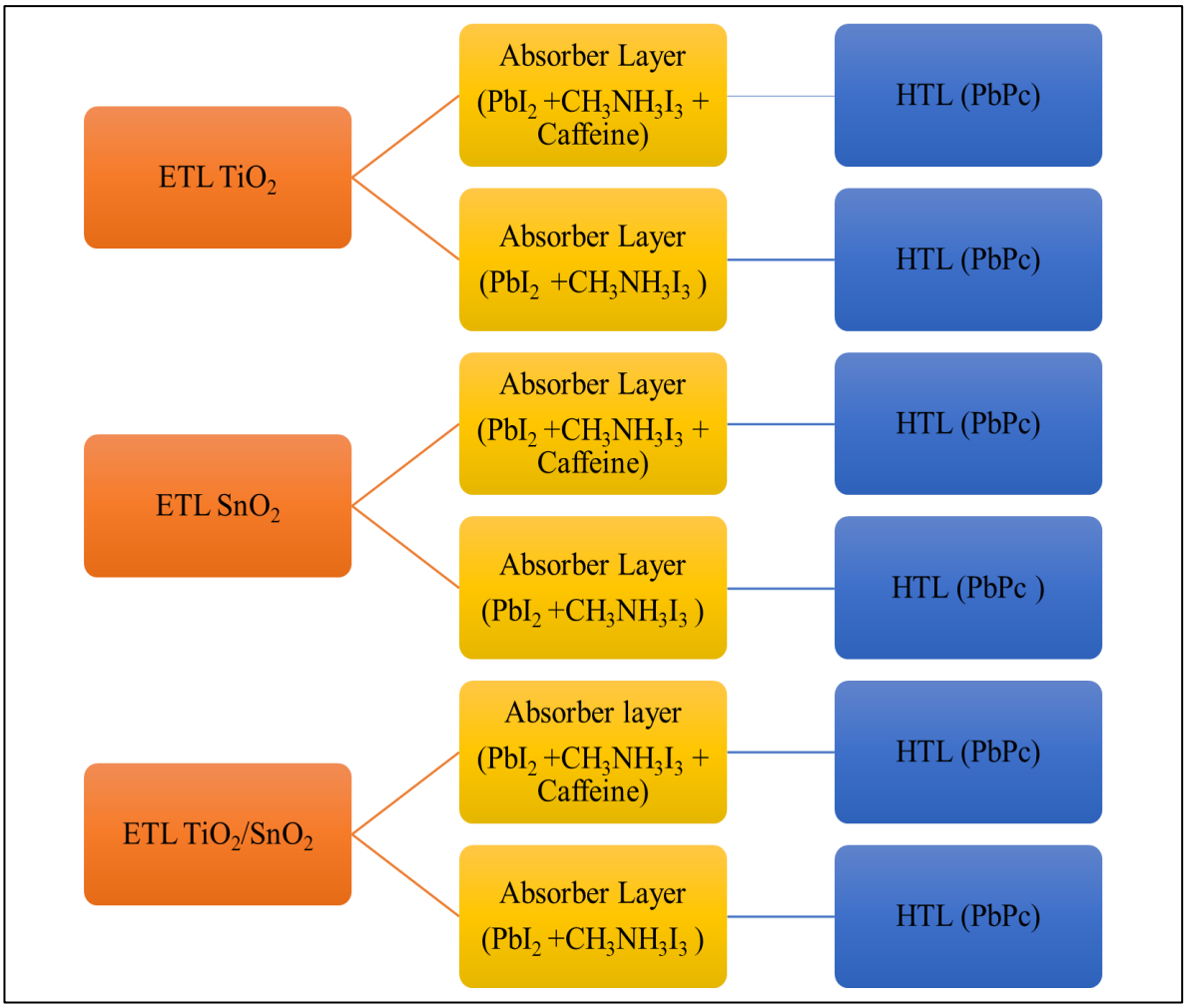

Figure 4.7 Configuration of the Cells Fabricated

4.5.2 Contact Deposition:

In order to complete the device fabrication, the silver contacts were deposited using Sputtering. Conductive Silver ink was also used. The pressure was raised up to exp-6 Torr and the thickness of the film was set to be 100 nm. The cell were further tested for efficiency measurement.

4.5.3 IV curve Measurement:

The cells were tested using 1 sun solar simulator, which gives the IV-curve. The graph gives the (Isc), (Voc) and Fill Factor (FF) for the device under consideration and this information can be used to compute the performance of the cell.

Summary:

This chapter explained all the experiments carried out for this research. For a complete device fabrication step wise fabrication of all the layers was performed. FTOs were cleaned and Materials chosen for ETL, TiO_2, SnO_2 and TiO_2/SnO_2 were fabricated using spin coating and two sets were made. The first set was further deposited with the Absorber layer (PbI_2+$CH_3NH_3I_3$ + Caffeine) and the second set was subjected to the deposition of Absorber layer (PbI_2+$CH_3NH_3I_3$) without Caffeine. HTL (PbPc) was thermally evaporated and deposited over the Absorber layer for all the cells. All the layers were individually characterized and tested using XRD, SEM/EDS, UV-Vis spectroscopy and Hall Effect. In the last contacts were deposited using RF sputtering. The device was then tested to calculate the cell efficiency using solar simulator.

References

[1] L. Wengeler, M. Schmitt, K. Peters, P. Scharfer, and W. Schabel, *Chemical engineering and processing : process intensification.*, vol. 68. Elsevier B.V, 2000

[2] S. Valligatla *et al.*, "High quality factor 1-D Er^3+-activated dielectric microcavity fabricated by RF-sputtering," , *Opt. Express*,20,19, (2012) 21214

[3] R. Liu *et al.*, "SnO $_2$ -rGO nanocomposite as an efficient electron transport layer for stable perovskite solar cells on AZO substrate," ,*Nanotechnology*, 30, 7, (2019) 075202

[4] Y. Hou *et al.*, "Low-Temperature and Hysteresis-Free Electron- Transporting Layers for Effi cient , Regular , and Planar Structure Perovskite Solar Cells," *Sci. China Chem.*, 62, 7, (2015) 800–809

[5] A. Fakharuddin, F. Di, I. Ahmed, Q. Wali, T. M. Brown, and R. Jose, "Role of morphology and crystallinity of nanorod and planar electron transport layers on the performance and long term durability of perovskite solar cells," , *J. Power Sources*, 283, (2015) 61–67

[6] W. Nanostructured, J. Choi, S. Song, M. T. Ho, H. J. Snaith, and T. Park, "Well-De fi ned Nanostructured, Single- Crystalline TiO 2 Electron Transport Layer for E ffi cient Planar Perovskite Solar Cells," *Adv. Funct. Mater.* 6, 17, (2016) 4746–4752

[7] D. Ouyang, Z. Huang, and W. C. H. Choy, "Solution-Processed Metal Oxide Nanocrystals as Carrier Transport Layers in Organic and Perovskite Solar Cells," *Adv. Funct. Mater.*, 29,1, (2019)1804660

[8] J. Ma *et al.*, "Highly Efficient and Stable Planar Perovskite Solar Cells With Large-Scale Manufacture of E-Beam Evaporated SnO_2 Toward Commercialization," *Sol. RRL*, 1, 10, (2017) 1700118

[9] Q. Liu *et al.*, "Enhanced Stability of Perovskite Solar Cells with Low-Temperature Hydrothermally Grown SnO $_2$ Electron Transport Layers," , *Adv. Funct. Mater.*, 26, 33, (2016)6069–6075

[10] J.-Y. Chen, C.-C. Chueh, Z. Zhu, W.-C. Chen, and A. K.-Y. Jen, "Low-temperature electrodeposited crystalline SnO2 as an efficient electron-transporting layer for conventional perovskite solar cells," , *Sol. Energy Mater. Sol. Cells*, 164, (2017) 47–55

[11] B. Bob, T.-B. Song, C.-C. Chen, Z. Xu, and Y. Yang, "Nanoscale Dispersions of Gelled SnO $_2$: Material Properties and Device Applications," ,*Chem. Mater.*, 25, 23, (2013) 4725–4730

[12] L. Xiong *et al.*, "Fully High-Temperature-Processed SnO $_2$ as Blocking Layer and Scaffold for Efficient, Stable, and Hysteresis-Free Mesoporous Perovskite Solar Cells," , *Adv. Funct. Mater.*, 28, 10, (2018) 1706276

[13] H. Shan, E. Rezaee, X. Leng, X. Wang, Q. Chen, and Z.-X. Xu, "Ultrasonic-Assisted Wet Chemistry Synthesis of Ultrafine SnO $_2$ Nanoparticles for the Electron-Transport Layer in Perovskite Solar Cells," , *ChemSusChem*, 11, 17, (2018) 3000–3006

[14] F. Prokert, "Neutron Scattering Studies on Phase Transitions and Phonon Dispersion in CsSrCl3," , *Phys. status solidi*, 104, 1, (1981) 261–265

[15] J. Rubin, E. Palacios, J. Bartolome, and J. Rodriguez-Carvajal, "A single-crystal neutron diffraction study of NH $_4$ MnF $_3$," , *J. Phys. Condens. Matter*, 7, 3 (1995)563–575

[16] A. Kojima, K. Teshima, Y. Shirai, and T. Miyasaka, "Organometal Halide Perovskites as Visible-Light Sensitizers for Photovoltaic Cells," , *J. Am. Chem. Soc.*, 131, 17, (2009) 6050–6051

[17] S. Hong *et al.*, "A facile and low-cost fabrication of TiO2 compact layer for efficient perovskite solar cells," , *Curr. Appl. Phys.*, 15, 5, (2015) 574–579

[18] N. Ahn, D.-Y. Son, I.-H. Jang, S. M. Kang, M. Choi, and N.-G. Park, "Highly

Reproducible Perovskite Solar Cells with Average Efficiency of 18.3%," , *J. Am. Chem. Soc.*, 137, 27, (2015) 8696–8699

S. Pitchaiya *et al.*, "A review on the classification of organic/inorganic/carbonaceous hole transporting materials for perovskite solar cell application," *Arab. J. Chem.*, 3111440, (2018) 1–12

[19] A. Dualeh, N. Tétreault, T. Moehl, P. Gao, M. K. Nazeeruddin, and M. Grätzel, "Effect of Annealing Temperature on Film Morphology of Organic-Inorganic Hybrid Pervoskite Solid-State Solar Cells," , *Adv. Funct. Mater.*, 24, 21, (2014) 3250–3258.

Chapter # 5

Results & Discussion

This chapter encompasses the results obtained from the characterization and testing methods employed for in-depth study of fabricated ETL. Different properties were studied using the various characterization techniques.

5.1 Tin Oxide Nanoparticle Synthesis

5.1.1 Optimization of SnO_2 Nanoparticles:

The nanoparticles were optimized at different pH levels and different Sintering temperatures. For optimization two major Characterization techniques, SEM and XRD was used. First the pH level was decided considering the % yield and size of the nanoparticles synthesized.

5.1.2 Structural Characterization

Varying the pH:

The nanoparticles were further optimized using different pH level. During the co-precipitation the pH, at which the reaction is to be stopped was varied from pH=5 to pH=8 and pH=11. The XRD comparative graph in figure 4 shows the peaks for pH 5, 8 and 11 respectively. The concentrations of H^+ and/or OH^- ions in the solution deeply effects the morphology of the solution processed synthesized SnO_2 [1]. The solution relatively more acidic at pH 5 will have less concentration of H^+ ions in comparison to OH^-. The NaOH reaction with the $SnCL_2.2H_2O$ causes the formation of $Sn(OH)_2$, during and later the chemical reaction the compound dissociates into Sn^{2+} and OH^- ions. Sn^{2+} plays an important role for SnO_2 nuclei formation when it surpasses the acute level. Nonetheless at pH 11, discrepancies in the OH^- ions concentration occur. Therefore on varying the pH from acidic to basic (5 to 11) the concentration of H^+ ions decreases and the OH^- ions increases, which encourages to form the desired structures [2]. In conclusion we can clearly see the increase in the pH shows reduction in the particle size, in the following XRD results figure 5.1 and table 5.1, the peak values given in the standard Reference code: 01-072-1147.

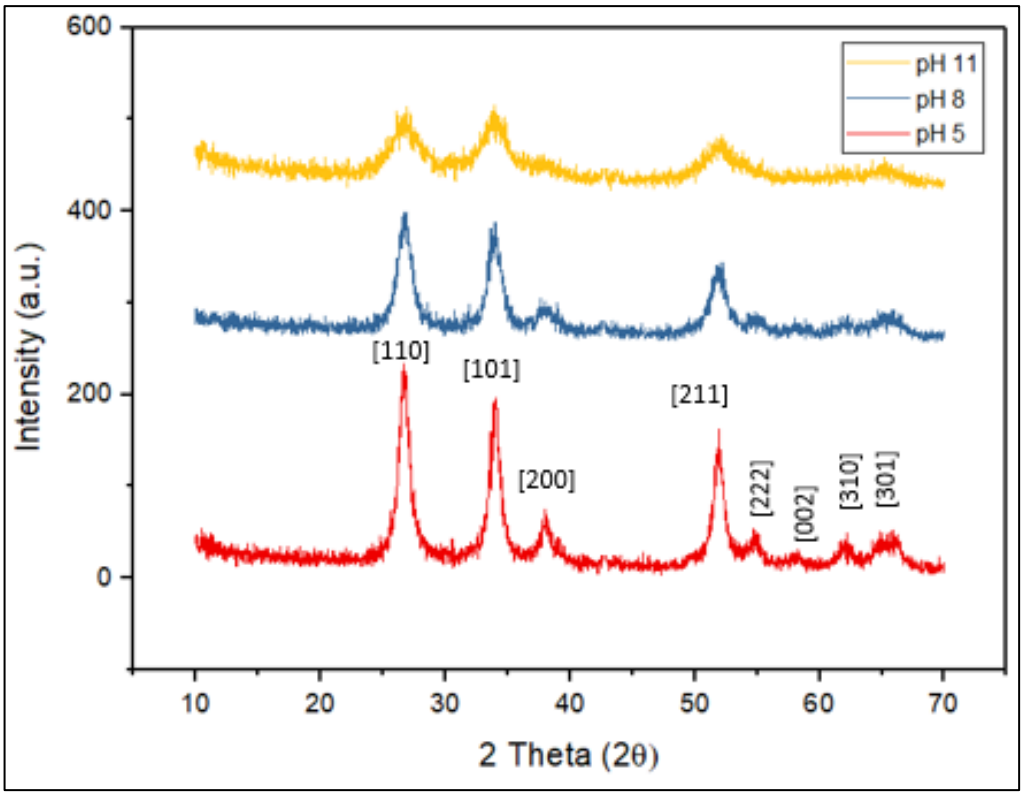

Figure 5.1 XRD pattern of SnO2 nanoparticles at different pH levels

Table 5.1 Effect of sintering temperature on various structural parameters

pH	Crystallite Size by Scherrer equation (nm)	Lattice parameters (Å)		Cell volume (Å^3)	a/c ratio
		a	C		
5	12.53	4.7370	3.1875	71.524	1.486
8	9.85	4.7370	3.1850	71.470	1.487
11	7.86	4.7370	3.180	71.356	1.489

Varying the sintering temperature:

The SnO_2 nanoparticles prepared at three different sintering temperatures have X-ray diffraction patterns as shown in Fig. 2. The XRD assisted to recognize the rutile phase, tetragonal structure of SnO_2 with the major peaks from [110] and [101] planes [3]. The diffraction peaks deduced were at (110), (101), (200), (211), (220), and (113) and were indexed using the software X'pert HighScore and the pikes are accurately alike with

the tetragonal rutile structure of SnO_2 [4], the peak values given in the standard Reference code: 01-072-1147.

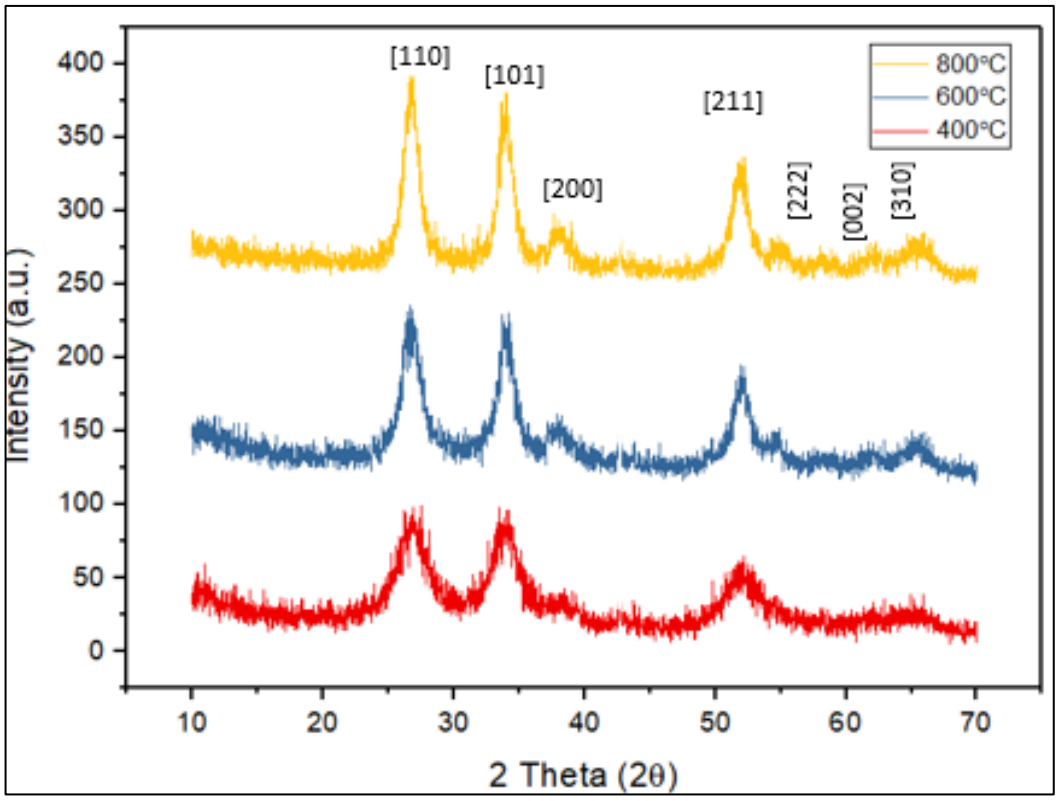

Figure 5.2 XRD pattern of SnO2 nanoparticles at various sintering temperature

The samples sintered at different temperatures has no shift in XRD peaks which indicates that there is no change in the rutile structure with incremental heating. The results demonstrate that as the sintering temperature increases the intensity of peaks has been narrowed expressively. The XRD results indicates that the heating time noticeably effects the crystallization. The experiments revealed that substantial particles start growing around 400°C for SnO_2. The increased temperature speeds up the growth. In addition, it has also been observed that lattice parameters and cell volume. The crystallite size also grow as a function of sintering temperature as given in Table 5.1.

Table 5.2 Effect of sintering temperature on various structural parameters

Sintering Temperature (^{0}C)	Crystallite Size by Scherrer equation (nm)	Lattice strain	Lattice parameters (Å)		Cell volume (Å^3)	a/c ratio
			a	C		
400°C	9.85	7.8×10-^{4}	4.7370	3.1850	71.470	1.487
600°C	16.21	23.5×10-^{4}	4.7401	3.1861	71.653	1.487
800°C	22.60	25.1×10-^{4}	4.7520	3.1875	72.234	1.490

The Debye Scherrer formula is used to calculate the crystallite grains, specified by equation ii

$$D_{hkl} = \frac{0.9\lambda}{\beta cos\theta} \qquad \textbf{(iii)}$$

Where, the wavelength is λ for the X-ray source, FWHM is β in radians unit and θ being angle of the diffraction of the peak in the tetragonal phase. The crystallite size increases with rise in temperature, and that can be because atomic diffusion occurs more at higher temperature.

Morphological Characterization:

The nanoparticles first optimized at different pH were characterized using SEM for morphological studies. The three different pH levels indicated the variations in size of the nanoparticles. The pH varied from 5 to 11 have the following SEM results figure 5.3.

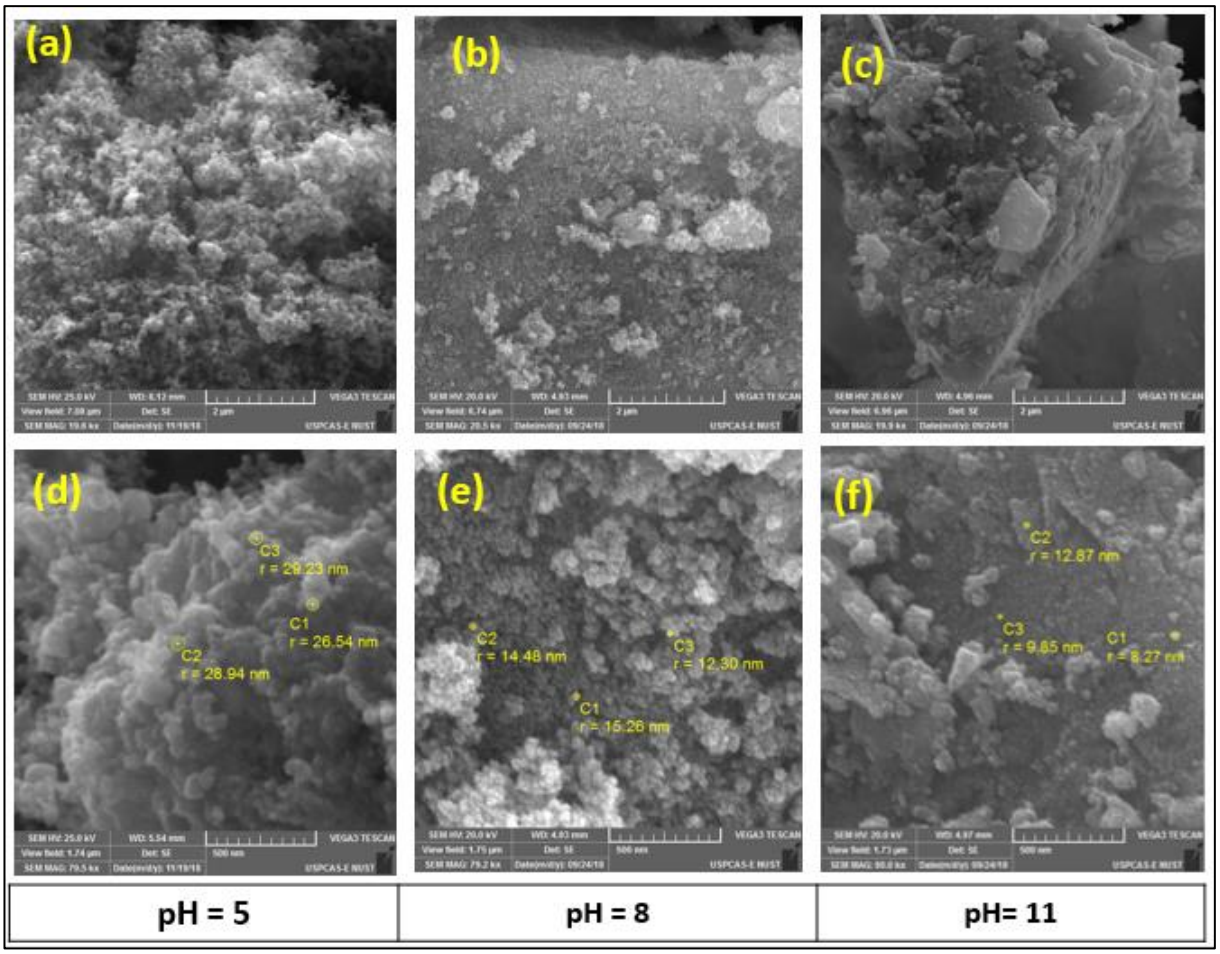

Figure 5.3 SEM images of SnO2 nanoparticles with pH 5, 8 and 11 at 2um (a, b & c) and 500nm (d, e &f)

After the finalization of pH, the sintering temperature was varied and studied the effect on morphological properties of the nanoparticles. The optimization was studied using SEM. The figure 5.4 depicts the SEM images at 2um, these nanoparticles prepared using same recipe were sintered at different sintering temperatures varied from 500 to 800 °C.

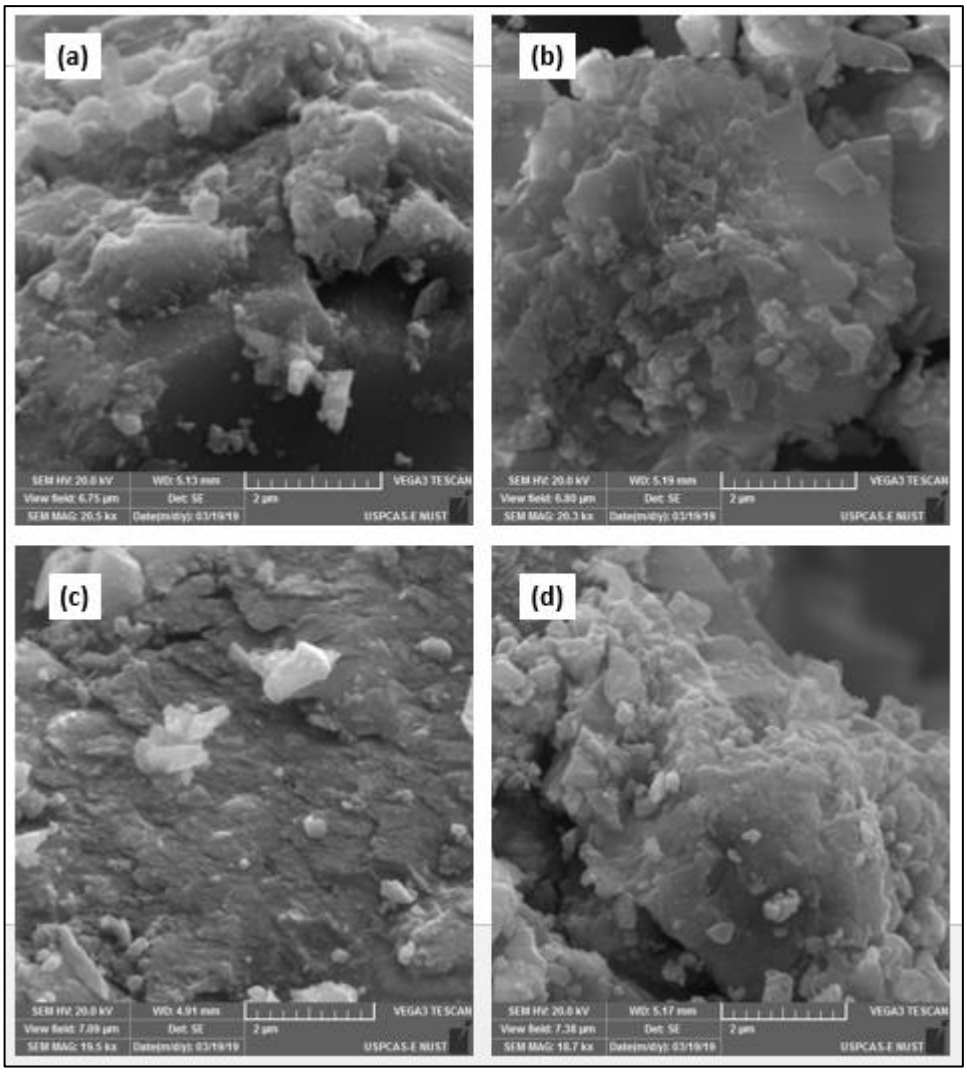

Figure 5.4 SEM images of SnO2 nanoparticles taken at different resolution 2um; varying sintering temperature (a) 500 °C, (b) 600 °C, (c) 700 °C and (d) 800 °C

SEM results shown in figure 5.5, also verify the comment deduced from the XRD data analysis that the particle size also decreases with rise in temperature. SEM images of Sample 1, which was sintered at 400°C showed grain like nano structures with grain size of d= 10.84 nm, sample 2, sintered at 600°C with a grain size of 16.23 nm and sample 3 being sintered at 800°C had a grain size of about 18.73 to 23.71 nm, was observed at 500 nm resolution scale.

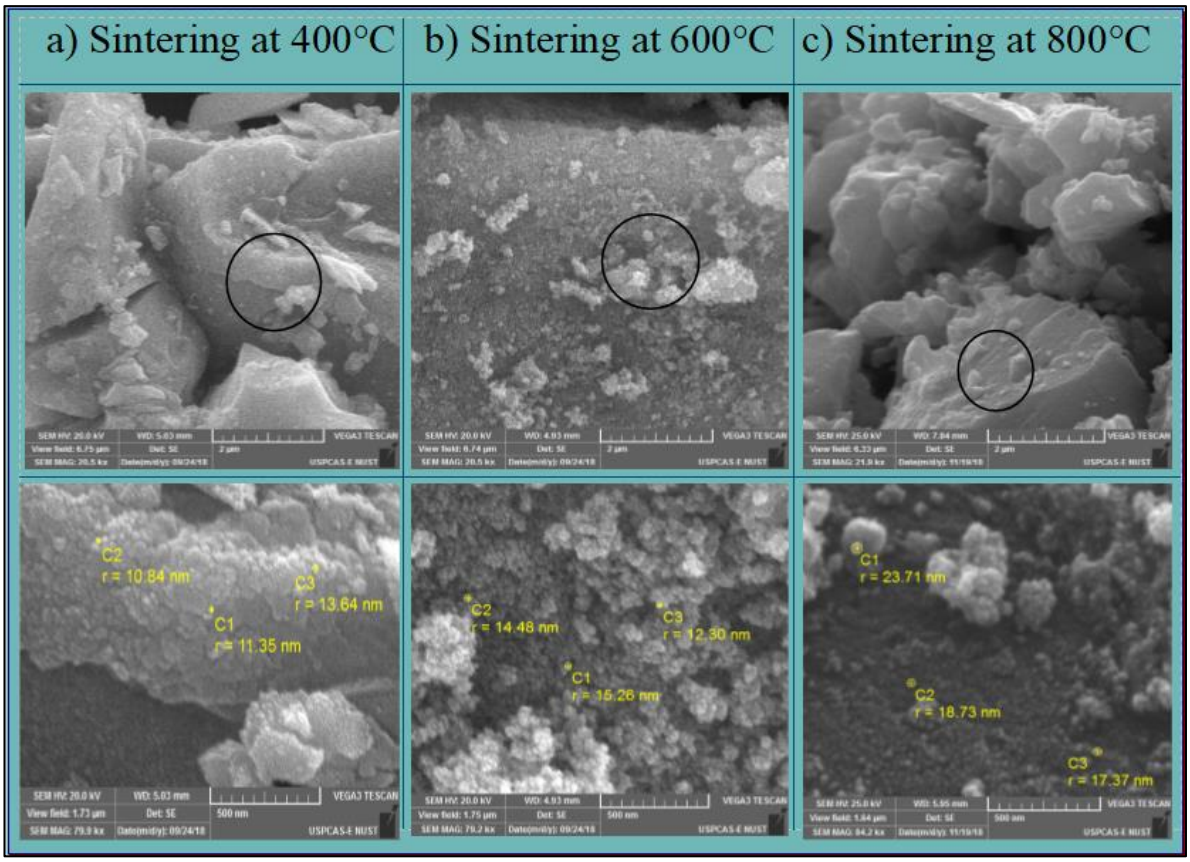

Figure 5.5 SEM images of SnO2 at various sintering temperatures

Once the tin oxide nanoparticles synthesis parameters were optimized, the major task of electron transport layer was started. The deposition of three different ETLs was carried out using spin coating.

5.2 TiO_2 ETL

The TiO_2 blocking layer paste already purchased, was spin coating on the cleaned FTOs. The procedure was first optimized and the results deduced from the optimized TiO_2 ETL were very satisfying.

5.2.1 Structural Characterization:

For structural characterization XRD was done for the phase identification of TiO_2 films being deposited on FTOs. The XRD of TiO_2 on FTO deposited via spin coating is shown in figure 5.6 and also in comparative graph in 5.10 in 2θ range of 20° to 80°. It shows major anatase peaks as per JCPDS card number 21-1272. The 2θ at peak 25.8° confirms the TiO_2 anatase structure [5]. There is no unwanted/false diffraction peak found in the sample, which shows that there is no impurity in the sample. The XRD pattern of TiO_2 shows peaks at 25.8°, 37.7°, 48.01°, 53.8° , 55.03° & 62.10° can be

assigned to [101], [112], [200], [105] , [211] & [204] planes respectively with tetragonal anatase structure [6]. Anatase phase of TiO_2 show properties like large mobility and wider optical absorption gap.

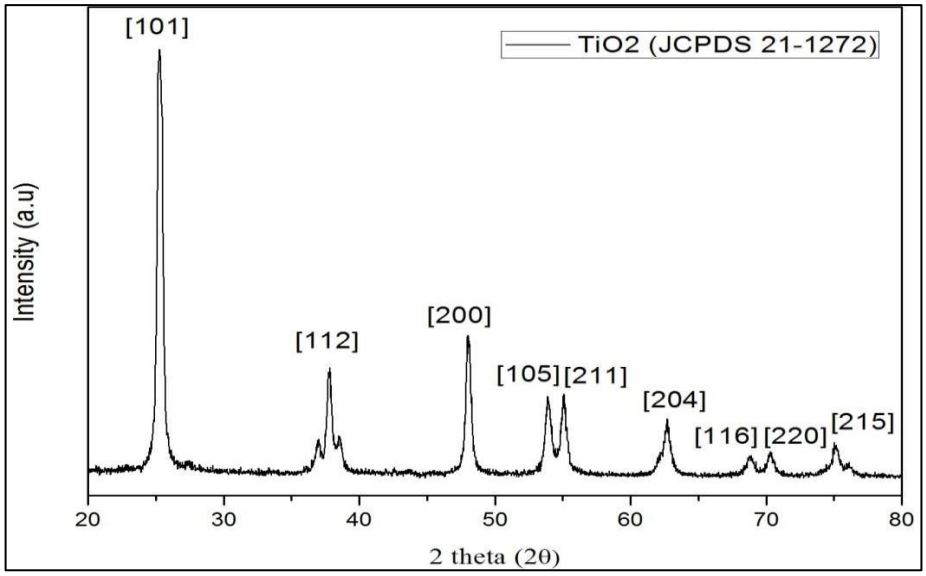

Figure 5.6 XRD pattern of TiO_2 on FTO

5.2.2 Morphological Characterization:

For morphological Analysis of the TiO_2 films deposited on FTO, SEM was conducted for the samples. The films were optimized using different rotation speed and spinning time. The first set was spin coated at 1500 rpm for 30 seconds and the second set was spin coated at 3000 rpm for 30 seconds. The film results were not so good, there was dispersion of the particles and the film was not homogenous. Figure 5.7 shows the first two sets of the TiO_2 films being deposited using spin coating.

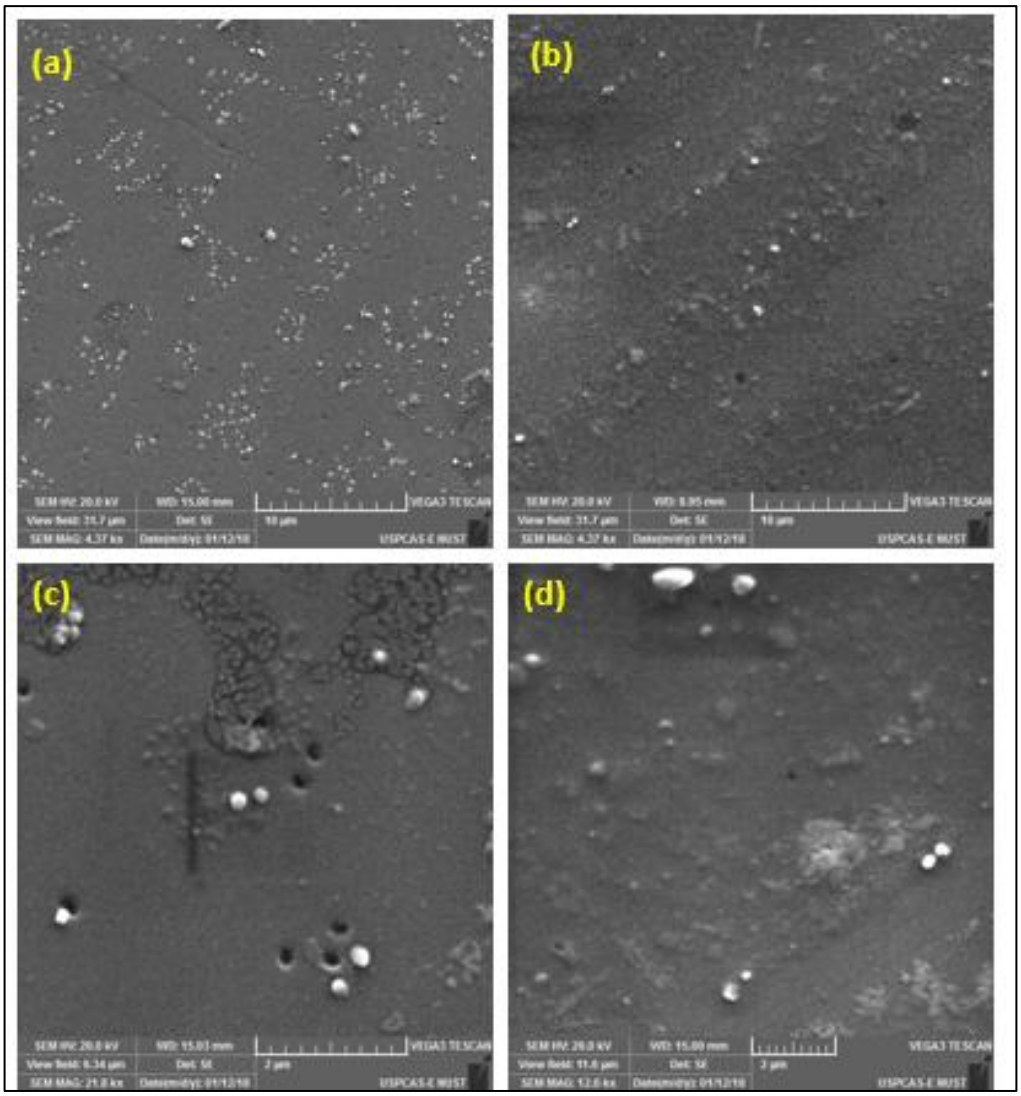

Figure 5.7 TiO_2 films deposited using spin coating at resolution 10um and 2um, (a &c) at 1500 rpm and (b & d) at 3000rpm

The experiments were then repeatedly undertaken for deposition of TiO_2 using spin coating to ultimately get a uniform and homogenous film with a good thickness. The rotation was increased from 3000 to 5000rpm and time was set at 50 sec. the films deposited were far better than the previous one but still had some cracks. These cracks were studied and compared with the literature and concluding the reasons because of the heating of the film [7]. The films were then dried after every film deposition with a step of 5°C per 2 minutes. Figure 5.8 shows the results obtained after step heating and before.

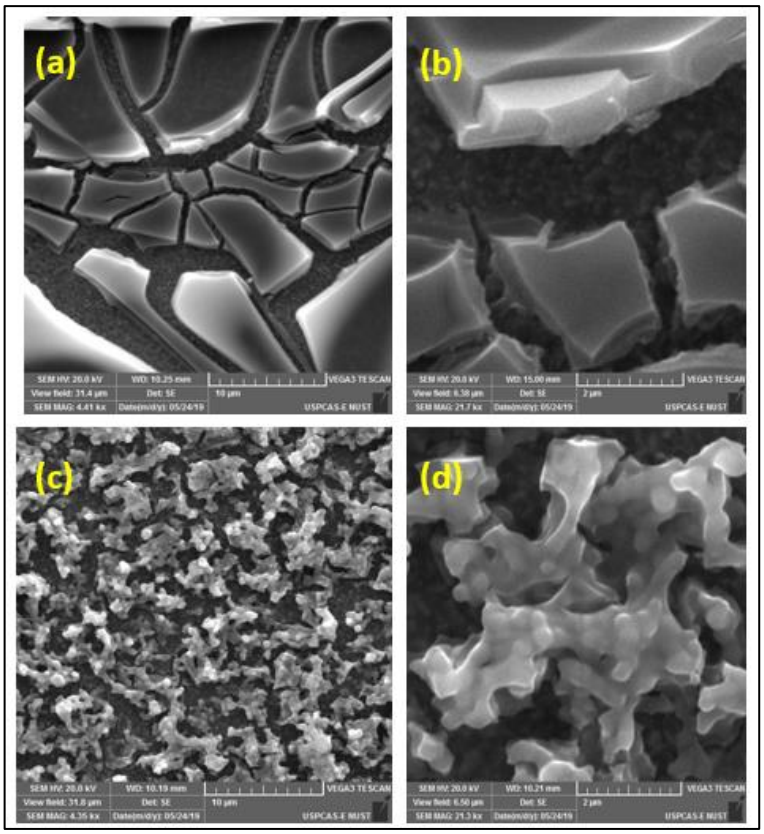

Figure 5.8 SEM images of TiO2 deposited at 5000 rpm for 50 seconds at 10um and 2um resolution, (a & b) direct annealing and (c & d) step annealing

The cracks in the films were further analyzed and hence via step annealing starting from 30°C to 90°C in a Mermet drying oven with a heating ramp of 5°C/2mins. The final films obtained were therefore homogenous and very thin up to 50nm. Figure 5.9 shows the SEM images of TiO_2 optimized at 5000 rpm and after step annealing. Further sintered at 475°C.

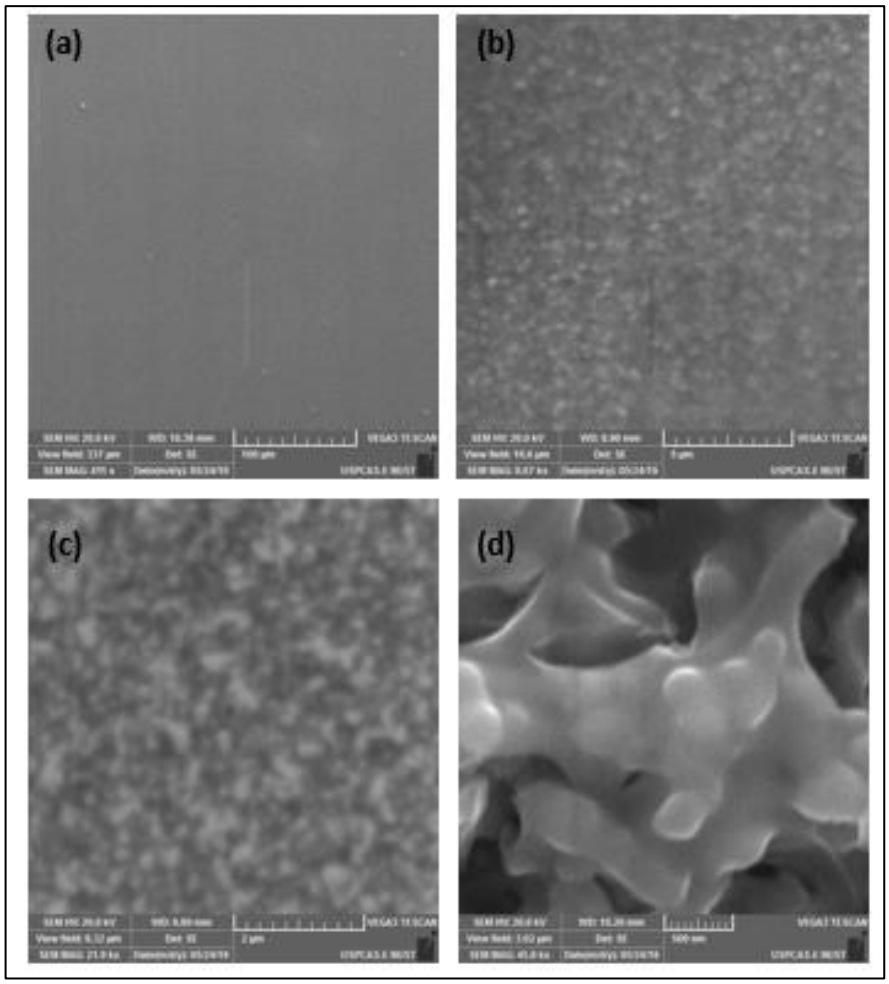

Figure 5.9 SEM images of TiO_2 deposited at 5000rpm and sintered at 475°C after step annealing at (a) 100um, (b) 5um, (c) 2um and (d) 500nm

5.3 SnO_2 ETL

The SnO_2ETL was spin coating on the cleaned FTOs. The material was prepared by using Co-precipitation Technique. The procedure was first optimized and the results deduced from the optimized SnO_2 ETL were very satisfying. Optimization of the films lead to very important results for ETL, leading to prove that the low temperature sintering had better results and hence low temperature processed ETL was fabricated.

5.3.1 Structural Characterization:

XRD pattern of SnO_2 film being deposited via spin coating is shown in figure 5.11 a and 5.11 b. SnO_2 is present in its rutile phase. The broad diffraction peak of SnO_2 at 26.3° shows its rutile phase. The XRD pattern in figure shows peaks at 26.3°, 33.6°, 52.8° and 62.8° can be assigned to planes of [110], [101],[211] and [310] respectively as per (reference card number: 01-077-0452). Like TiO_2 there is no false

peak present. Both of the SnO_2 films deposited via spin coating and differ by the sintering temperature of 90°C and 475°C showed the same plane orientation as shown in the graphs.

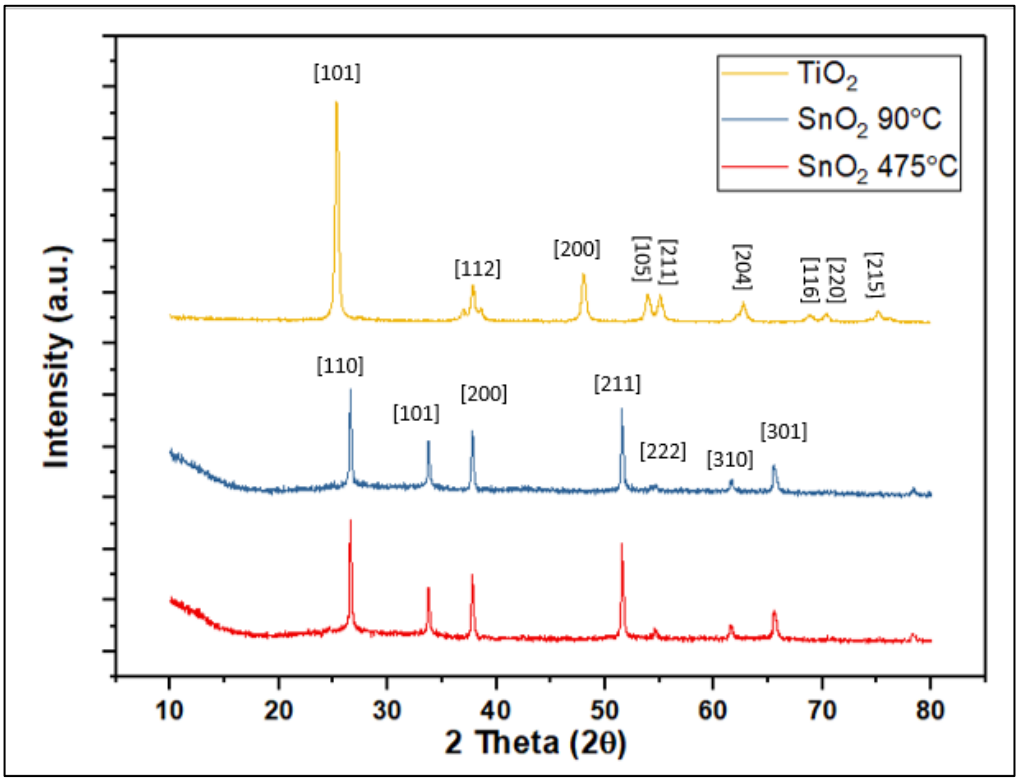

Figure 5.10 XRD comparative pattern of TiO2 and SnO2 sintered at 475°C and 90°C

5.3.2 Morphological Characterization:

For morphological Analysis of the SnO_2 films deposited on FTO, OM and SEM was conducted for the samples. The films were optimized using different rotation speed and spinning time. The first set was spin coated at 2500 rpm for 35 seconds and the second set was spin coated at 5000 rpm for 35 seconds. The third and fourth sample set was spin coated at 8000 and 10000 rpm. The film results were not so good, there was dispersion of the particles and the film was not homogenous. Figure 5.11 shows the first two sets of the SnO_2 films being deposited using spin coating. The first problem encountered was the cracks and uneven film distribution. The issues were resolved by step annealing and the optimization of the rpm.

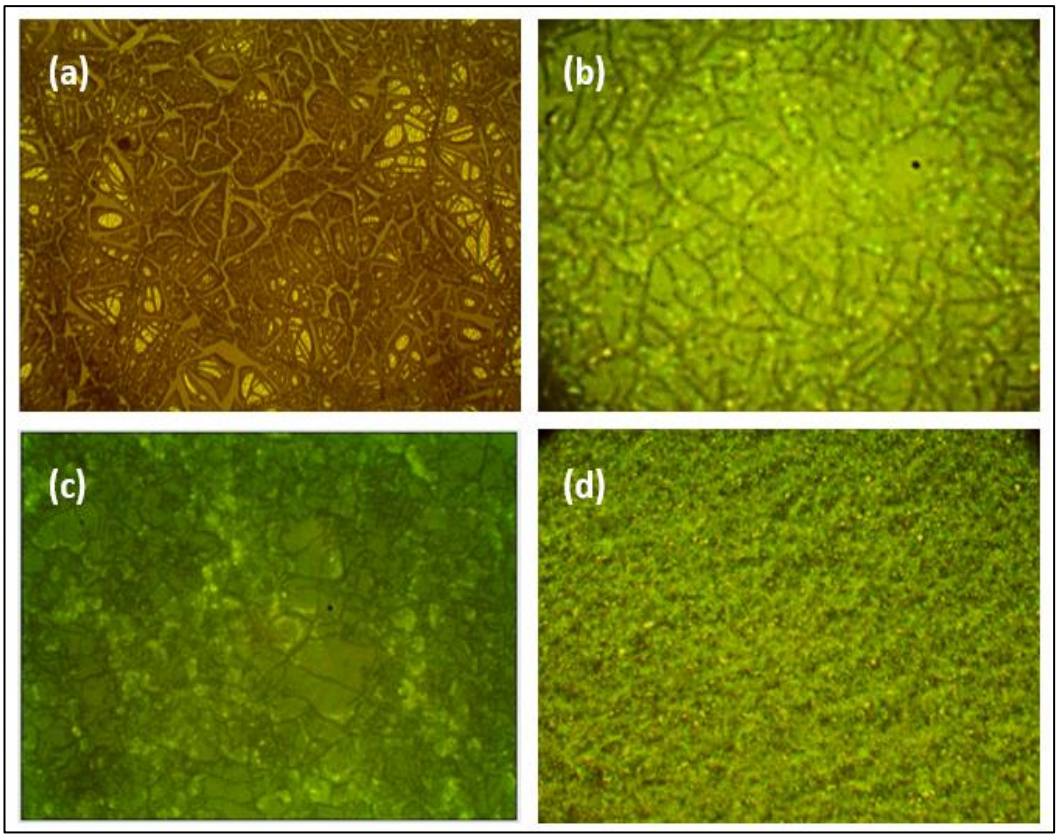

Figure 5.11 Optical Microscopic images of SnO2 films at x50 resolution, samples spin coated at (a) 2500rpm, (b) 5000 rpm, (c) 8000 rpm and (d) 10000 rpm

The SEM images can clearly show the cracks of the film without step annealing, figure 5.12. The cracks were studied and it was concluded that without the step annealing, the moisture trapped in each film escapes when heated in the end leaving the cracks.

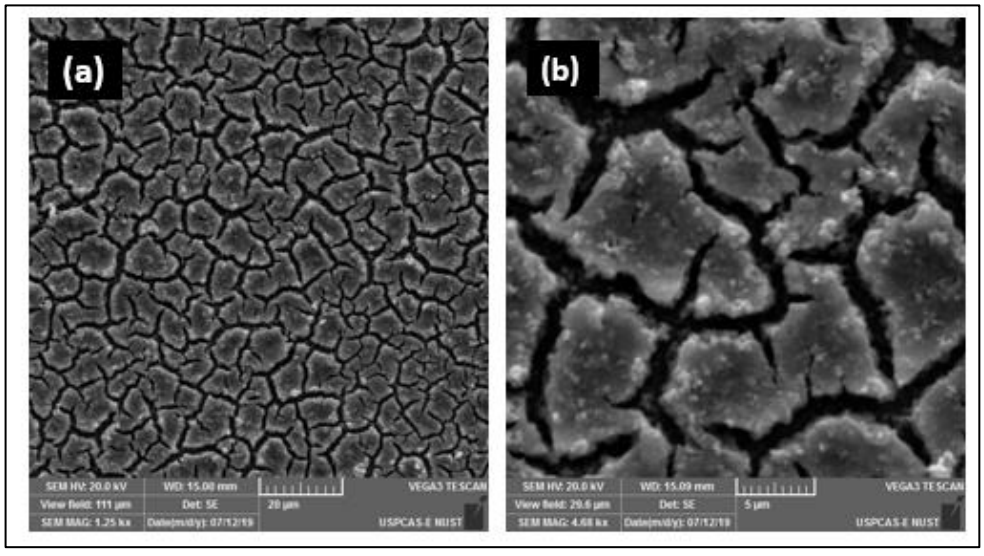

Figure 5.12 SEM images of SnO2 films without step annealing at (a) 20um and (b) 5um

Step annealing for each film after deposition was done from 40°C to 90°C and films obtained were homogenous and crack free. The final sintering at 90°C and 475°C of SnO_2 SEM images are shown in figure 5.13. The images of SnO_2 films depicting the grain like structure have been reported widely in literature [8][9][10] and the morphological properties revealed that the film does not need the high temperature sintering. The images are taken at different resolution of 5um, 2um and 500nm.

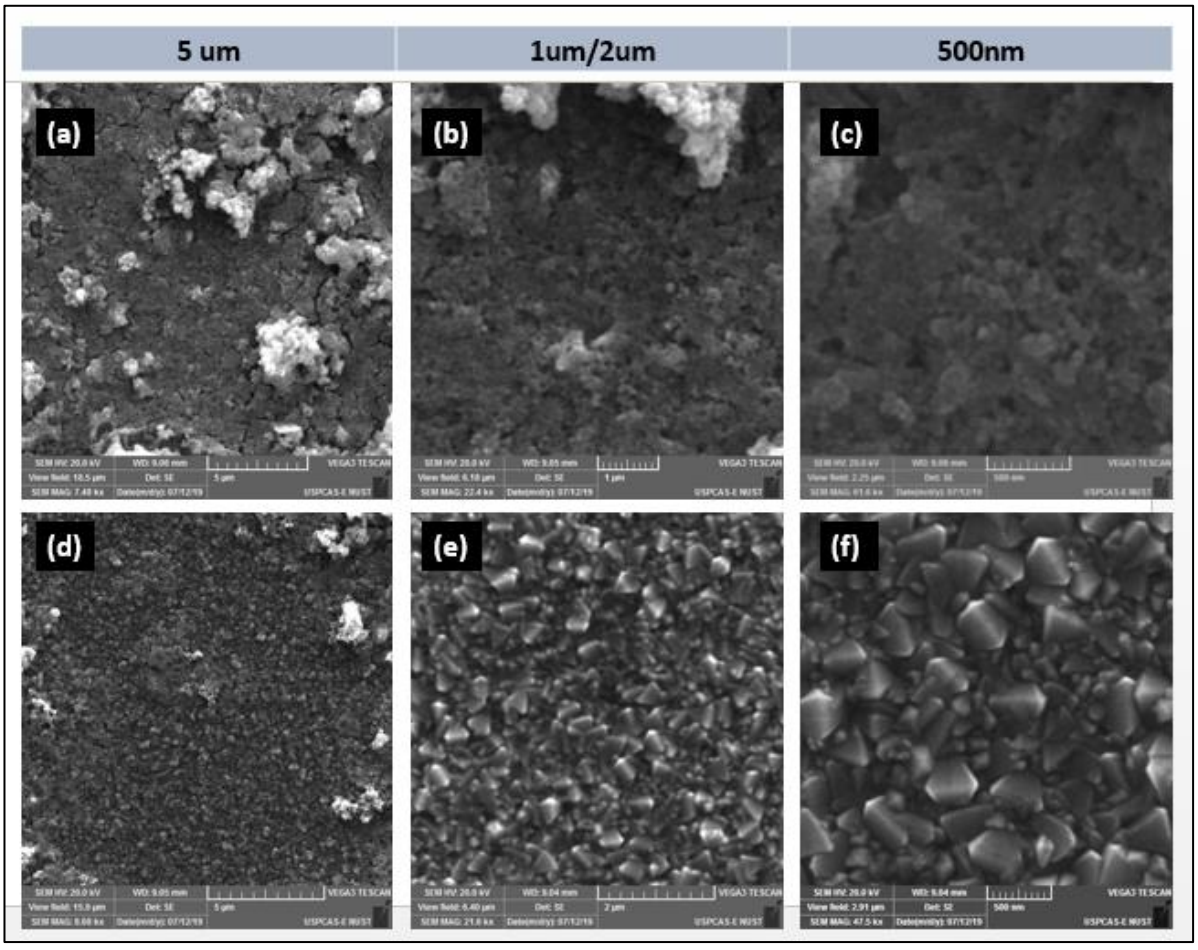

Figure 5.13 SEM images of SnO2 films at 5um, 1um/2um and 500nm of sample sintered at 475°C (a, b, c) and sintered at 90°C (d, e, f)

5.4TiO_2/SnO_2 ETL

5.4.1 Structural Characterization & Morphological Characterization

This ETL contains the both blocking layer composed of TiO_2 and then over that second layer composed of SnO_2. The structural analysis was done using XRD and because of SnO_2 film being on top the XRD spectra was of tin oxide, results displayed were identical of that figure 5.10. The morphological study of this multilayer ETL was done using SEM and the images obtained were same for the tin oxide ETL because of

the SnO_2 on the top as reported by various researchers in their published works [11][12][13] as already described in figure 5.13.

5.5 Comparative Analysis of Optical & Electrical Properties of ETLs

All the three ETLs, TiO_2, SnO_2 and the composite TiO_2/SnO_2 were compared by characterizing them for their optical and electrical properties.

5.5.1 Optical Characterization:

The transmittance and the absorbance spectra of TiO_2, SnO_2 and the composite TiO_2/SnO_2 were studied for optical characterization of the ETL using UV-Vis NIR spectrophotometer The visible light lies between the wavelengths of 400-800 nm. In view with that the graph in the figure shows that the around 60-70% of light for TiO_2 is passing within the visible region, reported widely [14]. The percentage of Transmittance for TiO_2 thin films decreases during annealing from 300°C to 600°C and the fabricated films are annealed around 500°C, this is attributed to the fact of increase in the light diffusion with the crystallite size [15]. Also, thin films having single layer show a higher transmittance in comparison to the films with multiple layers, hence the multiple coating on a samples results in a decrease in the %Transmittance, providing that three layers were spin coated for TiO_2 films and around 70% transmittance was achieved. Whereas for SnO_2 the % transmittance is a little higher than TiO_2 around 73%. SnO_2 with a larger bandgap then the TiO_2 [16]. But somehow for the composite layer TiO_2/SnO_2 the transmittance graph drops till 65%.

The Absorbance was measured through same procedure. Figure 5.14 a and 5.14 b shows the Transmittance and Absorbance spectra of the TiO_2, SnO_2 and the composite TiO_2/SnO_2 ETL proving it highly transmitting in visible region.

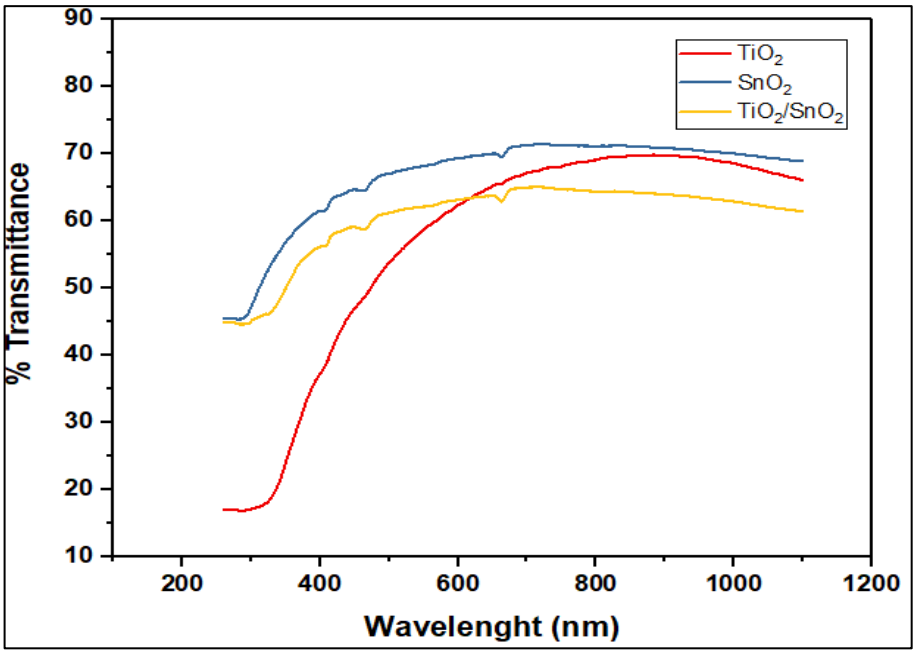

Figure 5.14 Comparison of %Transmittance for TiO2, SnO2 & TiO2/SnO2

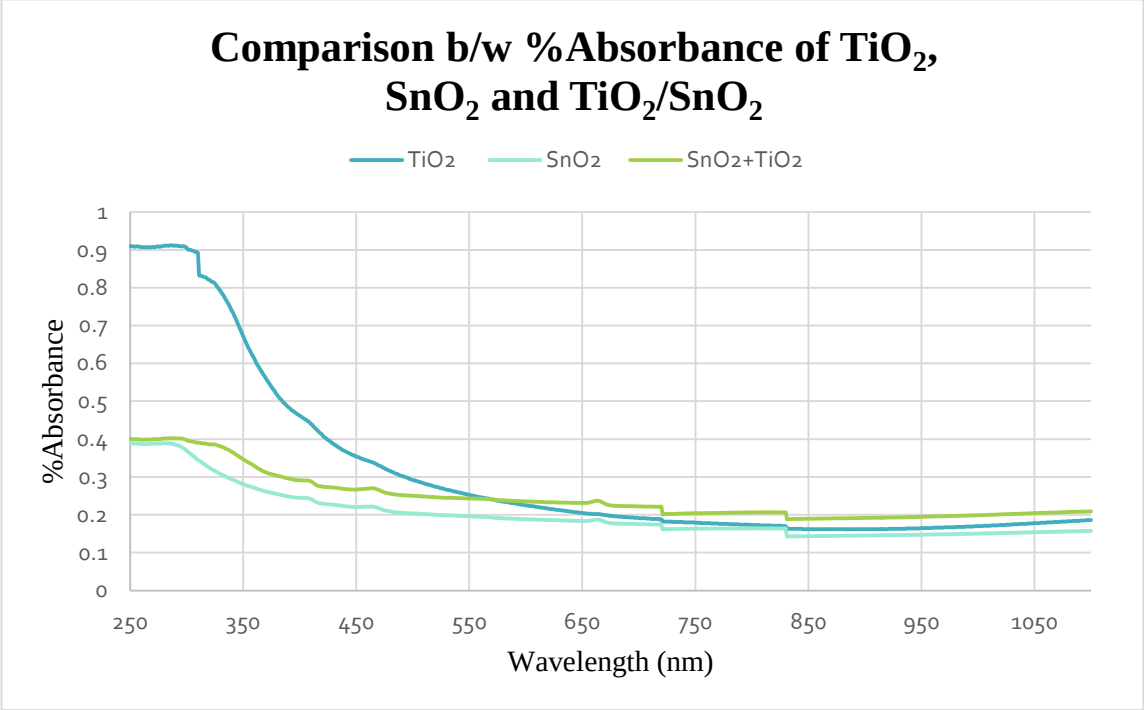

Figure 5.15 % Absorbance of TiO2, SnO2 & TiO2/SnO2

5.5.2 Electrical Properties:

Electrical properties of TiO_2, SnO_2 and the composite TiO_2/SnO_2 deposited on glass slide were studied using Hall Effect measurement system. The test also help

detecting the p or n type nature of the material in addition to providing the charge concentration, resistivity and conductivity values. TiO_2, SnO_2 and TiO_2/SnO_2, all three as an ETL were proved to be n-type material. The conductivity, mobility and carrier concentration of SnO_2 are shown in the table given.

Table 5.3: Hall Effect Measurements done for the ETLs

Sample	Mobility $cm^2 V_s^{-1}$	Carrier Concentration cm^{-3}	Conductivity (1/ Ω cm)	Resistivity Ω cm
TiO_2	$3.659x10^{1}$	$-5.150x10^{14}$	$3.019x10^{-3}$	$3.312x10^{2}$
SnO_2	$1.397x10^{-1}$	$-3.446x10^{16}$	$7.715x10^{-4}$	$1.296x10^{3}$
TiO_2/SnO_2	$1.72x10^{-1}$	$-9.700x10^{14}$	$2.738x10^{-5}$	$3.653x10^{4}$

A comparison of the R_s, ρ and σ values of the respective films shows that the conductive performance of the TiO_2 ETL is good. The TiO_2 resistivity values are up to exponent 2 as compared to the SnO_2 the resistivity values are up to exponent 3 which means the conductivity in fact for Tin oxide films is low than the TiO_2 films. The multilayer TiO_2/SnO_2 ETL showed resistivity higher than both the TiO_2 ETL and SnO_2 ETL.

5.6 Absorber Layer (Perovskite)

5.6.1 Morphological Characterization:

The morphological Analysis was done using SEM for the Absorber layer, Perovskite layer. The images were taken at 2um and 500nm. The structure of the absorber layer, MAI and lead iodide was depicted in the images. Figure 5.16

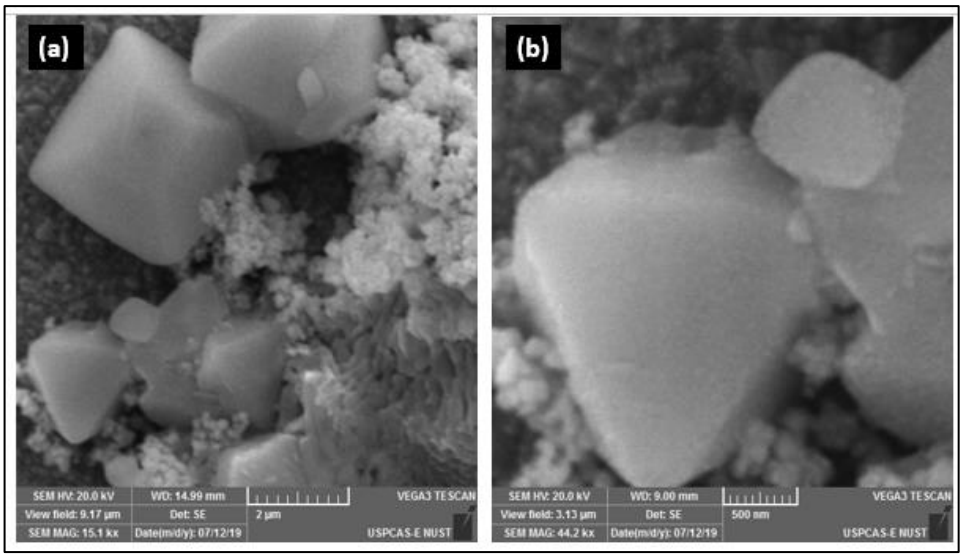

Figure 5.16 SEM images of Absorber Layer at (a) 2um and (b) 500nm

5.6.2 Optical Characterization

The transmittance and the absorbance spectra of the Absorber layer were studied for optical characterization using UV-Vis NIR spectrophotometer. The visible light lies between the wavelengths of 400-800 nm. Depending upon the absorbance range, the layer was optimized by varying compositional geometry. Starting from the $CsMAIPbI_3$ with equal ratios (1:1), the lead iodide first spin coated and then dip coated in MAI solution with Cesium. Another absorber layer with addition of caffeine in MAI layer was studied. $CsMAIPbI_3$ single step spin coated, and dual step spin-dip coated, $MAIPbI_3$ spin-dip coated with and without caffeine and the best shown absorbance window was obtained for $CsMAIPbI_3$ with two steps of spin and dip coating.

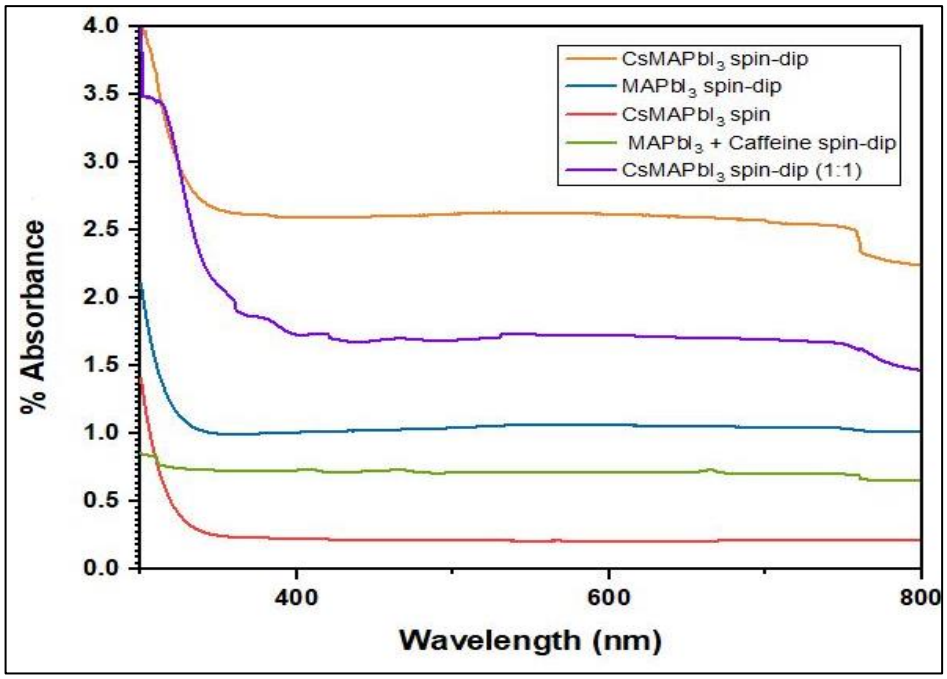

Figure 5.17Absorber Layer Optimization by varying compositional geometry

5.7 PbPc HTM

5.7.1 Morphological Characterization:

SEM with high intensity electron beam incident upon the surface of the specimen to attain information about the surface morphology.

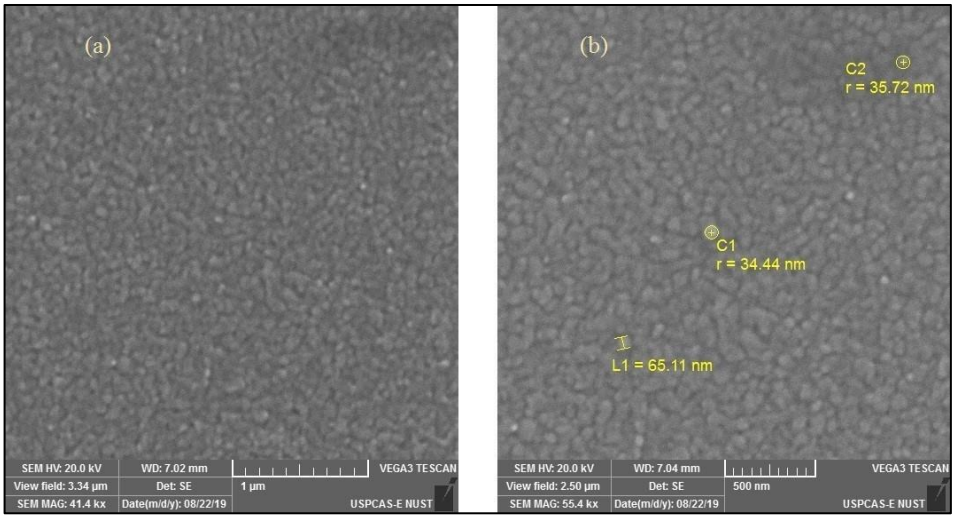

Figure 5.18 SEM of PbPc on FTO Glass at (a)1um and (b) 500nm

SEM was done at 5 um and 500 nm. The results show that films were smooth and evenly distributed even at the higher resolutions. The formation of such smooth and compact layers is due to high vacuum conditions, higher melting point of PbPc of around 230°C and the fact that it sublimes.

5.7.2 Structural Characterization

XRD peaks of the samples used relate to the peaks available for PbPc in literature. The peaks were found coherent to the α-phase of PbPc which objectively is responsible for hole transport purposes. The characteristic peaks at 12.61° and 16.51° correspond to the (320) and (420) monoclinic diffraction planes, respectively[17]. It suggests that thermal evaporation is the right tool to deposit PbPc on any surface.

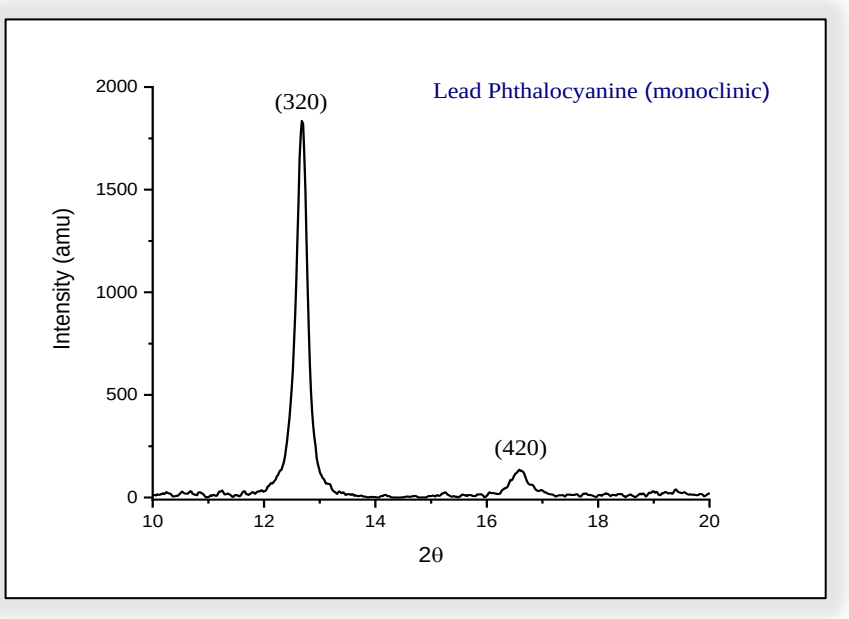

Figure 5.19 XRD of PbPc on FTO glass suggesting the peaks at □-phase

5.7.3 Optical Characterization

UV-Vis yields a spectrum of absorption and transmittance of light which provides knowledge about the light regions passing through various wavelengths. The visible light lies between the wavelengths of 400-800 nm. In view with that the graph in the figure shows that the around 35% of light for PbPc is passing within the visible region. As solar light which is harnessed for solar cell purposes lie within visible range, so, PbPc provides high transmittance for such light.

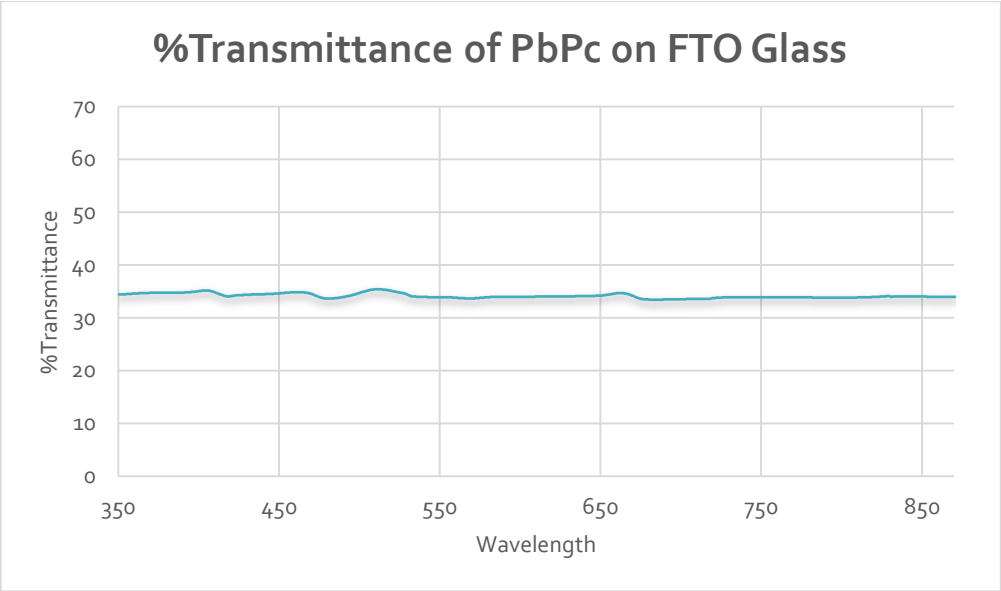

Figure 5.20 %transmittance of PbPc coated on FTO Glass using UV-VIS-NIR

5.7.4 Hydrophobicity Measurement

Contact angle for the fabricated PbPc films was observed using a goniometer. A 3-µm sized water droplet was poured upon the surface of slide. The contact angle of about 86.1° was observed which suffice the hydrophobic characteristics of the film. In general, the surfaces generating an angle of more than 90° are referred to as hydrophobic but with keeping view the viscosity of water, any angle closer to 90° is highly hydrophobic.

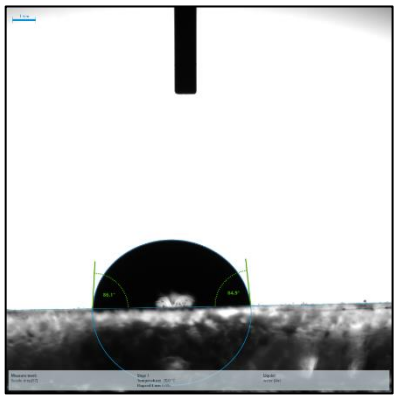

Figure 5.21 Contact Angle Measurement of PbPc on FTO Glass via Goniometer

5.8 I-V Characterization

PbPc based cells showed I-V character but with poor efficiency. There were some issues regarding perovskite layer deposition. So, I-V Curve generated showed very

little Current and Voltage value. Input power was taken as 0.1W/cm^2. Most of the cells showed short circuiting results.

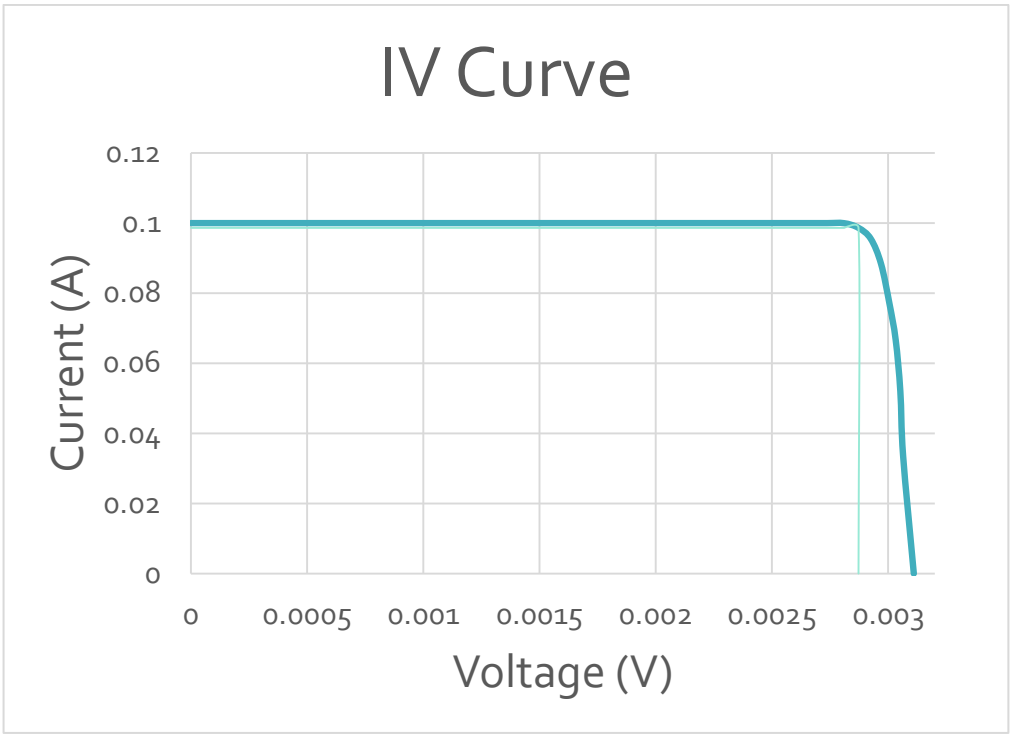

Figure 5.22 I-V Curve for PSC without caffeine

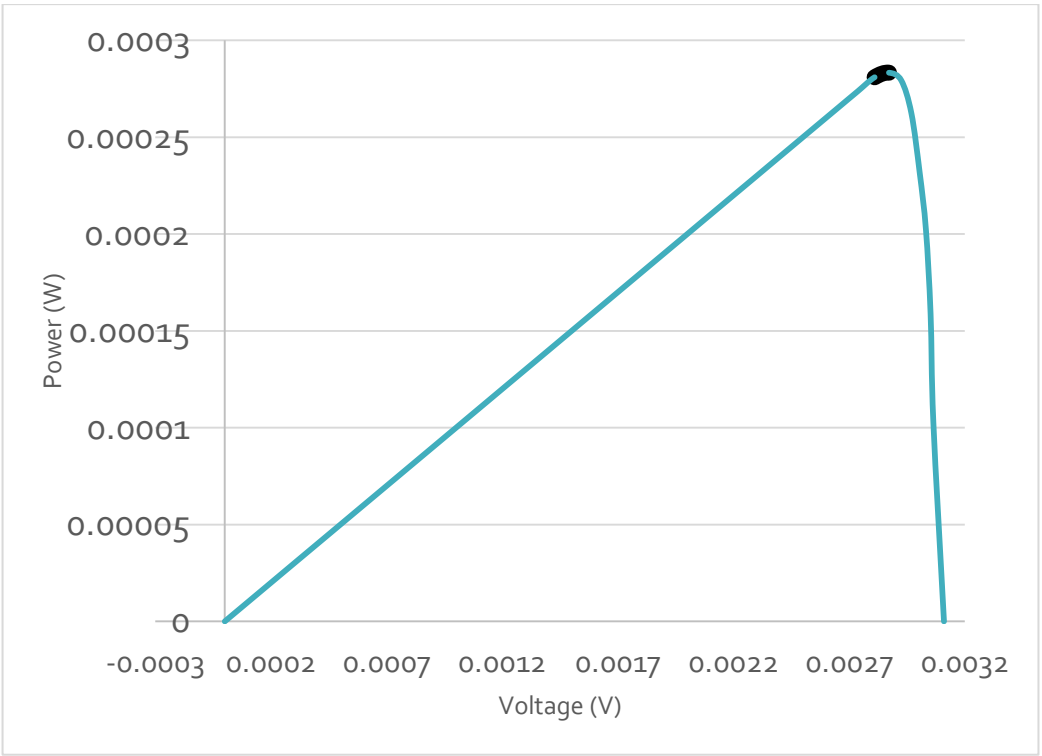

Figure 5.23 Power and Voltage curve for MPP

Table 5.4 Results drawn from IV Curve

Open Circuit Voltage	V_{oc} (V)	0.00311
Short Circuit Current	I_{sc} (A)	0.09999
Max. Power Point	M_{pp} (W)	0.00031
Voltage at M_{pp}	V_{mp} (V)	0.00287
Current at M_{pp}	I_{mp} (A)	0.09863
Fill Factor	F.F.	0.91091
Efficiency	η	0.28%

The reason behind such low efficiency is incomplete formation and degradation of perovskite layer. As dip coating was used for the absorber layer formation and a single solution of $CH_3NH_3PbI.PbI_2$, DMSO in DMF was used, which seems to be an unadvised option for further studies.

References:

[1] O. Rac, P. Suchorska-wo, M. Fiedot, and H. Teterycz, "Influence of stabilising agents and pH on the size of SnO 2 nanoparticles," , *Int. J. Solids Struct* 34. 4 (2014) 2192–2201

[2] M. Priya, S. Geetha, and A. Ramamurthi, "Effect of pH and annealing temperature on the properties of tin oxide nanoparticles prepared by sol – gel method,", *J. Mater. Sci. Mater. Electron.*, 58, 18, (2017) 675-689

[3] N. Hamdadou, "*Improved Properties Of Sno 2 Thin Films Obtained Via Spin Coating Method By Varying The Solution Concentration*," , *Mater. Sci. Pol.* 25, 7, (2018) 1–9

[4] P. Sarabadani, M. Sadeghi, M. Ghasemi, Z. Asadollahi, and N. Afshari, "Synthesis and Characterization of Tin Oxide Nanoparticles by Solid State Chemical Reaction," , *Adv. Funct. Mater* 78.(2011) 131–140

[5] Thirugnanasambandan Theivasanthi* and and Marimuthu Alagar, "XRD analysis of Titanium dioxide Nanoparticles.," *Chem. Mater*. 47. 23.(2014) 176-182

[6] T. Ye, Z. Suo, and A. G. Evans, "Thin film cracking and the roles of substrate and interface," *Int. J. Solids Struct.*, 29, 21,(1992) 2639–2648,

[7] K. Sujatha, T. Seethalakshmi, and O. L. Shanmugasundaram, “Synthesis, Characterization of Nano Tin Oxide via Co-precipitation Method,” , *Nanotechnol. Res. Pract.*, 11, 3, (2016) 98–105.

[8] B. Bob, T. Song, C. Chen, Z. Xu, and Y. Yang, “Nanoscale Dispersions of Gelled SnO 2 : Material Properties and Device Applications,” *Chem. Soc.*, 131, 17, (2013) 6050–6051

[9] S. Tazikeh, A. Akbari, A. Talebi, and E. Talebi, “Synthesis and characterization of tin oxide nanoparticles via the Co-precipitation method,” , *Mater. Sci. Pol.*, 32, 1, (2014) 98–101

[11] W. Zhao *et al.*, “Synthesis, characterization, and photocatalytic properties of SnO2/rutile TiO2/anatase TiO2 heterojunctions modified by Pt,” *J. Phys. Chem. C*, 118, 40,(2014) 23117–23125

[12] S. N. Kane, A. Mishra, and A. K. Dutta, “Preface: International Conference on Recent Trends in Physics (ICRTP 2016),” *J. Phys. Conf. Ser.*, 755, 1, (2016) 2–7

[13] C. Messaadi, M. Ghrib, H. Chenaina, M. Manso-Silván, and H. Ezzaouia, “Structural, optical and electrical properties of SnO2doped TiO2synthesized by the Sol–Gel method,” *J. Mater. Sci. Mater. Electron.*, 29, 4, (2018) 3095–3103,

[14] T. K. C. yu. M . Evushenko, S.V. Romanshkin, N.S. Trofimov, “optical properties of titanium dioxide films,” *Sci. direct Phys. Procedia*, 73, (2018) 100-107

[15] M. Ben Karoui, Z. Kaddachi, and R. Gharbi, “Optical properties of nanostructured TiO2 thin films,” , *J. Phys. Conf. Ser.*, 596, 1, (2015) 13-23

[16] I. Nanomaterials, “chapter 5 structural , optical and electrical properties of ni doped sno 2 nanoparticles,” *Adv. Funct. Mater* 26. (2017) 123–157.

[17] L. Ottaviano, L. Lozzi, A. R. Phani, A. Ciattoni, S. Santucci, and S. Di Nardo, “Thermally induced phase transition in crystalline lead phthalocyanine films investigated by XRD and atomic force microscopy,” *Appl. Surf. Sci.*, 136, 1, p(1998) 81–86,

Chapter # 6

Conclusions and Recommendations

This chapter sheds light on the conclusions drawn from the undertaken studies and what could possibly be recommended on their basis.

6.1 Conclusions

Following conclusions can be drawn from the results mentioned in precious chapter:

- Co-precipitation method yields very fine grain like nanoparticles of SnO_2 and the procedure was optimized by varying the pH and sintering temperature.
- The SnO_2 nanoparticle gel prepared through co-precipitation was spin coated and smooth films were obtained, thus the SnO_2 ETL was fabricated.
- TiO_2 blocking paste being spin coated and sintered lead to highly uniform and compact film as ETL.
- Both of the SnO_2 and TiO_2 films had great properties as ETLs and the characterizations showed very promising results to be used in Perovskite solar cell.
- The multilayer ETL comprising of TiO_2 and SnO_2 also showed favorable properties for electron transport.
- The Absorber layer fabrication was quite challenging for the case to avoid the moisture content to have an efficient cell.
- The so far optimized coating of the absorber layer did not operate so well in the cell structure for all the PSC's tested in the lab.
- Thermal Evaporation of PbPc yields smooth and compact films with the required α-phase structures, which are essential for hole mobility, thus proving the HTM nature.
- PbPc films bear good hydrophobic properties due to smooth and compact distribution of films hence making PbPc as a protective HTM for the PSCs.
- Contacts deposition was successful attempt using RF sputtering and fine films were achieved.

The final contact coating has to be done and the results for PSCs have to be collected which are going to be fruitful. Overall in this whole process of optimization and characterization of the films, the comparative analysis done for three different ETLs, between two majorly dip coated absorber layer and also the HTMS.

6.2Recommendations

- Various other synthesis techniques can be used for the Electron Transport materials and doping of different materials can be studied.
- The ETLs should be in-corporate within a cell to check its efficiency, provided that the Absorber layer is fully optimized and stable functioning.
- Other types of HTM can be also be studied and doping of the alkali metals can be consider. Also the carbon nanomaterials effect on the properties of the HTM should be studied for a protective and efficient HTL.

Other recommendations that can be suggested for the field of research are:

6.2.1 Optimization of Coating Processes:

The low-cost solution based coating techniques can be optimized to yield better thin films. Better properties and morphology of semiconductor thin films are beneficial for better working of the cell. Vacuum based techniques are expensive but they offer best compositional control of the films. Efforts should be made for quality improvements of the solution based coated thin films to match the product quality level of expensive methods.

6.2.2 Steps towards Better Stability of Perovskite Material Based Solar Cells

Stability and durability is a key issue for perovskite material based solar cells. This problem requires special attention as it is the biggest hurdle in the commercialization of perovskite material based solar cell. The instability mainly arises due to organic part of perovskite material which absorbs moisture and decomposed resulting shortening of solar cell. We have replaced organic part with inorganic which may likely increase the stability and this work provides basis for further investigation to enhance the stability of these third generation solar devices. Perovskite based solar cells are majorly fabricated through solution processing using spin coating technique if layers are not properly coated, then mismatch of layers interfaces caused shortening

of solar cell. Research should be done to enhance the efficiency of PSCs by improving the cell fabrication methods and also the stability.

Acknowledgments

All praise to Allah Almighty, the supreme Master of this universe who gave me the strength to successfully complete this dissertation. Completion of MS Degree has been a challenging yet interesting journey filled with life lessons. As my research has been completed, I would like to take this opportunity to express sincere gratitude to my advisor **Dr. Nadia Shahzad** for the continuous support of my MS study and adjacent research, for her patience, motivation, and immense knowledge. In addition to be an exceptional guide, she has incessantly encouraged and reinforced me to shine in my arena of research. I would also like to thank my guidance and evaluation committee: **Dr. Naseem Iqbal**, **Dr. Parvez Akhter** and **Dr. Afzal Hussain Kamboh** for their valuable feedback and insights which added value to this research.

I am truly grateful for the prodigious assistance of **Dr. Muhammad Imran Shahzad** who provided me the opportunity to conduct some of the essential experimental work at National Centre for Physics (NCP). Without his guidance and aid the research work would have been impossible.

I also appreciate the support of teaching and non-teaching faculty of U.S.-Pakistan Center for Advanced Studies in Energy for all the things that facilitated smooth work of my research.

I would particularly acknowledge the immense support of my dear **parents** who were like beacons of hope throughout this entire journey. I would also admire the wholehearted help of my friends and colleagues who always cheered for me and offered their support in every way possible.

Appendix 1 – Research Article

GRAPHICAL ABSTRACT:

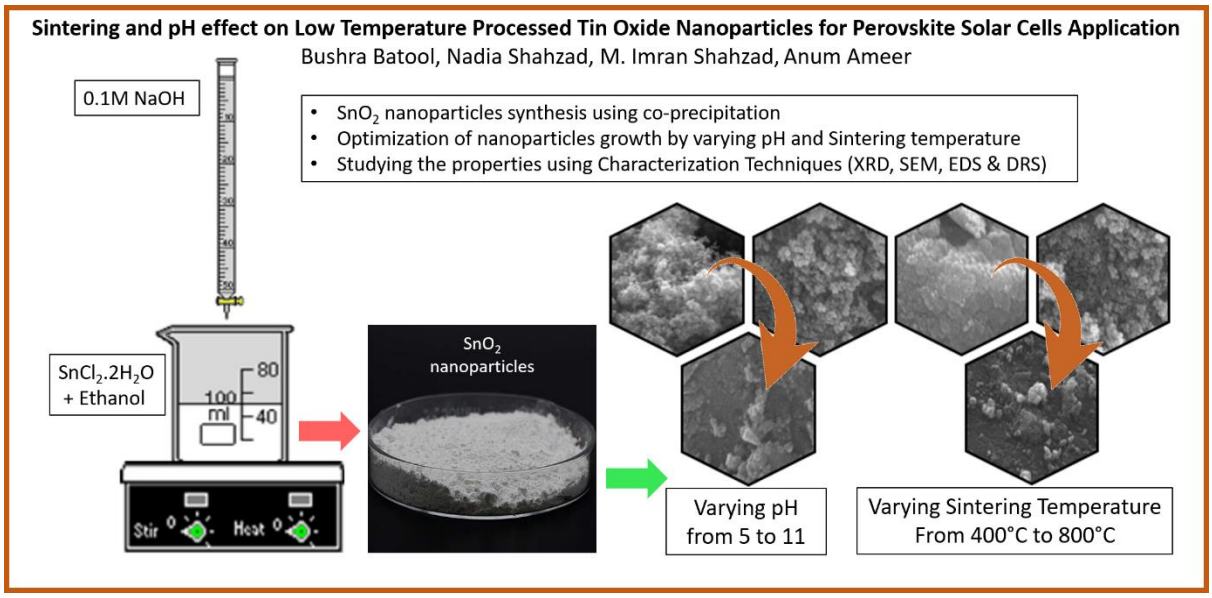

Sintering and pH effect on Low Temperature Processed Tin Oxide Nanoparticles for Perovskite Solar Cells Application

[a*]Bushra Batool, [a]Nadia Shahzad, [a]Anum Ameer, [b]M. Imran Shahzad

[a]*US-Pakistan Centre for Advanced Studies in Energy (USPCAS-E), National University of Science and Technology (NUST), 44000 Islamabad, Pakistan*

[b]*Nanosciences and Technology Department (NS&TD), National Centre for Physics (NCP), 44000 Islamabad, Pakistan*

[*] Corresponding author: e-mail: bushrakhtk@gmail.com, Tel. +92 334 5210841

Abstract:

With increasing worldwide energy consumption and environmental pollution, traditional fossil energy sources are not sufficient for the sustainable development of human society. Among a variety of new energy technologies, solar power is unquestionably one of the most promising technologies. Perovskite solar cells (PSCs)

are remarkably effective even at the very early stage of research. With an exceptional efficiency of 23.3% PSCs are considered as the future of solar energy. In many successful state of the art PSCs, Tin (IV) oxide (SnO_2) due to its favorable characteristics such as effective electron extraction, hole blocking and a better band alignment with perovskite absorber layer have been used as an Electron transport layer (ETL). SnO_2 despite of being a highly potential material puts a limitation to be frequently studied because of multiple oxidation states. In this study, low temperature processed, SnO_2 nanoparticles have been synthesized at different pH levels and sintering temperature using $SnCl_2.2H_2O$ as precursor salt. The as-synthesized SnO_2 nanoparticles were further characterized using X-ray Diffraction (XRD), Scanning Electron Microscopy (SEM), Energy Dispersive Spectroscopy (EDS) and Diffused Reflectance Spectroscopy (DRS) for studying the phase identification, morphological structure analysis, elemental analysis and band gap measurement of the material respectively. Here, the unique attributes of SnO_2 as an application for PSCs are described.

Keywords: *Tin Oxide; Nanoparticles; low temperature Synthesis; Perovskite Solar Cell*

1.1 Introduction:

The major concern today about energy crisis of the world is that the demands on the inadequate natural/conventional resources being used to power industrial and domestic sectors are deteriorating. The world's current Energy demand is increasing rapidly. The causes of this crisis include over- consumption, rapid increase in population, underprivileged infrastructure, wastage of energy and unexplored renewable energy options. The hour of need calls for Renewable energy resources like solar energy. Perovskite solar cells (PSCs) are considered as the most promising photovoltaic technology with an extraordinary efficiency of 23.3% PSCs due to its low manufacturing cost, feasible fabrication, and high power conversion efficiency (PCE) [1] . PSCs being the third generation of photovoltaic solar cells uses the nanostructured materials. Lately, Nanostructured materials have attracted a significant amount of consideration due to their exceptional electrical, physical, chemical, and magnetic properties as well as their potential for technological applications [7]. In past few years, Tin Oxide, SnO_2 has been used in PSCs as an Electron Transport layer (ETL) or hole blocking layer.

SnO_2 is known to be n-type semiconductor material and has an electronic band gap of 3.6 eV.

SnO_2 is well acknowledged for its potential applications in gas sensors, dye sensitized solar cells, and transparent conducting electrodes and as a catalyst support (Cheng *et al.*, 2004). Hence, there are many synthesizes techniques that have been recommended to synthesize SnO_2 nanostructures, such as sputtering from tin oxide as a target material and also from Tin metallic target followed by oxidation (in presence of oxygen gas), this is usually being done through DC/RF magnetron sputtering ('Solution Phase growth of Tin Oxide (SnO2) Nanostructures under Controlled Synthesis Conditions', 2017)(Fallah and Mokhtary, 2015) and e-beam deposition of Tin Oxide charge pellets, chemical vapor deposition (CVD), other processes includes solid state chemical reactions and wet chemical techniques like spray pyrolysis and sol-gel-related methods, co-precipitations (Bharat G Pawar *et al.*, 2012)(Park and Mackenzie, 1995), hydrothermally treated recipes are used to make tin oxide layers

(Sharma, Jha and Jindal, 2018), particles, and precipitates, few of these procedures also use template method to have defined nanostructures (Boran, Çetinkaya and Şahin, 2017)(Briois *et al.*, 2004)(Wang *et al.*, 2009)**.** The sol-gel technique, is widely used for the synthesis of nano ranged particles of SnO_2 and also have multiple benefits majorly involving low temperature processed nanostructures and providing homogeneity at high molecular level (Ahmed *et al.*, 2012) . Over-all, because of the ease of control and low-cost chemical input, the tin chlorides are chosen as precursors. The experiment can be carried out in more or less ambient conditions. Tin chloride has been used as precursor which is economical as compared to the granulated tin and tin alkoxide.

Lately, SnO_2 has attracted great considerations as ETL for PSCs, and it is being considered as the most encouraging substitute of TiO_2 because of certain reasons:

a) SnO_2 has a better energy band alignment with the major absorber layer and a deep conduction band. The excellent energy band alignment at ETL/perovskite interface will help improving the electron extraction and hole blocking [21-22].
b) High electron mobility of SnO_2 up to 240 $cm^2V^{-1}s^{-1}$ and comparatively greater conductivity helps for better the electron transport efficiency and prevents the recombination loss (Jiang, Zhang and You, 2018)
c) High transmittance over the visible region of spectrum and, wide optical band gap of SnO_2 (3.6 to 4.0 eV) ensures that the most of light is absorbed by the perovskite layer.
d) For a better compatibility with PSCs, flexible solar cells and tandem solar cells, SnO_2 can be simply processed by low-temperature techniques (Correa Baena *et al.*, 2015).
e) In comparison with TiO2 and other ETLs, SnO_2 depicted an excellent chemical stability, self-passivation property, UV resistance properties, and low photo-catalytic, proving it to be very suitable for complete device stability (Jiang *et al.*, 2018).

In this presented work, SnO_2 nano-powder was synthesized using co-precipitation method. The crystallinity and crystalline size of the as synthesized nano-crystalline SnO_2 powder was studied against different sintering temperature and also the pH effect on various structural and other properties of SnO_2 nanoparticles was studied.

1.2 Experimental

1.2.1 - Materials:

Stannous chloride dihydrate ($SnCl_2.2H_2O$), Ethyl Alcohol (C_2H_5OH) and sodium hydroxide (NaOH) were purchased from Merck-Sigma Aldrich with purity up to 99.9% trace metal basis. Glucose in a very small amount have been used as template.

1.2.2- Preparation of Tin Oxide Nanoparticles:

0.1M solution of $SnCl_2.2H_2O$ was prepared in ethanol and 0.1M solution of NaOH in distilled water was added drop wise to maintain a pH of 5. The solution was refluxed at 90°C for 4 hours in lab tech oven. After cooling, centrifugation was done at 3000 rpm for 15mins and repeated washing was done with water and later collecting the ensuing gel. It was then kept overnight in vacuum oven at 90°C. The sintering of the

obtained residue was done at 400°C. The nanoparticles were then crushed and refined powder was obtained for the further characterization. The pH effect was studied for the structural analysis of as synthesized SnO_2 by varying pH from 5 to 11. Once the pH was optimized, the nanoparticles growth was then analyzed by variation of sintering temperature. The samples were sintered at 400°C, 600°C and 800°C to obtain SnO_2 nano-powder. Finally, multiple samples of SnO_2 nano-powders were obtained and subjected to further characterizations.

1.2.3- Characterization:

A comprehensive explanation of the structure and composition was carried out by different characterization techniques. Structural characterization was carried out by X-ray diffraction using Rigaku X-ray Diffractometer with CuKα radiation wavelength λ = 1.5406Å in the 2θ range from 20^o to 80^o. The surface morphology of SnO_2 particles were analyzed by using the scanning electron microscope (SEM) (JOEL JSM 680 LA15 KV) (Fallah and Mokhtary, 2015). The Energy Dispersive spectroscopy EDS was done to find the elemental composition of the samples and to ensure no impurities were present in the synthesized product. The band gap of the nanoparticles were measured using Diffused reflectance measurement (DRS).

1.3- Results and Discussion

1.3.1- pH Variations

The nanoparticles were further optimized using different pH level. During the co-precipitation the pH, at which the reaction is to be stopped was varied from pH=5 to pH=8 and pH=11. The XRD comparative graph in figure 4 shows the peaks for pH 5, 8 and 11 respectively. The concentrations of H^+ and/or OH^- ions in the solution deeply effects the morphology of the solution processed synthesized SnO_2 (Rac *et al.*, 2014) (Periathai *et al.*, 2017). The solution relatively more acidic at pH 5 will have less concentration of H^+ ions in comparison to OH^-. The NaOH reaction with the $SnCL_2.2H_2O$ causes the formation of $Sn(OH)_2$, during and later the chemical reaction the compound dissociates into Sn^{2+} and OH^- ions. Sn^{2+} plays an important role for SnO_2 nuclei formation when it surpasses the acute level. Nonetheless at pH 11, discrepancies in the OH^- ions concentration occur. Therefore on varying the pH from acidic to basic (5 to 11) the concentration of H^+ ions decreases and the OH^- ions increases, which encourages to form the desired structures (Priya, Geetha and Ramamurthi, 2017)(Jiang *et al.*, 2005).In conclusion we can clearly see the increase in the pH shows reduction in the particle size, in the following XRD results figure 5.1 and table 5.1, the peak values given in the standard Reference code: 01-072-1147. In conclusion we can clearly see the increase in the pH shows reduction in the crystallite size, in the following XRD results (Figure 1 and Table 1).

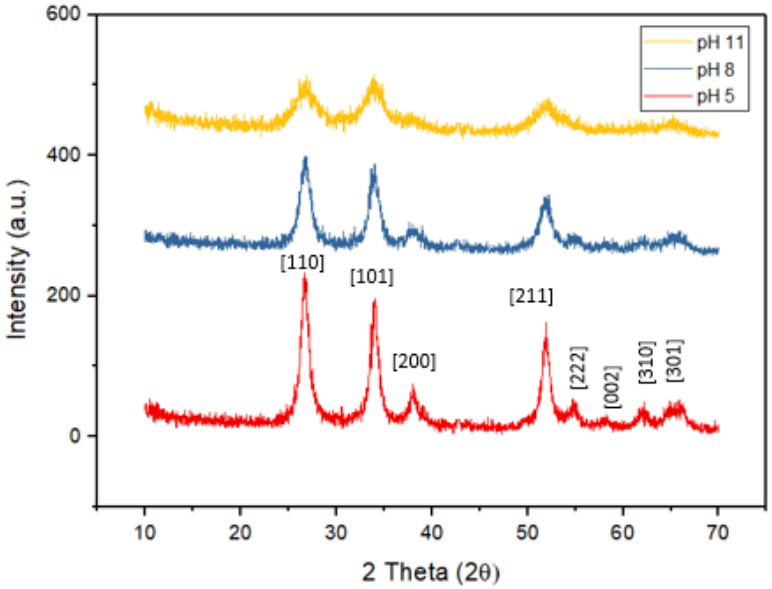

Figure 1: XRD pattern of the samples synthesized at pH 5, 8 and 1 1

Table 1: Effect of pH on various structural parameters

pH	Crystallite Size by Scherrer equation (nm)	Lattice parameters (Å)		Cell volume ($Å^3$)	a/c ratio
		a	C		
5	12.53	4.7370	3.1875	71.524	1.486
8	9.85	4.7370	3.1850	71.470	1.487
11	7.86	4.7370	3.180	71.356	1.489

The nanoparticles first optimized at different pH were characterized using SEM for morphological studies. The three different pH levels indicated the variations in size of the nanoparticles. The pH varied from 5 to 11 have the following SEM results figure 3. The morphology of nanoparticles was very homogenous and proper grain like structure were obtained at pH=8. Once the pH was optimized the temperature was varied for sintering and effect was studied.

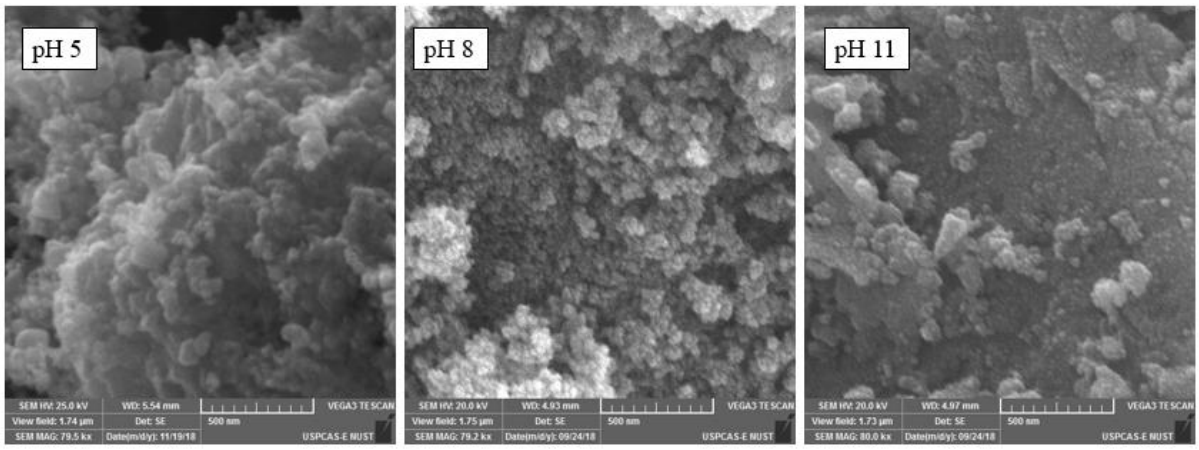

Figure 2: SEM images of SnO_2 nanoparticles with pH 5, 8 and 11 at 500nm

1.3.2- Varying the sintering temperature:

The SnO_2 nanoparticles prepared at three different sintering temperatures have X-ray diffraction patterns as shown in Fig. 2. The XRD helped to identify the tetragonal structure (rutile) of SnO2 with the maximum intensity peaks from (110) and (101) planes (Hamdadou, 2018).The diffraction peaks deduced were at (110), (101), (200), (211), (220), and (113) and were indexed using the software X'pert HighScore and the pikes are accurately alike with the tetragonal rutile structure of SnO_2 (Sarabadani *et al.*, 2011), the peak values given in the standard Reference code: 01-072-1147.

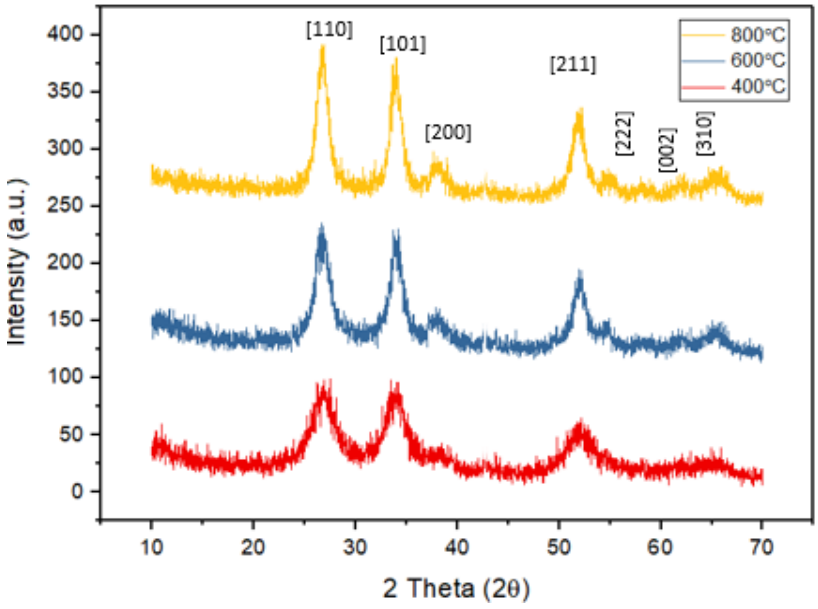

Figure 3 XRD patterns for SnO_2 nanoparticles sintered at 400°C, 600°C and 800°C

The samples sintered at different temperatures has no shift in XRD peaks which indicates that there is no change in the rutile structure with incremental heating. The results demonstrate that as the sintering temperature increases the intensity of peaks has been narrowed expressively. The XRD results indicates that the heating time noticeably effects the crystallization. The experiments revealed that substantial particles start growing around 400°C for SnO_2. The increased temperature speeds up the growth. In addition, it has also been observed that lattice parameters (a and c) and

cell volume also increase as a function of sintering temperature (Table 2) (Ahmed *et al.*, 2012). The Debye Scherrer formula is used to calculate the crystallite grains, specified by equation i (Wang *et al.*, 2009)

$$\mathbf{D_{hkl} = \frac{0.9\lambda}{\beta cos\theta}} \qquad \textbf{(Equation iii)}$$

Where, the wavelength is λ for the X-ray source (mostly λ = 1.54 A˚) and the full width at half maximum (FWHM) is β with unit in radians and θ being the angle of diffraction of the peak in the tetragonal phase (Illyaskutty *et al.*, 2015). The crystallite size increases with rise in temperature, and that can be because atomic diffusion occurs more at higher temperatures (Ahmed *et al.*, 2012).

Table 2: Effect of sintering temperature on various structural parameters

Sintering Temperature (^{0}C)	Crystallite Size by Scherrer equation (nm)	Lattice strain	Lattice parameters (Å)		Cell volume (Å^3)	a/c ratio
			a	C		
400°C	9.85	7.8×10-^{4}	4.7370	3.1850	71.470	1.487
600°C	16.21	23.5×10-^{4}	4.7401	3.1861	71.653	1.487
800°C	22.60	25.1×10-^{4}	4.7520	3.1875	72.234	1.490

SEM results shown in figure 4, also verify the comment deduced from the XRD data analysis that the particle size also decreases with rise in temperature. SEM images of Sample 1, which was sintered at 400°C showed grain like nano structures with grain size of d= 10.84 nm, sample 2, sintered at 600°C with a grain size of 16.23 nm and sample 3 being sintered at 800°C had a grain size of about 18.73 to 23.71 nm, was observed at 500 nm resolution scale.

At temperatures above 400 ºC, grain sizes are always larger than crystallite sizes. However, in that temperature range, the crystallite and grain sizes are of the same order of magnitude. This suggests that grain sizes are formed by a single crystal and that no geometrical changes occur during the sintering process, but only an increase in grain size (Leite *et al.*, 2003). It was also concluded that there was no change in pore geometry during the sintering process. Some researchers have also reported that with increasing temperature, the agglomeration also increased.

All the SEM images indicate that the particles have non-uniform size with high degree of agglomeration. For 400°C the nano-particles are amassed into bigger particles parting some pores between. In addition, the changes in the morphology of SnO_2 nano particles strongly depends on the annealing temperatures as observed for 600°C and 800°C, fine grain like nano structures were obtained. The samples exhibit a spherical shape with a high degree of agglomeration among fine particles. The SEM examinations reveal that when the calcination temperature increases the agglomeration of non-uniform particles increases (Bharat G. Pawar *et al.*, 2012) (Thamaraiselvi and Meenakshisundar, 2017).

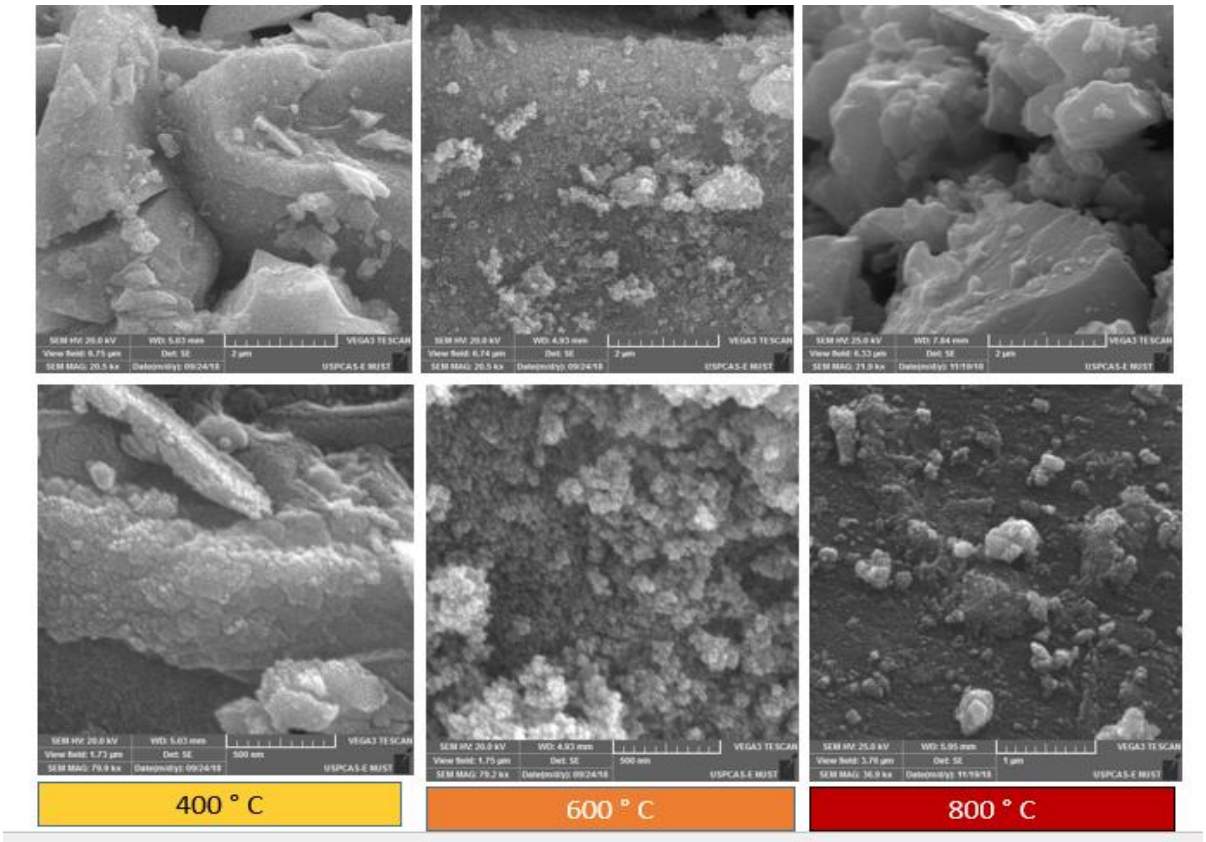

Figure 4: SEM images of SnO_2 nanoparticles at different sintering Temperatures

Energy Dispersive Spectroscopy (EDS); is a relatively easy method of explaining stoichiometry of material. EDS. EDS Graph shown in the figure 4 show the atomic weight of tin and oxygen particles but also ensures that no impurities were found in the sample.

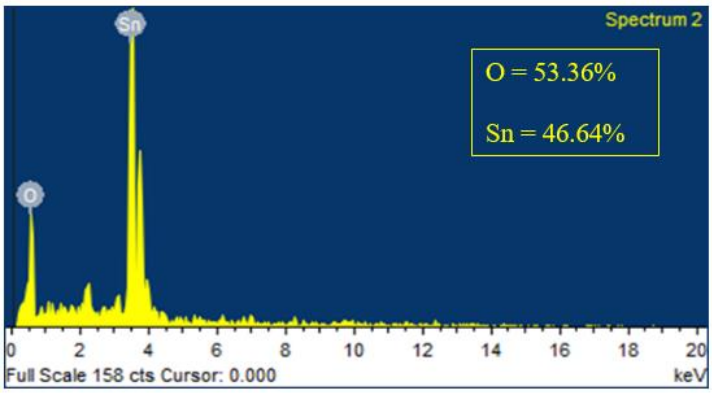

Figure 0.1 EDS of SnO_2 samples prepared

The band gaps of the nanoparticles were determined from the well-known Tauc relation (*J. Tauc, R. Grigorovici and A. Vancu, "Optical Properties and Electronic Structure of Amorphous Germanium," Physica Status Solidi (b), Vol. 15, No. 2, 1966, pp. 627-637. doi10.1002/pssb.19660150224 - References - Scientific Research Publishing*, no date) given by:

$$\alpha h\nu = A\,(h\nu - Eg)^{n} \qquad \textbf{(Equation 4)}$$

Where α =2.303A/t is called the absorption coefficient, A is the absorbance, t is the thickness of the cuvette, Eg is the band gap and n =2 for direct band gap semiconductor.

The band gap was determined by plotting the Tuac plot as shown in Figure 5. For the samples sintered at 400 °C band gap was E_g= 3.59 eV, for 600 °C E_g= 3.67 eV and for 800 °C E_g= 3.69 eV respectively. Hence with increasing the sintering temperature the trend of increasing band gap was observed.

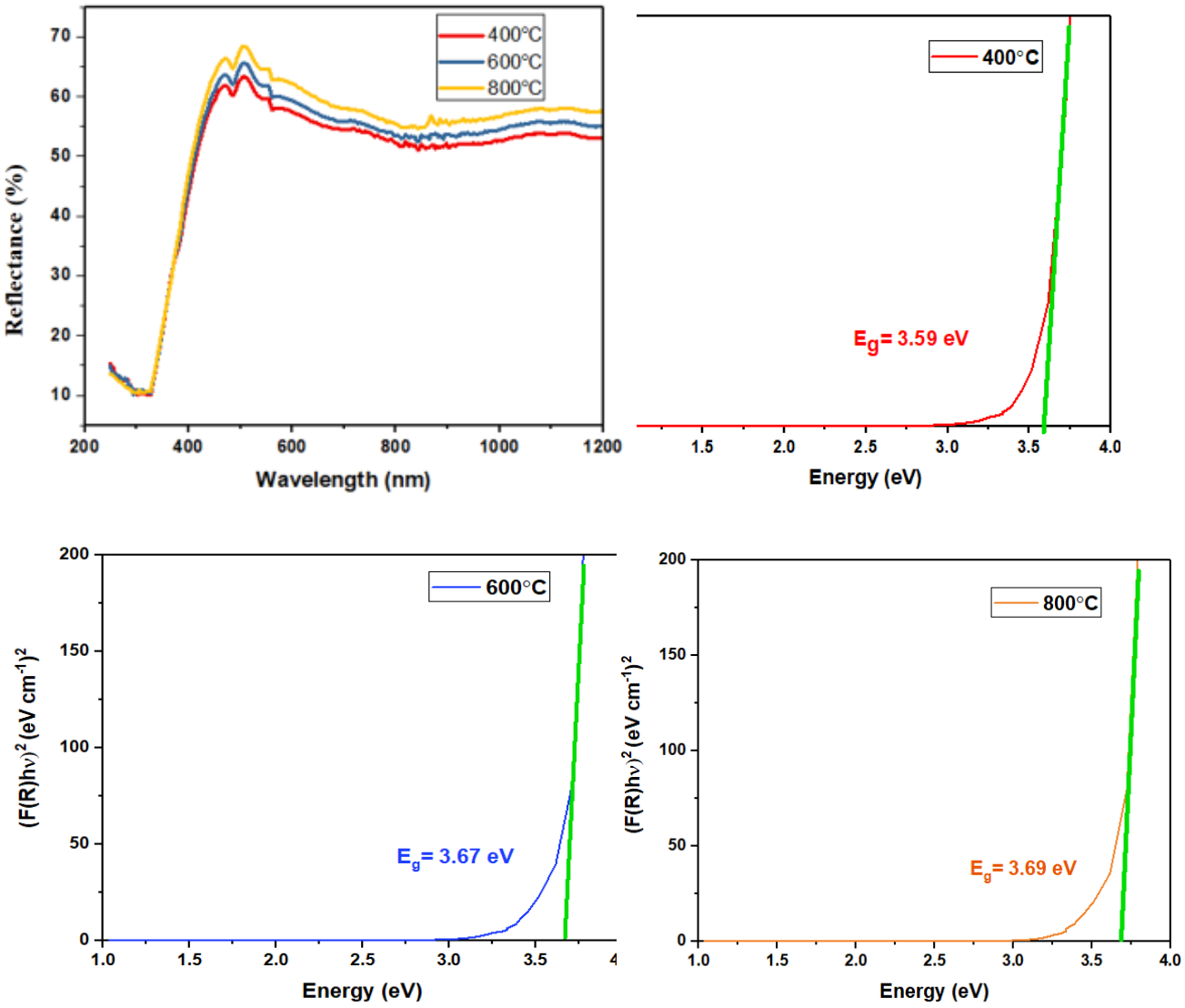

Figure 5: Graph representing %Reflectance and Band gap of SnO_2 sintered at different temperature

The increment in the band gap can be relate to the particle size of the nanomaterials. The trend of increasing band gap with increasing temperature is visible from 400°C to 600°C, but not with much difference at higher temperature. The concluded band gap values for the SnO_2 nanoparticles in this work coincides with the literature reported values. The recommended values of bandgap for SnO_2 to be used as an electron transport layer for Perovskite Solar Cells are 3.6eV or above.

1.4 Conclusions

In this work, we have synthesized and study the morphological, structural and optical properties of SnO_2 with reference to temperature and pH changes. The XRD aided to identify the tetragonal rutile structure of SnO_2 with the maximum intensity peaks from (110) and (101) planes. While the pH had totally opposite effect as that of sintering, the particle size clearly tend to reduce with increasing pH from 5 to 11. The variations from grain size ranging from r~10.84 nm to 23.71 nm was observed because of alternating the sintering temperature from 400°C to 800°C, which shows improved crystallinity of the samples. The bandgap measurement of the samples showed an increment whereas, for higher temperatures this increase is negligible. These facts show that the sintering temperature of 600°C or above are recommended to achieve SnO_2 nanoparticles with suitable properties to be employed as an effective ETL in Perovskite Solar Cells.

Acknowledgment:

The authors would like to thank Higher Education Commission, Pakistan for the financial support to conduct this research work.

1.5 Reference

[1] Ahmed, A. S. *et al.* (2012) 'Journal of Physics and Chemistry of Solids Temperature dependent structural and optical properties of tin oxide nanoparticles', *Journal of Physical and Chemistry of Solids*. Elsevier, 73(7), pp. 943–947. doi: 10.1016/j.jpcs.2012.02.030.

[2] Boran, F., Çetinkaya, S. and Şahin, M. (2017) 'Effect of Surfactant Types on the Size of Tin Oxide Nanoparticles', 132(3), pp. 546–548. doi: 10.12693/APhysPolA.132.546.

[3] Briois, V. *et al.* (2004) 'Solid-State and Solution Structural Study of Acetylacetone-Modified Tin(IV) Chloride Used as a Precursor of SnO_2 Nanoparticles Prepared by a Sol−Gel Route', *Chemistry of Materials*, 16(20), pp. 3885–3894. doi: 10.1021/cm040141q.

[4] Cheng, B. *et al.* (2004) 'Large-Scale, Solution-Phase Growth of Single-Crystalline SnO_2 Nanorods', *Journal of the American Chemical Society*, 126(19), pp. 5972–5973. doi: 10.1021/ja0493244.

[5] Correa Baena, J. P. *et al.* (2015) 'Highly efficient planar perovskite solar cells through band alignment engineering', *Energy and Environmental Science*. Royal Society of Chemistry, 8(10), pp. 2928–2934. doi: 10.1039/c5ee02608c.

[6] Fallah, N. S. and Mokhtary, M. (2015) 'Tin oxide nanoparticles (SnO 2 -NPs): An efficient catalyst for the one-pot synthesis of highly substituted imidazole

derivatives', *Integrative Medicine Research*. Taibah University, 9(4), pp. 531–537. doi: 10.1016/j.jtusci.2014.12.004.

[7] Hamdadou, N. (2018) 'IMPROVED PROPERTIES OF SnO 2 THIN FILMS OBTAINED VIA SPIN COATING METHOD BY VARYING THE SOLUTION CONCENTRATION', 25(7), pp. 1–9. doi: 10.1142/S0218625X18500920.

[8] Illyaskutty, N. *et al.* (2015) 'Thermally modulated multi sensor arrays of SnO2/additive/electrode combinations for enhanced gas identification', *Sensors and Actuators B: Chemical*. Elsevier, 217, pp. 2–12. doi: 10.1016/J.SNB.2015.03.018.

[9] *J. Tauc, R. Grigorovici and A. Vancu, "Optical Properties and Electronic Structure of Amorphous Germanium," Physica Status Solidi (b), Vol. 15, No. 2, 1966, pp. 627-637. doi10.1002/pssb.19660150224 - References - Scientific Research Publishing* (no date). Available at: http://www.scirp.org/(S(351jmbntvnsjt1aadkposzje))/reference/ReferencesPapers.aspx?ReferenceID=120791 (Accessed: 28 October 2019).

[10] Jiang, L. *et al.* (2005) 'Size-Controllable Synthesis of Monodispersed SnO 2 Nanoparticles and Application in Electrocatalysts', pp. 8774–8778.

[11] Jiang, Q. *et al.* (2018) 'Enhanced electron extraction using SnO2 for high-efficiency planar-structure HC(NH2)2PbI3-based perovskite solar cells', (November 2016). doi: 10.1038/nenergy.2016.177.

[12] Jiang, Q., Zhang, X. and You, J. (2018) 'SnO 2 : A Wonderful Electron Transport Layer for Perovskite Solar Cells', 1801154, pp. 1–14. doi: 10.1002/smll.201801154.

[13] Leite, E. R. *et al.* (2003) 'Sintering of undoped SnO2', *Cerâmica*. FapUNIFESP (SciELO), 49(310), pp. 87–91. doi: 10.1590/s0366-69132003000200005.

[14] Park, S.-S. and Mackenzie, J. D. (1995) 'Sol-gel-derived tin oxide thin films', *Thin Solid Films*, 258(1–2), pp. 268–273. doi: 10.1016/0040-6090(94)06404-0.

[15] Pawar, Bharat G. *et al.* (2012) ' Effect of Sintering Temperatures on the Synthesis of SnO2 Nanospheres ', *ISRN Chemical Engineering*. Hindawi Limited, 2012, pp. 1–7. doi: 10.5402/2012/954869.

[16] Pawar, Bharat G *et al.* (2012) 'Effect of Sintering Temperatures on the

Synthesis of SnO 2 Nanospheres', 2012. doi: 10.5402/2012/954869.

[17] Periathai, R. S. *et al.* (2017) 'Author ' s Accepted Manuscript Effect of pH on the electrical properties and Reference : To appear in : Physica B : Physics of Condensed Matter', *Physica B: Physics of Condensed Matter*. Elsevier. doi: 10.1016/j.physb.2017.01.002.

[18] Priya, M., Geetha, S. and Ramamurthi, A. (2017) 'Effect of pH and annealing temperature on the properties of tin oxide nanoparticles prepared by sol – gel method', *Journal of Materials Science: Materials in Electronics*. Springer US, 0(0), p. 0. doi: 10.1007/s10854-017-7959-2.

[19] Rac, O. *et al.* (2014) 'Influence of stabilising agents and pH on the size of SnO 2 nanoparticles', pp. 2192–2201. doi: 10.3762/bjnano.5.228.

[20] Sarabadani, P. *et al.* (2011) 'Synthesis and Characterization of Tin Oxide Nanoparticles by Solid State Chemical Reaction', pp. 131–140. doi: 10.1007/s10876-011-0350-1.

[21] Sharma, N., Jha, R. and Jindal, N. (2018) 'Hydrothermally Synthesized Stannic Oxide Nano-hexagons', *Materials Today: Proceedings*. Elsevier BV, 5(5), pp. 13807–13815. doi: 10.1016/j.matpr.2018.02.022.

[22] 'Solution Phase growth of Tin Oxide (SnO2) Nanostructures under Controlled Synthesis Conditions' (2017) *International Journal of Nanoparticle Research*. eSciPub LLC. doi: 10.28933/ijnr-2017-11-2502.

[23] Thamaraiselvi, E. and Meenakshisundar, S. (2017) 'Effect of temperature on Structural and Optical properties of SnO 2 nanoparticles', *IOSR Journal of Applied Physics*. doi: 10.9790/4861-17002036972.

[24] Wang, Y. *et al.* (2009) 'Antimony-Doped SnO_2 Nanopowders with High Crystallinity for Lithium-Ion Battery Electrode', *Chemistry of Materials*, 21(14), pp. 3202–3209. doi: 10.1021/cm9007014.